AD-A129 690 INTERACTION OF THE RADAR WAVES WITH THE CAPILLARY WAVES 1/3
ON THE OCEAN..(U) KANSAS UNIV/CENTER FOR RESEARCH INC
LAWRENCE REMOTE SENSING L.. S BARKESHLI ET AL. MAY 83
UNCLASSIFIED CRINC/RSL-TR-419-1 N00014-79-C-0533 F/G 17/9 NL

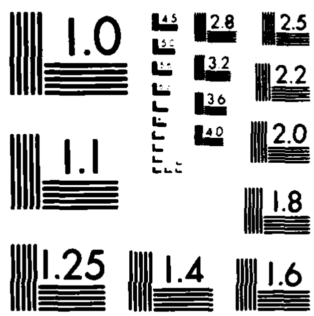

MICROCOPY RESOLUTION TEST CHART
NATIONAL BUREAU OF STANDARDS-1963-A

CRINC

REMOTE SENSING LABORATORY

12

ADA 129690

DTIC FILE COPY

JUN 2 2 1983

A

THE UNIVERSITY OF KANSAS CENTER FOR RESEARCH, INC.

2291 Irving Hill Drive—Campus West
Lawrence, Kansas 66045

83 06 21 023

INTERACTION OF THE RADAR WAVES
WITH
THE CAPILLARY WAVES ON THE OCEAN

by

S. Barkeshli
R.K. Moore

Remote Sensing Laboratory
Center for Research, Inc.
The University of Kansas
Lawrence, Kansas 66045

RSL Technical Report
RSL TR 419-1
May 1983

Supported by:

OFFICE OF NAVAL RESEARCH
Department of the Navy
800 N. Quincy Street
Arlington, Virginia 22213

CONTRACT N00014-79-C-0533

Unclassified

SECURITY CLASSIFICATION OF THIS PAGE (When Data Entered)

REPORT DOCUMENTATION PAGE		READ INSTRUCTIONS BEFORE COMPLETING FORM
1. REPORT NUMBER RSL TR 419-1	2. GOVT ACCESSION NO. AD-A129 690	3. RECIPIENT'S CATALOG NUMBER
4. TITLE (and Subtitle) Interaction of the Radar Waves with the Capillary Waves on the Ocean		5. TYPE OF REPORT & PERIOD COVERED Interim-Technical Report
		6. PERFORMING ORG. REPORT NUMBER
7. AUTHOR(s) S. Barkeshli and R.K. Moore		8. CONTRACT OR GRANT NUMBER(s) N00014-79-C-0533
9. PERFORMING ORGANIZATION NAME AND ADDRESS Remote Sensing Laboratory; University of Kansas Center for Research, Inc.; 2291 Irving Hill Drive-Campus West; Lawrence, Kansas 66045		10. PROGRAM ELEMENT, PROJECT, TASK AREA & WORK UNIT NUMBERS
11. CONTROLLING OFFICE NAME AND ADDRESS Office of Naval Research Dept. of the Navy 800 N. Quincy St.; Arlington, Va. 22213		12. REPORT DATE May 1983
		13. NUMBER OF PAGES 192
14. MONITORING AGENCY NAME & ADDRESS(if different from Controlling Office)		15. SECURITY CLASS. (of this report) Unclassified
		15a. DECLASSIFICATION/DOWNGRADING SCHEDULE

16. DISTRIBUTION STATEMENT (of this Report)

Approved for public release; distribution unlimited

17. DISTRIBUTION STATEMENT (of the abstract entered in Block 20, if different from Report)

18. SUPPLEMENTARY NOTES

19. KEY WORDS (Continue on reverse side if necessary and identify by block number)

20. ABSTRACT (Continue on reverse side if necessary and identify by block number)

Measurements of the radar cross-section of the sea were made from the Noordwijk platform off the Dutch coast during September-November 1979 as part of Project MARSEN using an FM microwave spectrometer over the 8-18 GHz frequency range. A set of techniques for studying the modulation of the capillary waves on the ocean surface was developed for use in analyzing the entire observation set and is presented here as applied to a single set of observations. Thus, the results given here are only of limited oceanographic

DD FORM 1 JAN 73 1473 EDITION OF 1 NOV 65 IS OBSOLETE

S/N 0102-LF-014-6601

Unclassified

SECURITY CLASSIFICATION OF THIS PAGE (When Data Entered)

significance, but illustrate the types of analysis to be performed when these techniques are applied to more data.

Measured scattering coefficient based on instantaneous radar antenna footprint was cross-correlated with wave height and slope for measurements at the Noordwijk tower on 21 September 1979. The scattering coefficient leads the wave height by about 104° and leads the slope by about 77°. A new modulation index concept, $\mu(t)$, the ratio of the measured scattering coefficient (based on instantaneous radar antenna footprint) to the theoretical scattering coefficient (based on uniform capillary modulation and instantaneous resonance with the K-spectrum) has been presented. The RMS value of $\mu(t)$ is 0.876 with standard deviation 0.349 for HH-polarization and 0.673 with standard deviation of 0.044 for VV-polarization. The cross-correlation of $\mu(t)$ and wave height shows that the peak of the modulation leads the wave height by about 153°. Cross-correlation of $\mu(t)$ and slope shows that the peaks of the modulation are located at about the minima of the dominant slope, 165° away from both sides of the maximum. An algorithm for transformation from temporal to spatial domain has been developed, and the modulation transfer function based on Plant's definition [1979] has been calculated.

TABLE OF CONTENTS

LIST OF FIGURES

LIST OF TABLES

1.0 ABSTRACT

Measurements of the radar cross-section of the sea were made from the Noordwijk platform off the Dutch coast during September-November 1979 as part of Project MARSEN using an FM microwave spectrometer over the 8-18 GHz frequency range. A set of techniques for studying the modulation of the capillary waves on the ocean surface was developed for use in analyzing the entire observation set and is presented here as applied to a single set of observations. Thus, the results given here are only of limited oceanographic significance, but illustrate the types of analysis to be performed when these techniques are applied to more data.

Measured scattering coefficient based on instantaneous radar antenna footprint was cross-correlated with wave height and slope for measurements at the Noordwijk tower on 21 September 1979. The scattering coefficient leads the wave height by about 104° and leads the slope by about 77°. A new modulation index concept, $\mu(t)$, the ratio of the measured scattering coefficient (based on instantaneous radar antenna footprint) to the theoretical scattering coefficient (based on uniform capillary modulation and instantaneous resonance with the K-spectrum) has been presented. The RMS value of $\mu(t)$ is 0.876 with standard deviation 0.349 for HH-polarization and 0.673 with standard deviaton of 0.044 for VV-polarization. The cross-correlation of $\mu(t)$ and wave height shows that the peak of the modulation leads the wave height by about 153°. Cross-correlation of $\mu(t)$ and slope shows that the peaks of the modulation are located at about the minima of the dominant slope, 165° away from both sides of the maximum. An algorithm for transformation from temporal to spatial domain has been developed,

and the modulation transfer function based on Plant's definition [1979] has been calculated.

2.0 INTRODUCTION

Radar backscatter from the ocean can be used to monitor the wind velocity with a scatterometer that observes at two or more directions relative to the wind vector, to determine wave heights and ocean elevation (and from it currents) with an altimeter, and to monitor features of the wave spectrum, bottom topography, internal waves, ship wakes, and oil spills with an imaging radar. Since the radar backscatter represents a confusing ''clutter'' for radars observing targets such as ships and periscopes, studies of the radar backscatter have been conducted since the early days of radar before the direct applications listed above were developed.

The relatively recent advent of spaceborne scatterometers, altimeters, and synthetic-aperture imaging radars has led to greatly increased interest in the nature of radar backscatter from the sea. Furthermore, the use of these instruments calls for different kinds of understanding (consequently theory and measurements) than those required for earlier clutter measurements. To aid in improving this understanding, several major international measurement programs have been conducted in recent years. Project MARSEN, of which this research is a part, is one of the more recent programs. This program was conducted in the fall of 1979 in two instrumented areas in the North Sea: off the German coast near the Helgoland Bight and off the Dutch coast near Noordwijk. This is a report of part of one of the studies conducted from the Noordwijk platform of the Dutch Department of Water Control.

Measurements of radar backscatter from instrumented towers in the sea are based on the need for observations under more carefully

controlled conditions than are possible with measurements from aircraft and spacecraft, and to study with a greater variety of conditions than can be encountered with measurements from aircraft whose flight times are limited. A goal of measurement programs such as MARSEN is to perform many measurements of different kinds from towers and aircraft so that the synergism of data comparisons may lead to better understanding than would be obtained with isolated measurement programs by small groups of investigators.

Radar measurements were made at the Noordwijk platform by three groups: The University of Kansas, a Dutch group of experimenters from the Physics Research Laboratory of National Defence and the Technical University of Delft, and a French group from the Institut Francaise du Petrole. A JPL group made measurements with a capillary wave gauge and near-surface wind probes, and a British group made measurements of breaking waves with special buoys deployed from the platform. In addition, overflights were made by a NASA aircraft carrying a scatterometer and by several imaging radars from the U.S., Germany, France, and the Netherlands. The object of the aircraft measurements over the Noordwijk platform was to allow comparison with the platform measurements.

Major goals of the University of Kansas measurements, most of which were shared by the other radar investigators on the platform were:

1. To establish the variation of the capillary-wave amplitude over the underlying larger waves, and to establish the portion of the underlying waves contributing the strongest radar signals. This is important because the nature of a synthetic-aperture image of

the larger waves depends on the local velocities associated with the strongest scattering centers, and these velocities are different for different parts of the larger waves. The nature of the University of Kansas radar allowed it to be used as a ''radar wave gauge'' to measure the wave height at the center of the radar beam, so the type of analysis conducted to meet this objective was unique—no other radar measurements have been made where the wave height was measured exactly at the radar observation spot.

2. To establish the variations of the capillary-wave component of the ocean-wave spectrum for different wind speeds and directions relative to that of the wind. This is important because the radar backscatter from the sea at angles of 20° or more from vertical is known to be governed by resonance with these capillary and near-capillary waves. In fact, the determination of the spectrum from the radar measurements is based on this known resonance phenomenon. With the University of Kansas radar's capability of measuring over wavelengths from about 1.7 cm to 3.3 cm and that of the French radar from 3.3 cm to 25 cm, this experiment provided an unparallelled opportunity to observe the capillary spectrum.

3. To determine empirically the variation of radar scattering coefficient from the sea over a wide range of angles of incidence, angles relative to the wind direction, frequencies, and polarizations. This is important in scatterometry, radar design, and clutter rejection studies. Although many previous measurements of this nature have been performed from aircraft and stationary platforms, none has allowed measurements with such a variety of radar parameters at one time. Furthermore, although

aircraft and spacecraft measurements have allowed development of successful wind-vector measurement systems using scatterometers, one of the greatest unknowns is the exact relationship between scattering coefficient and wind speed—the previous measurements have led to considerable scatter in the values of the coefficients in this relationsip.

4. To establish the variation of the quantities determined under objectives 1–3 when an oil spill is present on the surface. Oil is known to damp the shorter components of the ocean-wave spectrum, and this fact is used as the basis for oil-spill monitoring radar systems used by several countries, although quantitative measurements of the effect are scarce.

The study reported here is related to object (1) above, the determination of the modulation of the capillary waves associated with the underlying larger waves. This report is primarily concerned with development of the methodology for a later study of the more complete data set. However, the preliminary results reported for a single set of data have value in their own right.

One of the approaches commonly used for describing this modulation is to calculate a ''modulation transfer function'' (MTF) in the frequency domain. The MTF amplitude shows the underlying-wave frequencies at which the capillary amplitude correlates best with the underlying waves, and the phase indicates the location of the relevant capillary components on the individual frequency components of the underlying waves.

In this report an alternate time-domain approach is presented that is based on the cross-correlation function between the radar signal and

the underlying waves. The cross-correlaton function tends to show the principal effects in a more compact and understandable form than the MTF. So that this relation may be understood better, the cross-correlation function is calculated for the capillary modulation alone by using as an input the ratio of the observed signal to the one that would be observed if the capillary waves were of uniform amplitude (changes in the slope of the underlying wave would cause all variations in the received signal if this were true). This ''instantaneous modulation'' can only be calculated in the time domain.

During the course of the investigation of the data the presence of strong-signal ''events'' was observed. These are presumably the same as the ''sea spikes'' that have been reported by numerous previous investigators. To determine the capillary-wave effects, one must first remove these anomalously large signals from the time series of the signal. Methods for doing this have been devised, and the result of the removal is a significant improvement in the repeatability of the modulation-study results.

This study was intended primarily to develop methodology, so only one data set was used—this was for a wind speed of 8.8 m/sec with the radar looking in the upwind direction. The dominant wave period was 5.8 seconds, and the maximum of the measured scattering coefficient was found to occur 1.8 seconds, or 104°, before the crest of the oncoming wave—it is therefore on the front face of the wave and nearer the trough than the crest. The location of the maximum instantaneous modulation (ratio of observed signal to that predicted if the capillary waves were uniformly distributed) is 153° ahead of the crest, a location almost in the trough. Furthermore, a secondary maximum was

found at 62° behind the crest, or well up on the back face of the wave.

Correlations were also performed between the scattered signal and the instantaneous slope of the waves. The slope spectrum has a higher peak frequency than the wave-height spectrum, so these correlations lead to different separations between maximum of the slope and maximum radar signal than would be observed if a single sine wave were observed. That is, one should be able to obtain the location of the peak signal on the slope of a single sine-wave component from the height record alone, but with a complex wave pattern this is no longer possible. Interpretation of the relation between peak radar scatter and slope remains to be worked out.

Most of the analyses were performed on time records, since the wave heights were measured at the fixed center of the radar footprint as time histories. However, one can determine the spatial picture over a limited distance from a time record by suitably summing a series in distance using the Fourier coefficients of the time series. The method for doing this was also developed here and will be used in future studies of the measurements.

3.0 Background of Theory and Experiment

The phenomenon of sea scatter and its theoretical basis has been of interest since the advent of the practical radar system. It has been generally agreed [Wright (1968), Chan and Fung (1973), Wu and Fung (1972), Long (1974)] that the scattering properties of the sea surface can be explained fairly well in terms of a two-scale slightly rough surface model, where the small-scale capillary waves are assumed to satisfy the small perturbation assumption, and the large-scale waves are assumed to satisfy the Kirchhoff approximation. This theory, verified to a large extent by experiment, indicates that backscatter at microwave frequencies is from those wavelength components of the ocean-wave spectrum that are resonant to the radar probing wavelength (Figure 3.1). In general, the scattering cross-section per unit area, σ^o, depends on the local angle of incidence (Figure 3.2), and also on the small capillary waves which are tilted by the large-scale wave slope. This angle depends on the position of the capillary waves with respect to the large-scale waves. The amplitudes of the small capillary waves are modified by a variety of hydrodynamic interactions with the large-scale waves. The local scattering cross-section depends on this amplitude. In fact, in first-order scattering theory, the cross-section and power spectrum amplitude are proportional(Section 4.3.1). Therefore, it is the modulation of scattering by the large-scale waves which makes them detectable by microwave radar. If the small capillary wave amplitude is modulated, so is the stress. A modulated stress, if of the proper phase, results in larger wave-growth. Table 3.1 shows the list of symbols for the following analysis.

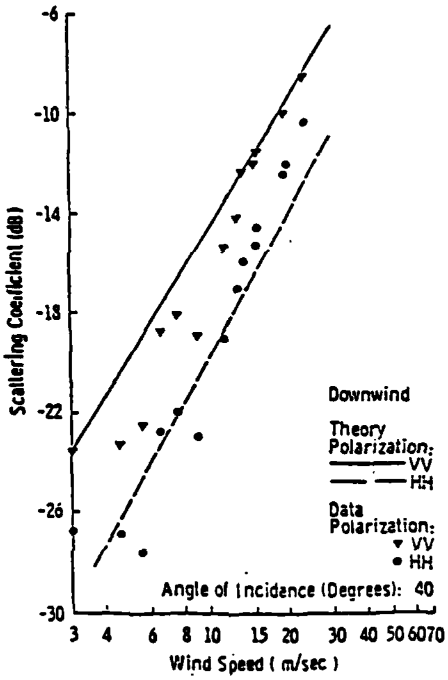

Figure 3.1: Comparison between theoretical and measured σ^{o}_{pp} for vertical and horizontal polarizations at 40° incidence angle for downwind observation with a 13.9 GHz radar. This illustrates close correspondence between experiment and theory based on resonance with capillary waves.

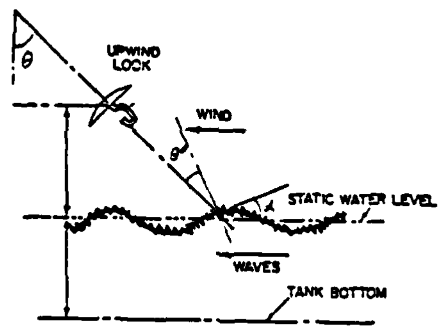

Figure 3.2: Dependence of scattering coefficient on local angle of incidence, θ' and small capillaries which are tilted by the large-scale wave slope.

TABLE 3.1
LIST OF SYMBOLS

$u*$	Air friction velocity
θ	Angle of incidence (angle between vertical and radar-wave direction)
k_x	Component of wave number in x direction
$cg, cg°$	Group speed of wind-generated wave with and without plunger-generated wave
u	Horizontal component of orbital velocity of plunger-generated wave
$e(t)$	Linearly-detected, rectified, received signal
θ'	Local angle of incidence (angle between normal to local surface and radar-wave direction)
M	Measured fractional modulation
r	Measured peak-peak modulation of R(0)
k_o	Microwave number
P	Modulation index of received signal
u_o	Modulation of u
$u(t)$	Periodic constituent of e(t)
$f,(k)$	Perturbation of surface displacement spectrum
ϕ	Phase angle
C	Phase speed of plunger-generated wave
C_o	Phase speed of wind-generated wave in absence of plunger-generated wave
k	Plunger-generated wave number
S	Plunger-generated wave slope
ω	Radian frequency of plunger-generated wave
Ω	Radian frequency of wind-generated wave
$f(t)$	Random (wind-generated) constituent of e(t)
P	Received power
P_o	Received power in absence of plunger
γ	Straining constant
B	Straining function
D	Straining function
τ	Time lag
β	Wind-generated wave growth rate
β_r	Wind-generated wave relaxation rate
H	Wind-wave interaction functional
F, F_o	Wind-wave surface displacement spectrum

Keller and Wright [1975] suggested a two-scale scattering theory called 'the relaxation time model,' and state that the small capillary waves, if perturbed from equilibrium, will relax back at an exponential rate called 'the relaxation rate.' The relaxation rate is a function of the small capillary-wave spectrum.

They found that these waves grew exponentially over several orders of magnitude in spectral intensity. The energy influx from the wind to a wave of given wave number must be balanced by transfer to other wave numbers for dissipation or growth of the wave. The transport equation gives this balance. In the case of growth along a single cartesian coordinate x in the direction of the wind, it may be written:

$$\frac{\partial F}{\partial t} + C_g \frac{\partial F}{\partial x} = \beta F + H(F, k, u^*) \qquad (3.1)$$

where F(k,x,t) is the surface displacement spectrum, cg is the group velocity, β is the exponential growth rate, H(F,k.u*) is a function which accounts for nonlinear transfer to other waves and non-linear dissipation, all evaluated at wave number k. The quantities $\frac{\partial F}{\partial x}$ and F may be obtained directly in wave-tank experiments from the intensities of the first-order Bragg line in the Doppler spectra (Figure 3.3a). β is the initial temporal growth rate, provided nonlinear interactions are negligible in the initial stages of growth [Keller and Wright, 1975]. The quantities $\frac{\beta F}{F_m}$, (C_g/F_m) and $\frac{S_{nl}}{F_m} = (C_g(\frac{\partial F}{\partial x}) - \beta F)/F_m$. where F_m is the maximum value of F observed under the conditions of the measurement, are shown in Figure 3.3b for some cases reported by Plant and Wright [1977]. The difference $C_g(\frac{\partial F}{\partial x})/F_m - \beta F/F_m$ can be matched, for the cases shown, by values of

S_{nl}/F_{max} calculated from the second-order gravity-capillary wave-wave interaction. When the nonlinear interactions bring the wave to a steady state or equilibrium, the vertical flux βF from the wind is large compared to horizontal flux $C_g\left(\frac{\partial F}{\partial x}\right)$. The difference is dissipated either by the breaking of the wave itself or by the transfer to other wave numbers for subsequent dissipation, but in either case, the equilibrium is spatially localized. It is the perturbation of this equilibrium by the fluid motions associated with the large waves which modulates the small-wave amplitude, and in consequence, the scattering cross-section.

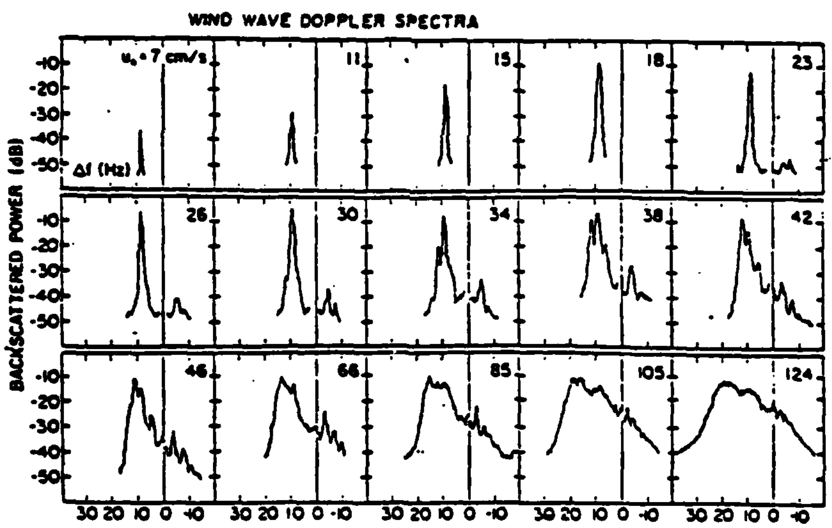

Figure 3.3a
Evolution of Doppler spectra of backscattered microwaves with increasing wind speed at fixed fetch. The wavelength was 6.9 cm (f = 4.35 GHz), the depression angle was 30°, and the Bragg wavelength was 4.05 cm.

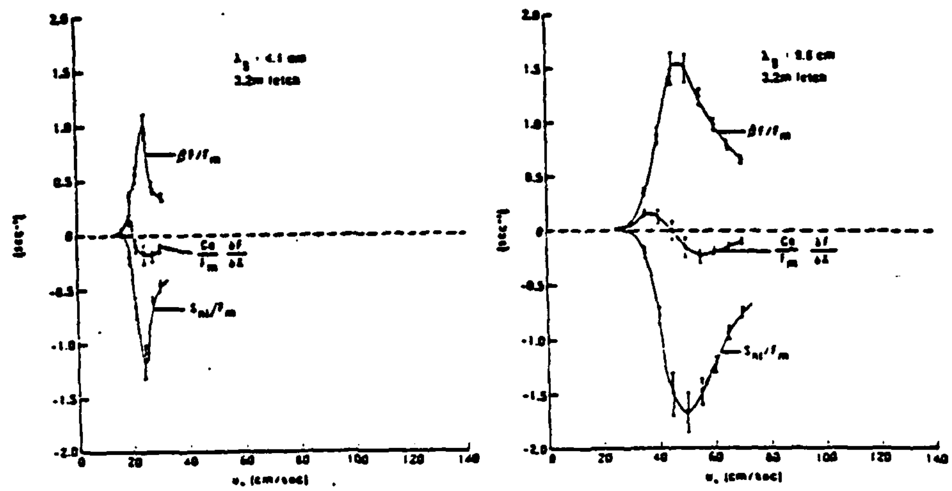

Figure 3.3b
Terms in the equilibrium transport equation for gravity-capillary waves. The curve labeled S_{nl}/F_m is the difference of the other two curves, i.e., $S_{nl}/F_m \equiv (C_g(\partial F/\partial x) - \beta F)/F_m$. The Bragg wavelength is denoted by λ_B.

A phenomenological model of the perturbation of this equilibrium by the horizontal component of orbital speed of a large wave [Keller and Wright, 1975] can be constructed after including the effect of the horizontal current u(x,t) in the transport equation

$$\frac{\partial F}{\partial t} + C_g \frac{\partial F}{\partial x} - \frac{\partial \omega}{\partial x} \frac{\partial F}{\partial k} = \beta F + \gamma(k) F \frac{\partial u}{\partial x} + H(F, k, u^*) \qquad (3.2)$$

where:

$$\omega = \omega_0 + \bar{k} \cdot \bar{u} \qquad (3.3)$$

$$c_g = \frac{\partial \omega}{\partial k} \tag{3.4}$$

The quantity is the angular freqency of the small wave under consideration. The term on the right containing (k), the straining constant, is called the radiation stress and

$$\gamma(k) = 1 - c_g^{\circ}/c^{\circ} \tag{3.5}$$

where c_g° and c° are the group and phase speed, respectively, of the small wave in the absence of the current u.

Let $F_0(k,x)$ be the surface displacement spectrum in the absence of the current u(x,t) which we now assume to have the form

$$u(x,t) = u_0 \, e^{j(kx - \Omega t)} \tag{3.6}$$

This is the current which perturbs the equilibrium spectrum. In consequence we expand the resultant surface displacement spectrum in a perturbation series in (u_0/c), where $c = \Omega/k$ is the phase speed of the large wave.

$$F = F_0 + (u_0/c) f_1(k) \, e^{j(kx - \Omega t)} + \ldots\ldots \tag{3.7}$$

The key assumption is that the increment in the nonlinear transfer can be written:

$$\delta H = \left(\delta H / \delta F \right)_{F = F_0} \left(u_0/c \right) f_1 \tag{3.8}$$

This is called the relaxation time appproximation. It is now straightforward to solve (3.2) and (3.7) to first order in (u_0/c)

$$\frac{f_1}{F_0} = \frac{-\left(\frac{\Omega}{\beta_r}\right)^2 \left(1 - c_g^0/c\right)\left(\frac{k}{F_0}\frac{\partial F_0}{\partial k} - \gamma\right) + \frac{\Omega}{\beta_r}\frac{1}{kF_0}\frac{\partial F_0}{\partial x}}{1 + \left(1 - c_g^0/c\right)^2 \left(\Omega/\beta_r\right)^2} -$$

$$\delta\,\frac{\left(\Omega/\beta_r\right)\left(\frac{k}{F_0}\frac{\partial F_0}{\partial k} - \gamma\right) + \left(\Omega/\beta_r\right)^2 \left(1 - c_g^0/c\right)\frac{1}{kF_0}\frac{\partial F_0}{\partial x}}{1 + \left(1 - c_g^0/c\right)^2 \left(\Omega/\beta_r\right)^2} \tag{3.9}$$

where the relaxation rate

$$\beta_r \equiv \left(\delta H/\delta F\right)_{F=\bar{F}_0} - \beta \tag{3.10}$$

has been introduced [Wright, 1977].

The first order in (u_0/c) terms in the expansion adequately describes the response of the wind-generated waves for winds of less than 7 to 8 m/sec and $u_0/c < 0.1$.

Modulation of backscattering cross-sections have been measured at 9.35 GHz and depression angle of 45 degrees (Bragg wavelength = 2.3 cm) by Keller and Wright [1975, 1976]. The linearly detected signal, proportional to the scattered electromagnetic field was ratified and filtered to remove frequency a and phase modulation and cross-correlated.

The measured auto-covariance function, $R(\tau)$ exhibited a spike at $\tau = 0$, due to the longer short-gravity waves of the wind-generated wave system, a mean value proportional to the square of the mean scattered field and a periodic portion due to modulating plunger-generated wave:

$$R(\tau) = \frac{1}{T_a}\int_0^{T_a} e(t)\,e(t+\tau)\,dt \tag{3.11}$$

$$e(t) = f(t) + p\bar{f}\,u(t) \tag{3.12}$$

$$R(0) = \overline{f^2}(t) \tag{3.13}$$

If $$u(t) = \cos(\Omega t) \tag{3.14}$$

$$R(\tau) = \frac{1}{T_a}\int_0^{T_a} f(t)\,f(t+\tau)\,dt + \frac{p^2}{2}(\bar{f})^2\cos(\Omega\tau) \tag{3.15}$$

The ratio of the peak-to-peak amplitude of the periodic portion of $R(\tau)$, r, to R(0), which latter quantity is proportional to the main scattered power is called the fractional modulation, m (Figure 3.4). So

$$r = p^2(\bar{f})^2 \tag{3.16}$$

and

$$M = \frac{r}{R(0)} \tag{3.17}$$

where M is fractional modulation.

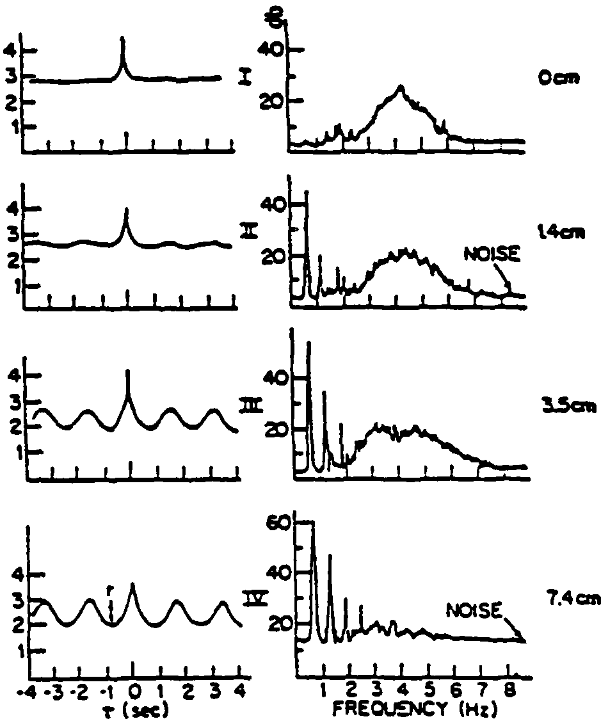

Figure 3.4
Autocorrelation functions of the microwave return (left) and wind-wave spectra (right) for various wave amplitudes at $u^* = 16.5$ cm sec^{-1}

If we represent p, power return as

$$p = p_0 \left(1 + m \cos(\Omega t + \phi)\right) \tag{3.18}$$

where

$$m = \left(B^2 + D^2 + T^2 \pm 2DT\right)\left(u_0/c\right) \tag{3.19}$$

and

$$\phi = \tan^{-1}\left((D \pm T)/B\right) \tag{3.20}$$

then

$$M = \left(\frac{m^2}{4}\right)\left(\frac{\overline{f^2}}{(\bar{f})^2}\right) \tag{3.21}$$

or

$$M = \left(\frac{m^2}{4}\right)\left(\frac{R(0)}{(\bar{f})^2}\right) \tag{3.22}$$

Positive and negative signs refer to upwind and downwind-looking antenna orientations, respectively.

The calculated theoretical curves and fractional modulation, are nonetheless an excellent fit to the measured value for winds of less than 8 m/sec and $u_0/c < 0.1$. For these winds, larger wave amplitudes, the fractional modulations saturated, i.e., they ceased to increase with increasing modulation wave amplitude, (Figures 3.5a,b).

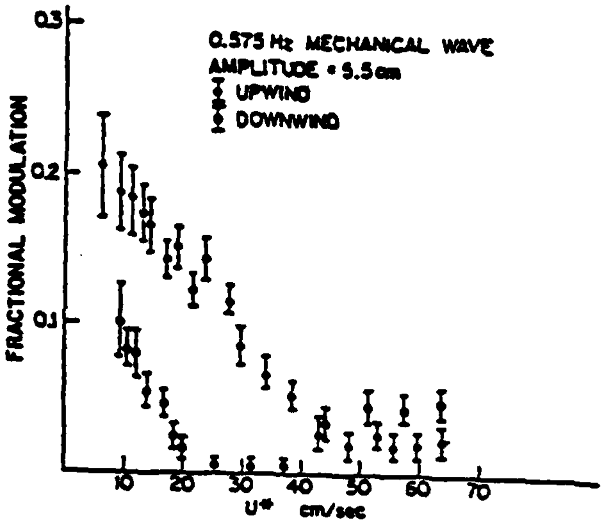

Figure 3.5a
Fractional modulation vs. air friction velocity for 0.575 Hz wave, $U_o/C = 0.091$; solid circles, upwind; open circles, downwind

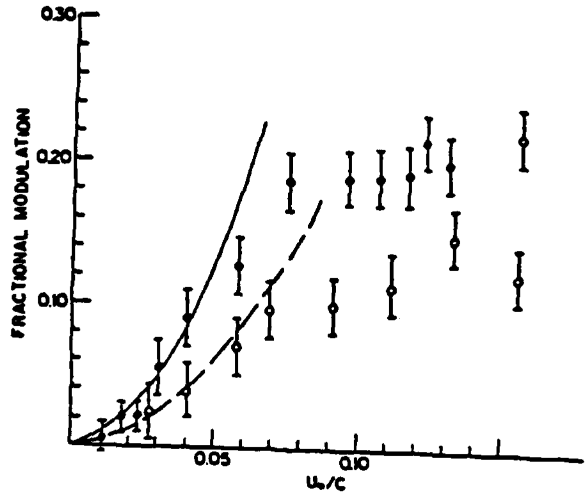

Figure 3.5b
Comparison of theoretical and measured fractional modulations looking upwind vs orbital velocity of 0.575 Hz waves. Solid data points and solid line are for $u^* = 16.5$ cm sec^{-1}. Open data points and dashed line are for $u^* = 30$ cm sec^{-1}.

Keller and Wright [1976] stated that at the higher wind speed there is definitely another phenomenon present unaccounted for by the relaxation theory. They believe that, at present, the tneory is phenomenological and the relaxation rate is an adjustable parameter. The reasons for choosing certain values for this and other incompletely known parameters become clearer upon consideration of relaxation of a pair of waves which simulate short gravity waves coupled to capillary waves by the second-order resonant interaction [Valenzuela and Laing, 1972, Plant and Wright, 1977, Plant 1979].

In a consequent study of sea surface backscatter phenomena, Plant, Keller and Wright [1978] conducted an experiment to measure the modulation of small capillary wind-generated waves by those with typical ocean wave periods. They stated that tne horizontal component of the orbital velocity of shoaling waves much exceeds tne vertical component exception in the region near the wave crests. Hence the relative importance of modulation due to tilting is much reduced over most of the large-scale wave, so the shoaling waves beyond the surf zone provide easily understood modulating conditions. The power spectra of e(t), rectified scattered field strength e(t), and the line-of- sight speed v(t), here show contributions both from the crests and low-amplitude quasi-periodic portions of the waves. The narrow peaks in the spectra were used to obtain quantitative measurements of the modulation. They also were used to calculate 'fractional modulation M' (Figures 3.6a,b and c).

In the most recent work by Plant et al. [1980] the modulation transfer function is calculated.

Let p(t), the square of the homodyne-detected [King, 1978]

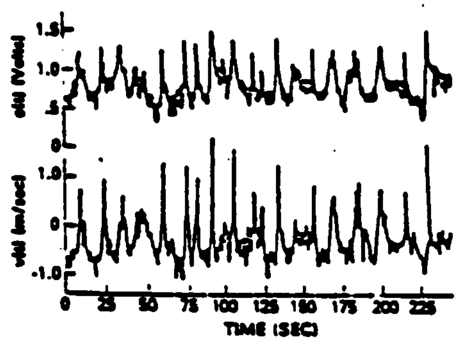

(a)

Processed microwave return from shoaling waves. The top trace is the rectified signal amplitude e(t), while the lower trace is the line-of-sight speed v(t), delayed by 1.25 s from the top trace. Both signals have been low-pass-filtered with a 0.6 Hz cutoff.

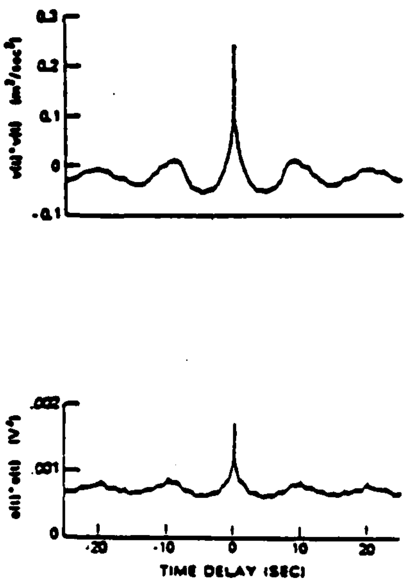

(b)

Autocovariance functions of line-of-sight speed v(t) and rectified backscattered signal amplitude e(t).

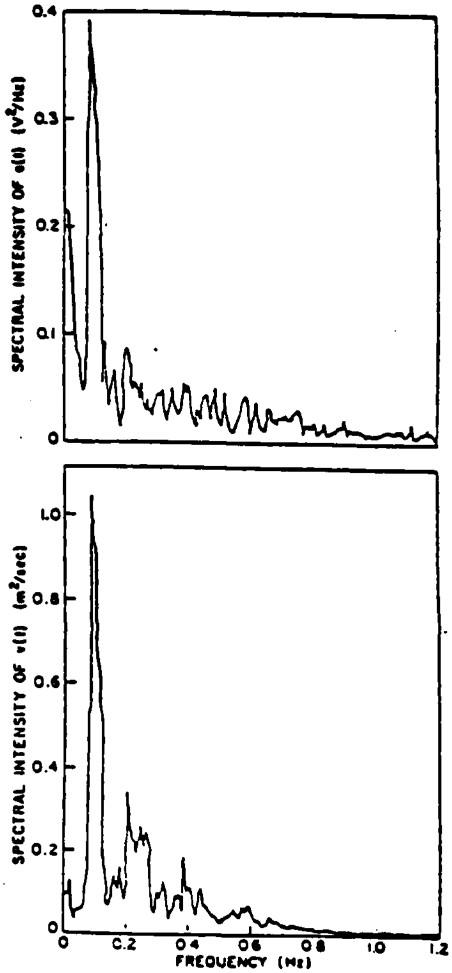

(c)

Power spectra of rectified back-scattered signal amplitude e(t) and line-of-sight speed v(t).

Figure 3.6

microwave voltage, which in turn is proportional to the backscattered electromagnetic field, be called the instantaneously received power. Let $v(t)$ be the instantaneous line-of-sight speed. If G_{pv} is the cross-spectrum of instantaneously received power and instantaneous line-of-sight speed and G_{vv} is the autospectrum of the latter, define

$$m(\Omega) = \frac{C(\Omega)}{\bar{\rho}} \frac{G_{\rho v}(\Omega)}{G_{vv}(\Omega)} \tag{3.23}$$

The phase speed $C(\Omega)$ and mean received power $\bar{\rho}$ normalize the modulation transfer function, $m(\Omega)$ making it dimensionless. $G_{pv}(\Omega)$ is, of course, complex. To fix ideas, suppose the plane of incidence (the plane containing the microwave propagation vector) and the normal to the undisturbed ocean surface, also contain the direction of a monochromatic, modulating surface wave of frequency Ω and wave number K, propagating in water of depth D, and the depression angle is θ, then:

$$V(t) = V_0 \cos(\Omega t + \varphi_s) \tag{3.24}$$

$$\tan(\varphi_s) = \tanh(KD)\tan(\theta) \tag{3.25}$$

$$V_0/u_0 = \left(\sin^2\theta + \cos^2\theta \tanh^2(KD)\right) \tag{3.26}$$

and

$$\rho = \bar{\rho}\left(1 + m(u_0/c)\cos(\Omega t + \varphi)\right) \qquad (3.27)$$

where φ_s is the phase angle by which the line-of-sight speed leads the horizontal component of orbital speed, $u = u_0$ (Ωt) (Figure 3.7).

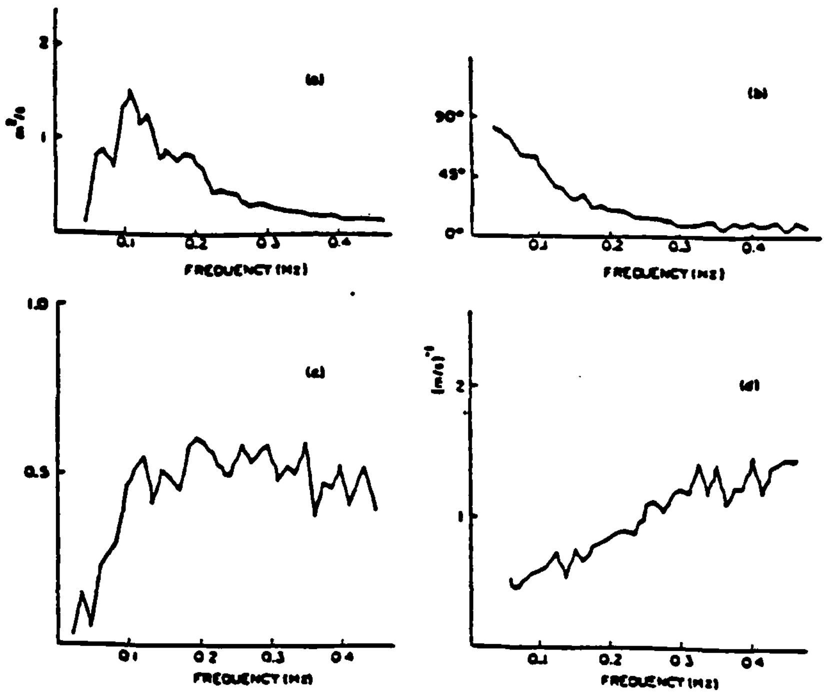

Figure 3.7
Modulation spectra of the demodulated return of the 9.375 GHz radar. Wind speed = 7.5 m/s.
(a) Line-of-sight component of orbital speed;
(b) phase of the modulation transfer function;
(c) coherence;
(d) modulus of the modulation transfer function divided by the ocean wave phase speed, m/c.

The transfer functions and their phase shown in Figures 3.8 to 3.11 are referred to the line-of-sight velocity as defined by (3.24). The transfer function which refers to the horizontal component of orbital speed (a more useful quantity for interpretive purposes) is obtained by multiplying m by V_0/u_0 given by (3.26). Although the transfer function, before averaging over the wind speed bands, exhibited scatter as large as a factor of 2, the finally averaged

modules (Figure 3.12a) and phase (Figure 3.12b) show smooth, stable dependence on modulating frequency and wind speed.

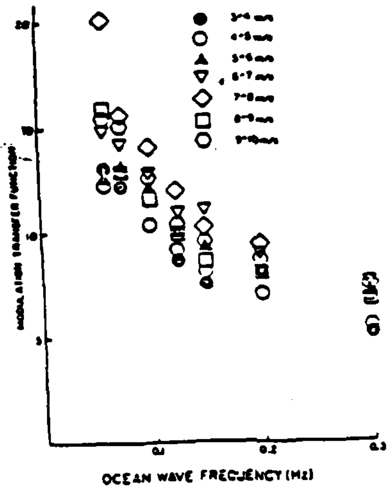

Figure 3.8
Modulus of the 1.5 GHz (Bragg wavelength = 13 cm) transfer functions.

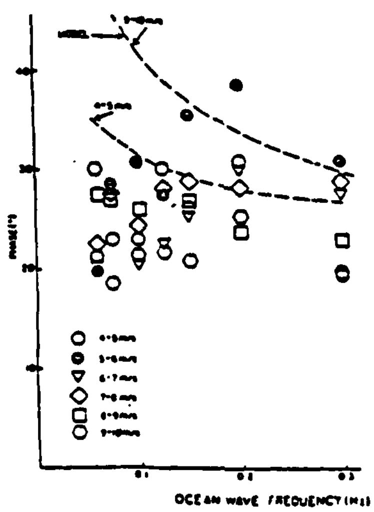

Figure 3.9
Phase of the 1.5 GHz (Bragg wavelength = 13 cm) transfer functions. Phases are measured from wave crests and are positive leading the crest. Dashed lines are theoretical predictions assuming modulation caused solely by straining. [Plant, Keller and Wright, 1980]

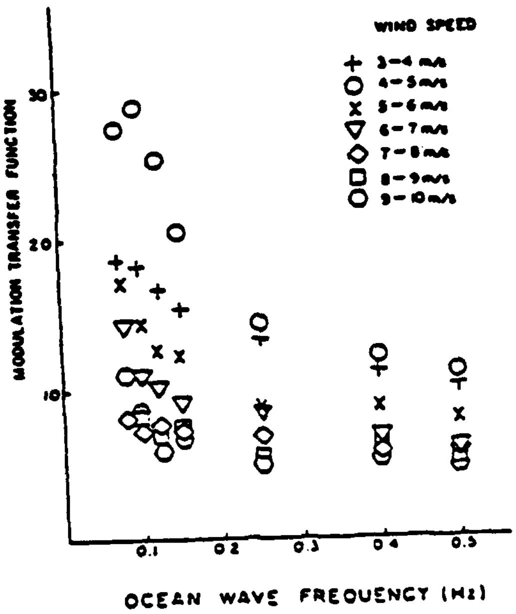

Figure 3.10
Modulus of the 9.375 GHz (Bragg wavelength = 2.3 cm) transfer functions

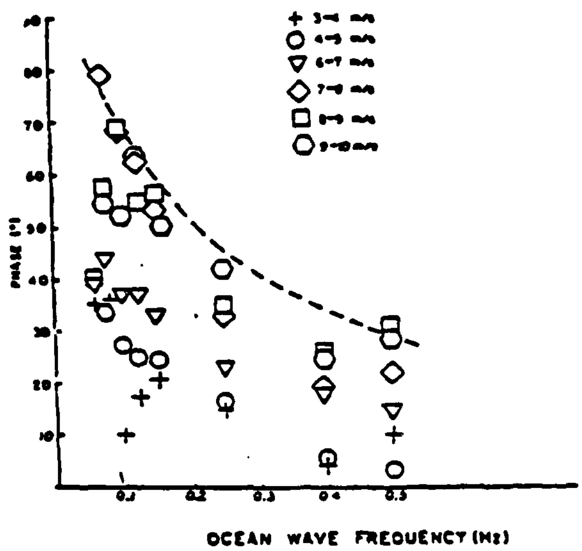

Figure 3.11
Phase of the 9.375 GHz (Bragg-wavelength = 2.3 cm) transfer functions. Phases are measured from wave crests and are positive leading the crest. Dashed line is a theoretical prediction assuming modulation caused only by straining.

Although the total averaged MTF looks very smooth and corresponds reasonably well with the theory, we believe the MTF concept is especially difficult for radar theorists who are not involved in pure theoretical hydrodynamics and fluid mechanics equations. We think that 'modulation index', $\mu(t)$, (Section 4.4.2), would, if it could be treated well, be an easily interpreted concept that could be used to make a simple statement about phase relationships between the peak of capillary and large-scale waves.

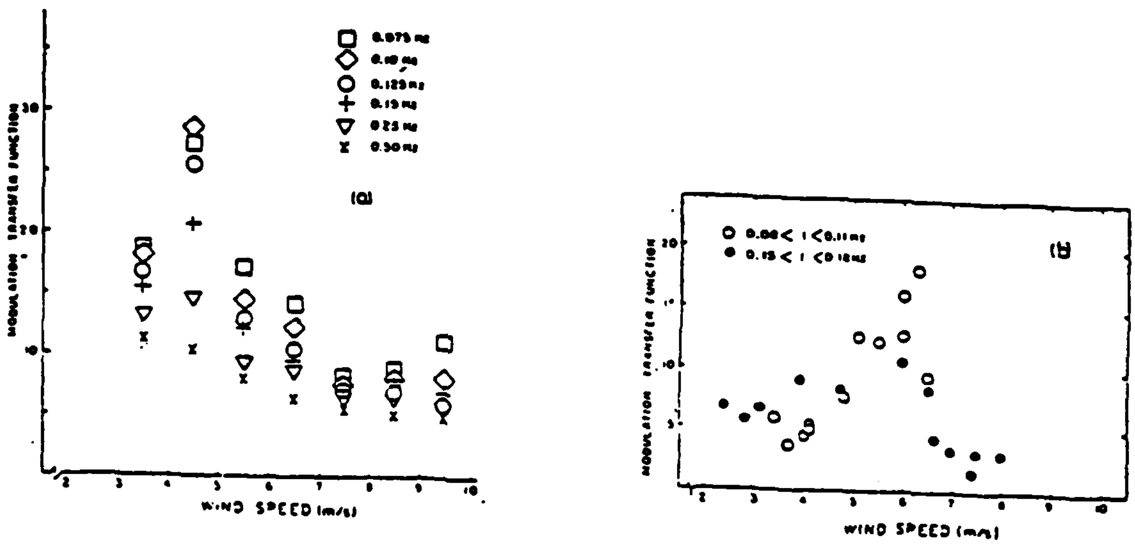

Figure 3.12
Wind speed dependence of 9.375 GHz modulation transfer functions. (a) NOSC tower; (b) Nags Head, North Carolina [Plant et al., 1978].

4.0 THEORY OF OCEAN WAVES

4.1 Ocean Wave Phenomena

4.1.1 The Theory of Wave Motion

Waves on the actual ocean are extraordinarily complex phenomena. A distinction must be made between the idealized classical wave motions of hydrodynamics and the much more complex (and far less well understood) wave motions that occur in nature. There is a distinction between deep water and shallow water waves depending on the ratio between wavelength and water depth.

4.1.2 Definition of Periodicity

The solution of the classical equations for ocean waves takes the form of a sum of periodic functions (Section 4.1.3). A function $f(t)$ is periodic of period T if and only if $f(t) = f(t+T)$ for all t. Records of the rise and fall of the water surface as a function of time at a fixed point on the ocean surface do not satisfy the above definition. Water waves in nature are not periodic. Hence, the sum is in principle infinite and representable by a continuous spectrum.

For all types of truly periodic traveling-wave motion

$$\lambda = CT \tag{4.1}$$

where λ is the distance between the crests of the waves, C is the speed with which the crests move and T is the time required for the water surface to go through one complete oscillation at a fixed point.

The period and length of a wave are rather cumbersome notations and it is possible to replace them by the concepts of wave number and angular frequency.

$$k = \frac{2\pi}{\lambda} \tag{4.2}$$

$$\omega = \frac{2\pi}{T} \tag{4.3}$$

4.1.3 General Gravity, Large-Scale Wave Theory

The simplest wave motion is that of a simple harmonic long-crested traveling wave in the +x direction whose equation would be given by

$$h(x,t) = a \cos\left(\frac{2\pi x}{\lambda} - \frac{2\pi}{T}t\right) \tag{4.4}$$

It is possible to write

$$h(x,t) = a \cos\left((x - ct)\frac{2\pi}{\lambda}\right) \tag{4.4a}$$

In the following derivation it is assumed that the earth is flat, that the water is of constant depth h, that the Coriolis force is negligible, that the density of the air can be neglected compared with the density of the water, that the water is of constant density, that the body of water is infinite in extent and completely covered by waves, and that the viscosity and surface tension can be neglected. Moreover, it is assumed that there is no variation in wave propagation

in the y direction. The equations are unsolvable in closed form, as they are nonlinear. A perturbation technique must be employed to linearize these equations and to obtain a useful result.

Assume that the unknown functions in hydrodynamic equations can be expanded in powers of a small dimensionless parameter ϵ , so that the solution is a power series in ϵ that will converge if enough terms are taken. These expansions are substituted into the equations, and all terms to the same power in ϵ are collected. It is possible, in general, to obtain terms to zero power in ϵ , to the first power in ϵ , to the second power in , and so on. Depending upon the power of ϵ used in the expansion, successively higher and more nearly correct approximations to the solution of the complete equation are obtained [Neumann and Pierson, 1966].

The steady, time-independent wave equation can be shown to be

$$g a \cos(Kx) - \frac{a C_o^2 \cosh(Kh)}{\sinh(Kh)} K \cos(Kx) = 0 \qquad (4.5)$$

where

$$C_o^2 = \frac{g}{k} \tanh(Kh) \qquad (4.6)$$

where g is the gravitational acceleration (9.8 m/sec).

Equation (4.6) relates the phase speed C to the wave number K and the depth of the water h. For a given depth there is only one possible value for the wave speed given the wavelength (or the wave number).

Equation (4.6) can be simplified for two situations with reference to the values of h and K. The hyperbolic tangent of a function varies between zero and 1 for positive values of the argument. The hyperbolic tangent approaches the value 1 very closely for values of the argument that are very large Thus, if the product of K and h is such that the hyperbolic tangent is essentially 1, (4.6) reduces to the much simpler form given by

$$C_o^2 = \frac{g}{k} \qquad (4.7)$$

The waves that satisfy this simplified form of the equation are called short waves, or 'deep water' waves. The second approximation occurs if the product of K and h is very small. Under these circumstances the hyperbolic tangent of Kh is approximately equal to Kh and if this substitution is made, (4.6) will be

$$C_o^2 = gh \qquad (4.8)$$

Waves that satisfy this equation, relating the phase speed to the depth since the length of the wave no longer determines the phase speed, are called long waves, or 'shallow-water' waves.

Table 4.1 shows the various relations for deep-water waves between the different parameters.

	L	C_0	T	ω	k	C_g
L	L	$(gL/2\pi)^{1/2}$	$(2\pi L/g)^{1/2}$	$(2\pi g/L)^{1/2}$	$2\pi/L$	$\frac{1}{2}(gL/2\pi)^{1/2}$
C_0	$2\pi C_0^2/g$	C_0	$2\pi C_0/g$	g/C_0	g/C_0^2	$C_0/2$
T	$gT^2/2\pi$	$gT/2\pi$	T	$2\pi/T$	$4\pi^2/gT^2$	$gT/4\pi$
ω	$2\pi g/\omega^2$	g/ω	$2\pi/\omega$	ω	ω^2/g	$g/2\omega$
k	$2\pi/k$	$(g/k)^{1/2}$	$2\pi/(gk)^{1/2}$	$(gk)^{1/2}$	k	$\frac{1}{2}(g/k)^{1/2}$
C_g	$8\pi C_g^2/g$	$2C_g$	$4\pi C_g/g$	$g/2C_g$	$g/4C_g^2$	C_g

Table 4.1
Relationship between wavelength, phase speed, period, angular frequency wave number, and group velocity for deep water linear periodic gravity waves. Read down to express the quantity in the top row in terms of the quantity in the left-hand column [Neumann and Pierson (1966]

4.1.4 General Solution for Large-Scale Gravity Waves

The linear solution that has been obtained can be used as a basis for second-order solutions. One could proceed to third and even higher orders. In general one can show

$$h(x) = \sum_i a_i \cos(k_i x + \varphi_i) \qquad (4.9)$$

It is possible to transform the solution to the form in which the presence of a current to produce the steady motion is eliminated. The general solution for the moving wave profile would then be given by

$$h(x,t) = \sum_i a_i \cos(k_i(x + C_i t) + \varphi_i) \qquad (4.10)$$

It is worthwhile to mention that C_i in general is not equal to $C_0 = \sqrt{\frac{g}{k}}$. C_i and C_0 have nonlinear relations, but it is very difficult to find the exact nonlinear relationships. In the following analysis we assume a linear relationship between C_i and C_0, where:

$$C_i = C_o \tag{4.11}$$

4.2 Capillary Waves

4.2.1 Capillary Phenomena

If the surface tension of the water is important, as it is for very short waves, additional restoring force due to curvature of the free surface enters the Bernoulli equation.

In linearized theory, the equation for the phase speed is:

$$C_o = \left(\frac{g}{k} + \frac{Tk}{\rho} \right)^{1/2} \tag{4.12}$$

where ρ is the sea water density. Perturbation techniques were applied to the problem by Pierson and Fife [1961]. In general, waves have a phase speed that increases with increasing wave amplitude. However, in linear theory the speed and amplitude are independent.

When capillary waves interact with large-scale waves the capillaries appear at times to be concentrated on the forward face of the large-scale wave just before the sharp crest. In this case, perturbation techniques are rather difficult to apply, because the effect of surface tension is not uniform over the whole disturbed surface. Longuet-Higgins [1963] introduced surface tension as a perturbation effect on large-scale waves in the region of the sharp crest and has shown the reason for the occurrence of this phenomenon.

4.2.2 Capillary Generation by Wind

One of the universal features of wind-generated wave systems is

the modulation of velocity and amplitude of small capillary waves by large-scale gravity waves. These modulations are of practical importance. For example, the imaging properties of microwave radars used for remote-sensing of ocean waves depend on the modulation of surface scatterer density, amplitude, and velocity. Furthermore, the short gravity and capillary waves can support the entire stress of the wind on the water [Larson and Wright, 1975]. If the large-scale waves modulate the small capillary wave amplitudes, they also modulate the stress. The component of this modulation stress which is in phase with the horizontal component of orbital speed of the large-scale wave will work on the large-scale wave and cause it to grow. The mechanism of energy transfer between short and long waves, discussed by Hasselman [1971] also depends on the phase and amplitude of this modulation.

4.2.3 Sources of Modulations

At least three sources of modulation have been noted so far: modulation of the orientation of small capillary waves (called tilting), modulation of the amplitude of the small capillary waves exemplified by the straining of the capillary waves by the horizontal component of the orbital velocity of the large-scale waves [Longuet-Higgins and Stewart (1964), Phillips (1966)], and modulation due to wave-induced airflow. The last type of modulation, wave-induced airflow, is a principal result in the recent work of Wright, Plant and Keller [1980]. The dependence of modulation on modulating ocean wave frequency and, partially, upon wind speed are qualitatively consistent with wave-induced airflow as a modulator, but positive identification of the modulation sources remains to be made.

4.3 Current Theory of Scattering from the Ocean

4.3.1 History and Basis of Equations

The current scatter theory is a refinement of the two-scale model developed in the 1960's [Bass and Fuks (1968), Fuks (1969), Valenzuela (1967, 1968)]. The success of such a theory in explaining dependence on wind speed, wind direction, angle of incidence and frequency depends almost exclusively upon the adequacy of knowledge of the sea spectrum.

The derivation of the average backscattering coefficient for the sea surface involves two major steps: (1) compute the backscattering coefficient for the capillary waves using standard perturbation techniques [Valenzuela (1967), Wright (1966)] and (2) account for the tilting effect of the large-scale waves. The expression for the polarized scattering coefficients from step (1) is well known [Valenzuela (1967), Chan and Fung (1973)] and is

$$\sigma^{o}_{pp}(\theta, \varphi) = 8k^4 |\alpha_{pp}|^2 W(\theta, \varphi) \tag{4.13}$$

where for horizontal polarization p=h and for vertical polarization p=v, k is the electromagnetic wave number, θ is the incidence angle, is the aspect angle relative to the upwind direction, and $W(\theta, \varphi)$ is the roughness spectrum of the sea surface. The coefficients, α_{pp}, for different polarization states are defined as

$$\alpha_{hh} = R_h \cos(\theta) \tag{4.14}$$

$$\alpha_{vv} = R_v \cos^2(\theta) + (k'^2 - k^2) T_v^2 \sin^2\theta / 2k'^2 \qquad (4.15)$$

where θ is the incidence angle, φ is the aspect angle relative to the upwind direction, k' is the wave number in sea water, R_h, R_v are Fresnel reflection coefficients for horizontal and vertical polarizations, respectively, and $T_v = 1 + R_v$. The depolarization scattering coefficient is also known [Valenzuela, 1967].

$$\begin{aligned} \alpha_{hv}(\theta,\varphi) &= \alpha_{vh}(\theta,\varphi) \\ &= \frac{2}{\pi} k^4 \left|(k'^2 - k^2)(R_v - R_h)\cos\theta\right|^2 \\ &\iint_{-\infty}^{\infty} mn\, W(m^+, n^+)\, W(m^-, n^-)\, |D|^{-2}\, dm\, dn \end{aligned} \qquad (4.16)$$

where:

$$D = k^2 (k'^2 - m^2 - n^2)^{1/2} + k'^2 (k^2 - m^2 - n^2)^{1/2} \qquad (4.17)$$

$$m^{\pm} = n \sin(\varphi) + (m \pm k \sin\theta) \cos(\varphi) \qquad (4.18)$$

$$n^{\pm} = n \cos(\varphi) - (m \pm k \sin\theta) \sin(\varphi) \qquad (4.19)$$

To account for the tilting effect of large-scale waves, it is necessary to identify polarization changes due to tilting and then to

average the resulting expression for the scattering coefficient of the capillary waves over the slope distribution of the large-scale waves. The concept involved in considering polarization changes can be described in terms of two sets of coordinates: (1) the reference coordinates in which the scatter problem is posed, and (2) the local coordinates in which scattering due to capillary waves is computed. Let $\hat{v}$, $\hat{h}$, be the unit vertical and horizontal polarization vectors in the reference frame and $\hat{v}'$, $\hat{h}'$ be the corresponding unit vectors in the local frame. Let the incident field be $\mathcal{E}_o$. Then components of the local incident fields are:

$$\mathcal{E}^{i}_{h'} = \hat{h}' \cdot \vec{\mathcal{E}}_o \tag{4.20}$$

and

$$\mathcal{E}^{i}_{v'} = \hat{v}' \cdot \vec{\mathcal{E}}_o \tag{4.21}$$

Upon scattering by the capillary waves, each of the above incident field components is depolarized so that the scattered fields are

$$\mathcal{E}^{s}_{v'} = S_{v'h'}\, \mathcal{E}^{i}_{h'} + S_{v'v'}\, \mathcal{E}^{i}_{v'} \tag{4.22}$$

and

$$\mathcal{E}_{h'}^{s} = S_{h'h'} \mathcal{E}_{h'}^{i} + S_{h'v'} \mathcal{E}_{v'}^{i} \tag{4.23}$$

where S_{pq} is the scattering function for the capillary waves. The scattered fields in the reference frame become

$$\mathcal{E}_{v}^{s} = (\hat{v}\cdot\hat{h}')\mathcal{E}_{h'}^{s} + (\hat{v}\cdot\hat{v}')\mathcal{E}_{v'}^{s} \tag{4.24}$$

$$\mathcal{E}_{h}^{s} = (\hat{h}\cdot\hat{h}')\mathcal{E}_{h'}^{s} + (\hat{h}\cdot\hat{v}')\mathcal{E}_{v'}^{s} \tag{4.25}$$

It is clear from (4.13) that to compute the scattering coefficient for horizontal polarization the local vertically-polarized scattered field is needed and vice versa. Furthermore, there is a term involving the product of $\mathcal{E}_{h'}^{s}$ and $\mathcal{E}_{v'}^{s}$.

Special cases where $S_{h'v'}$, $S_{v'h'}$ are zero and tilt angles are small have been treated by Wright [1968], and cases where the tilt angle is restricted to the plane perpendicular to the plane of incidence have been studied by Valenzuela [1968]. Note that Valenzuela did not average over the tilt angles as Wright did. Thus, his results show the effect of polarization changes. The study of these special cases indicates that the polarization effects due to tilting are unimportant for vertical polarization. The same statement can be made for horizontal polarization when the incidence angle is restricted to less than about 70°. Hence, when averaging is included, the scattering coefficient for polarization scattering is approximately

$$\sigma^{\circ}_{pp}(\theta,\varphi) = \int_{-\infty}^{\infty}\int_{-\cot\theta}^{\infty} \sigma^{\circ}_{pp}(\theta',\varphi)\, P_{\theta}(Z_{x'}, Z_{y'})\, dZ_{x'}\, dZ_{y'} \tag{4.26}$$

where $\sigma^{\circ}_{pp}(\theta',\varphi)$ is given (4.1), θ' is the local angle of incidence, $P_0(Z_{x'},Z_{y'})$ is the slope distribution of the large-scale waves as viewed at an incidence angle, θ, and is defined in the prime coordinate whose x' axis is parallel to the wind direction. $Z_{x'},Z_{y'}$ are partial derivatives of Z. It is assumed that the plane of incidence is the x-z plane and that the angle between the x axis and the x' axis is φ, (Figure 4.1) so that an upwind observation occurs when $\varphi=0$. The relations between the primed and unprimed coordinates are

$$Z_{x'} = Z_x \cos(\varphi) - Z_y \sin(\varphi) \tag{4.27}$$

$$Z_{y'} = Z_y \cos(\varphi) - Z_x \sin(\varphi) \tag{4.28}$$

The cross-polarized scattering coefficient, including polarization and averaging effects for small tilts, is approximately

$$\sigma^{\circ}_{hv}(\theta,\varphi) = \int_{-\infty}^{\infty}\int_{-\cot\theta}^{\infty} \left[\sigma^{\circ}_{hv'}(\theta',\varphi) + \sigma^{\circ}_{hv}(\theta',\varphi)\right] P_{\theta}(Z_{x'}, Z_{y'})\, dZ_x\, dZ_y \tag{4.29}$$

where

$$\sigma^{\circ}_{hv}(\theta',\varphi) = 8 k^4 \left| Z_y (\alpha_{vv} - \alpha_{hh}) / \sin\theta' \right|^2 W(\theta',\varphi) \tag{4.30}$$

and $\sigma^{\circ}_{hv}(\theta',\varphi)$ is given by (4.1).

The relation between the slope and density function $P_{\theta}(Z_{x'},Z_{y'})$ and function $P_{0}(Z_{x'},Z_{y'})$ defined by Cox and Munk [1954] is

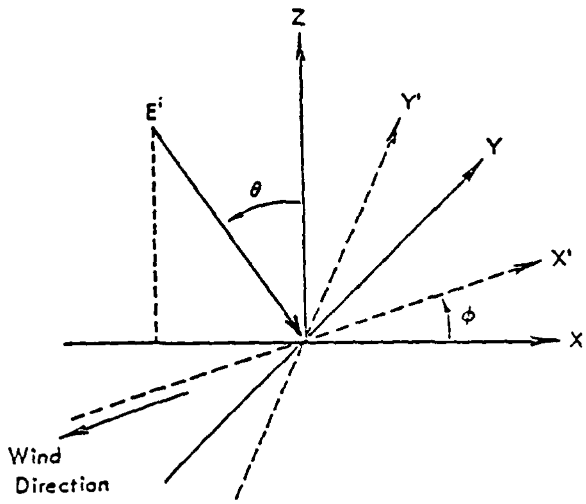

Figure 4.1
Diagram of the relation between
(Z,X,Y) and (Z,X',Y') coordinates.
[Chan and Fung, 1977]

$$P_\theta(Z_{x'}, Z_{y'}) = (1 + Z_x \tan\theta) P(Z_{x'}, Z_{y'}) \qquad (4.31)$$

The form of $P(Z_{x'}, Z_{y'})$ has been found to be a Grom-Charlier series [Cox and Munk (1954), Longuet-Higgins (1963), Pierson (1975)]. However, the values of the slope-variance parameters in the function require further studies. The slope variances, σ_u^2, σ_c^2, given by Cox and Munk [1954] are not restricted to large-scale waves. It is not clear at the present time how the slope variances for the large-scale wave alone can be obtained at a given microwave frequency. It has been suggested that one possible way to compute these slope variances is to integrate the low-frequency portion of the slope spectrum of the sea surface [Chan and Fung, 1977]. If we assume that some suitable slope variance parameters can be found, then all the quantities in the scattering coefficient have been discussed except the sea spectrum for the sea spectrum $W(\theta, \varphi)$ to be discussed in the following section.

4.3.2 The Sea Spectrum

The high-frequency portion of the sea spectrum has undergone intense study in recent years [Pierson (1973), Mitsuyasu and Honda (1974), Afarani (1975)]. The general form of the directional sea spectrum is

$$S(K,\varphi) = S(K)\left(a_0 + a_1 \cos(2\varphi)\right) \qquad (4.32)$$

when higher order terms in φ are neglected [Pierson, 1973]. The quantity determined from measurement is S(K). One form for S(K) proposed by Pierson [1975] for the fully-developed sea is as follows: [The large-K regions are based on wave-tank measurements. It should be noted that further revision of S(K) is being contemplated [Pierson, 1978].]

$$S(K) = S_i(K) \qquad K_{i-1} < K < K_i \qquad (4.33)$$

$$S_1(K) = \frac{a}{K^3} \exp\left[-\frac{0.74 g^2}{K^2 u(u^*)^4}\right] \qquad 0 < K < K_1 \qquad (4.34)$$

$$S_2(K) = a K_1^{-1/2} K^{-5/2} \qquad K_1 < K < K_2 \qquad (4.35)$$

$$S_3(K) = S_4(K_3)\left(K/K_3\right)^{q} \qquad K_2 < K < K_3 \qquad (4.36)$$

$$S_4(K) = 0.438\,(2\pi)^{P-1} \frac{g + 3gK^2/13.1769}{\left(gK + gK^3/13.1769\right)^{P+1/2}} \qquad K_3 < K < K_4 \qquad (4.37)$$

$$S_5(K) = 1.473\times10^{-4}\, u^{*3} K_m^6 K^{-9} \qquad K_4 < K < \infty \qquad (4.38)$$

K_4 can be found numerically by setting $S_4(K_4)$ equal to $S_5(K_4)$. Other parameters are as follows:

u^* = friction velocity $u^* > u^*_m$

$K_m = (13.1769)$

$q = \log[S_8(K_2)/S_4(K_3)]/\log[K_2/K_3]$

$p_1 = 5.0 - \log u^*$

$Z_0 = 0.684/u^* + 4.28 \times 10^{-5} u^{*2} - 4.43 \times 10^{-2}$

$u(u^*) = u^*/0.4 \; \mathrm{Ln}(Z/Z_0)$ cm/sec.

$a = 4.05 \times 10^{-3}$

$g = 980$ cm/sec.

$u^*_m = 12$ cm/sec.

Note that this sea spectrum shows that the capillary waves (i.e., $S_4(K)$) grow with the wind and that the higher the K value the faster the growth. The parameters a_0 and a_1 have been derived by Chan and Fung [1977] and the relation between $W(\theta', \varphi)$ in (2) and (3) and $S(K, \varphi)$ has been found to be:

$$W(\theta', \varphi) = \frac{S(K)}{2\pi K}\left[1 + 2\left(\frac{1-V}{1+V}\right)\cos(2\varphi)\right] \tag{4.39}$$

where $K = 2k\sin\theta'$, $V = \sigma_{c\tau}^2/\sigma_{u\tau}^2$, $\sigma_{c\tau}^2$, $\sigma_{u\tau}^2$ are the slope variances of the sea surface along the crosswind and upwind directions. A possible way of estimating V is to use the slope variance parameters given by Cox and Munk [1954] for their clean sea model. Note that $W(\theta', \varphi)$ is resricted to that portion of the sea spectrum which satisfies the assumptions in the perturbation theory. Thus, the value of K has a lower bound which is a function of the electromagnetic wavelength.

With the sea spectrum given in the preceding section, the sea-scatter model given by (4.14) can be evaluated. Figure 4.2 shows a comparison of the theoretical σ^o versus azimuth angle curves with experimental data taken on two different AAFE RADSCAT flights [Jones,

Schroeder and Mitchell, 1977, 1978]. Figure 4.3 illustrates the relation between scattering coefficient and wind speed at three angles for horizontal polarization and 13.9 GHz frequency, along with experimental points obtained with the AAFE RADSCAT instrument. The lines on the figures are theoretical values based on the σ° model and spectrum of Section 4.3.2.

Our following analysis for determination of theoretical scattering coefficient σ^{o}, is based on having instantaneous slope. One can Theory derive instantaneous local angle of incidence, θ', and also roughness spectrum $W(\theta', \varphi)$ and directly calculate the instantaneous

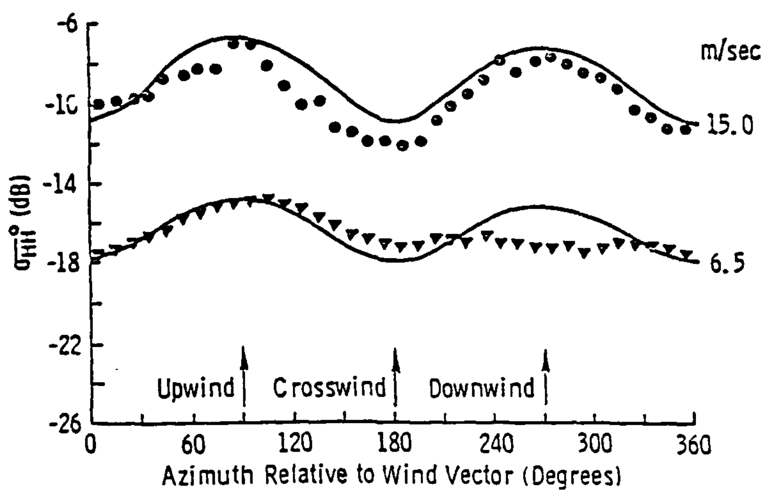

Figure 4.2
Comparison of theoretical results with a sample AAFE run [Chan and Fung, 1977].

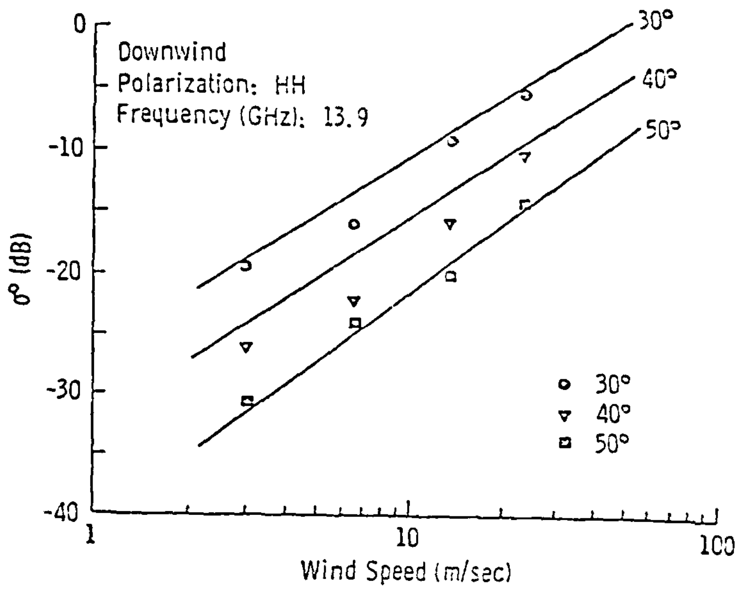

Figure 4.3
Example of theoretical and observed values of σ^{o} plotted versus wind speed. AAFE Radscat data.

theoretical scattering coefficient, σ^{o}_{theory}, Section 6.2.

$$\sigma^{o}_{pp}(\theta', \varphi) = 8k^4 |\alpha_{pp}|^2 W(\theta', \varphi) \tag{4.40}$$

Note that α_{pp} and K are also functions of local angle of incidence, and that the above theory assumes that the shorter waves are uniformly distributed over the longer waves. When modulation of the amplitude of the shorter waves takes place, the analysis must be modified.

4.4 Theoretical Basis of Capillary Modulation Distribution

4.4.1 Modulation Phenomena

Short gravity-capillary waves, the equilibrium excitation of the ocean surface, are spatially and temporally modulated by large-scale ocean waves. Remote sensing of ocean waves by microwave radar depends

on these modulations [Wright, 1977] which may also induce transfer of substantial energy between short capillary and long large-scale waves.

An FM radar, such as that used by K.U., is a self-contained two-scale wave probe. The measure of the large-scale waves (several meters in length) is the instantaneous wave height, which is obtained from time-delay of the received signal (slant range) (Section 5.3). At appropriately chosen viewing angles the primary scatterers are capillary waves, a few centimeters in length. Hence the amplitude modulation of the received signal is a measure of the modulation of the capillary waves. Two important sources of modulation of scattered microwave power have been noted: modulation of the orientation of the capillary waves, called tilting, and modulation of the amplitude of the capillary waves, exemplified by the straining of the short capillary waves by the horizontal component of orbital velocity of the large waves.

If one assumes that the capillary wave amplitudes are uniform over the large-scale waves, the modulation of the received signal is completely governed by the variation of the local angle of incidence (tilting effect) caused by slope changes. Note that the instantaneous large-scale wave slope can easily be derived from the instantaneous wave height time profile, provided a long-crested assumption is made.

If one knows the spectrum of the capillary waves S(K) and the slope of the large-scale waves, the scattering coefficient can also be established (Section 6.2). Since the capillary wave amplitudes are not the same at all points on the large-scale waves, due to modulation, one of the major goals is to establish their distribution. This task can be done by comparing the radar signals calculated as mentioned above with the actual radar signal observed. The difference must be due to a

change in the amplitude of the capillary waves at the Bragg-resonant wavelength. When the variation of this amplitude difference is cross-correlated with the height or slope of the large-scale waves, an estimate of the phase relations of the peak of the distribution of 'apparent' capillary wave amplitude (with the crest of the wave or point of maximum slope) can be obtained (Section 8.0).

The term 'apparent' is used because interactions between the larger wavelength ocean waves and the capillary wave can result in stretching or compressing a persistent train of capillary waves, so that the wavelength associated with a particular pair of wave crests may be different, depending upon their position on the large-scale wave. Since the Bragg resonant condition for the radar can not follow these expansions and contractions of the wavelengths for a wave train, the signal observed might actually come from different wavelets, depending upon their position on the large-scale waves, even if the local angle of incidence were to remain the same.

4.4.2 Definition of the Modulation Index

Note that the scattering coefficient, σ°_{total}, can be resolved into the two components: contribution of backscattering due to orientation modulation (tilting) σ°_{tilt}, and contribution of backscattering due to amplitude modulation, σ°_{mod}. Hence

$$\sigma^{\circ}_{total} = \sigma^{\circ}_{tilt} + \sigma^{\circ}_{mod} \tag{4.41}$$

but

$$\sigma^{\circ}_{Theory} = \sigma^{\circ}_{tilt} \tag{4.42}$$

so

$$\sigma^{\circ}_{total} = \sigma^{\circ}_{Theory}\left(1 + \frac{\sigma^{\circ}_{mod}}{\sigma^{\circ}_{Theory}}\right) \tag{4.43}$$

Let

$$\mu = \frac{\sigma^{\circ}{}_{mod}}{\sigma^{\circ}{}_{Theory}} \tag{4.44}$$

so

$$\sigma^{\circ}_{total} = \sigma^{\circ}_{Theory}\left(1 + \mu\right) \tag{4.45}$$

where μ is called the 'modulation index.'

The concept of the modulation index is fairly straightforward. It is simply the ratio of the contribution of amplitude modulation to the contribution of tilting to the backscatter. The phase relations of the modulation index with respect to the crest and slope are discussed in Section 8.0.

5.0 EXPERIMENTAL SET-UP, MEASUREMENT TECHNIQUES AND 'EVENT' SOLUTION

5.1 Experimental Set-Up and System Description

The University of Kansas system was an FM radar operated over the band from 8-18 GHz, Ku-band. The block diagram of the system is shown in Figure 5.1. The platform near the Dutch coast was instrumented with both microwave and ocean-wave equipment for measurement of waves, currents and tides (Figures 5.2a and 5.2b).

5.2 Basis of Experiment

The microwave antenna was mounted just below the helicopter deck of the platform (Figures 5.3a and 5.3b). It illuminated a portion of the ocean surface that was small in comparison with the wavelength of any modulating (large-scale) ocean wave of interest. The short capillary waves, the predominant microwave scatterers are advected about by the large waves. The backscatter field caused by Bragg-resonant phenomena was measured at the receiver. From the frequency difference between transmitted and received signals, the slant range between the radar and the centroid of the illuminated area could be found and converted to wave height. From the signal return and the instantaneous area of the observed spot, the scattering coefficient could be determined. The result of these conversions would be a sample time profile of wave height in the center of the scattering-measurement area which is comparable with that obtained by a wave gauge at the tower and a simultaneous time history of the scattering coefficient. Brief remarks on radar equations and calculation of scattering coefficients and range follow. Note that the simplification of the radar equation when the radar parameters remain

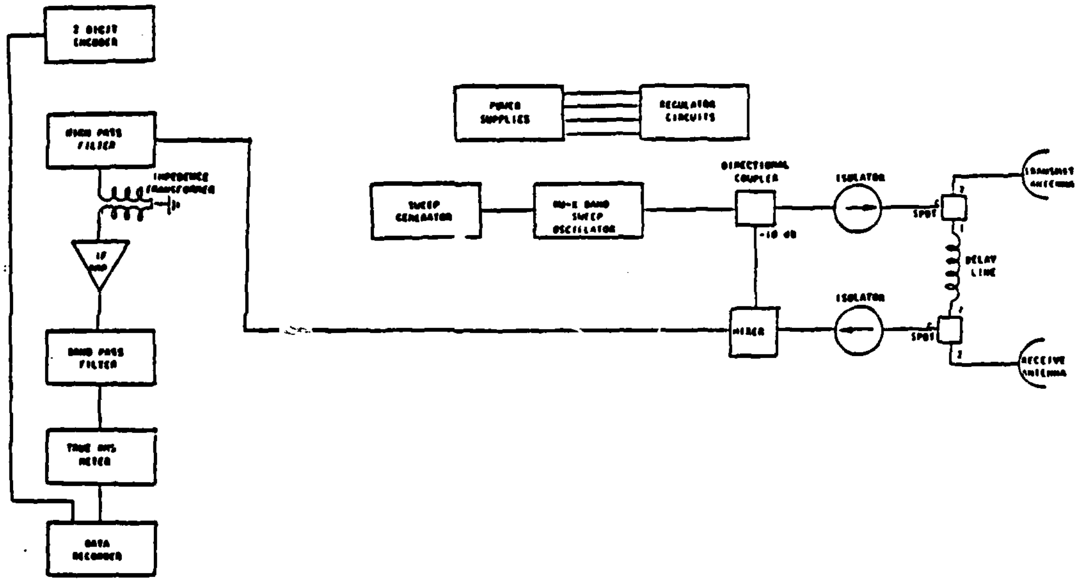

Figure 5.1
The block diagram of the radar system (TRAMAS)
used in the Noordwijk experiment

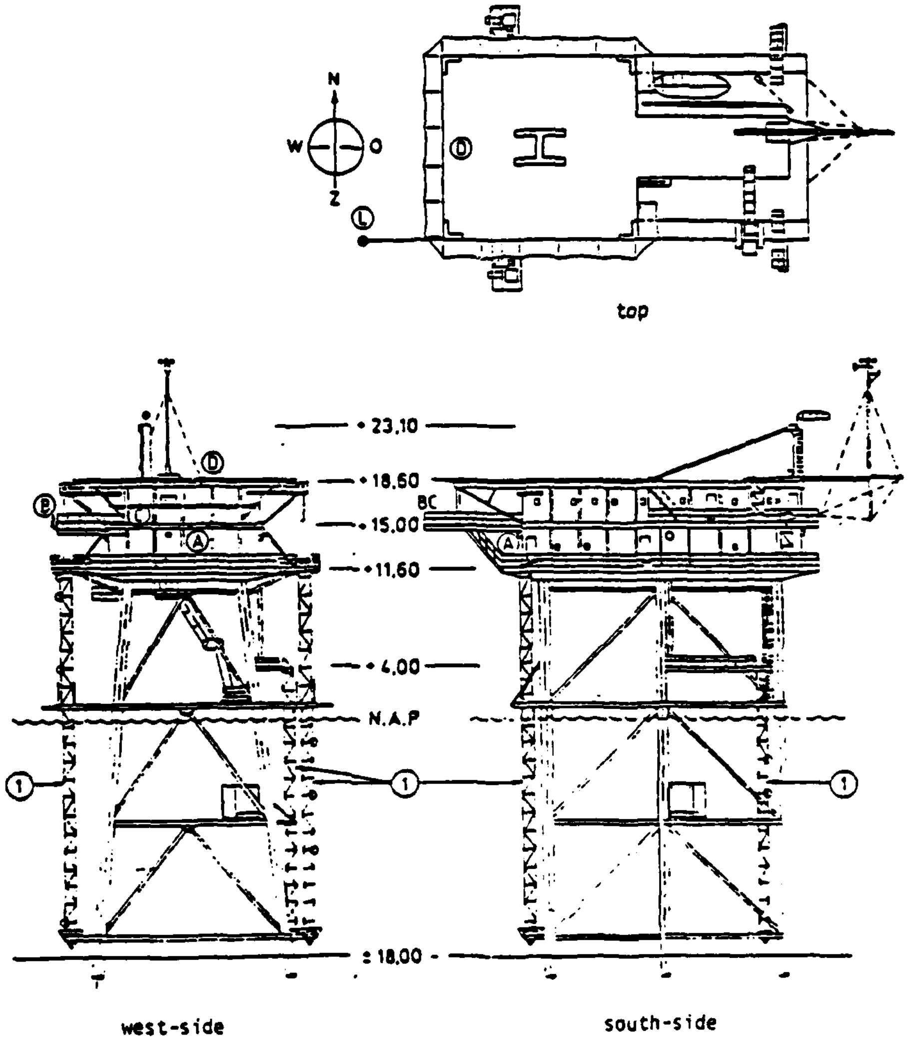

1. poles with oceanographic sensors
A. place of FM/CW measuring radar in 1977
B. ditto in 1978
C. place of French RAMSES system
D. place of 8 mm navigation radar
L. luneberg lens, protruding from helicopter deck (calibration)

Figure 5.2a
Measurement platform Noordwijk

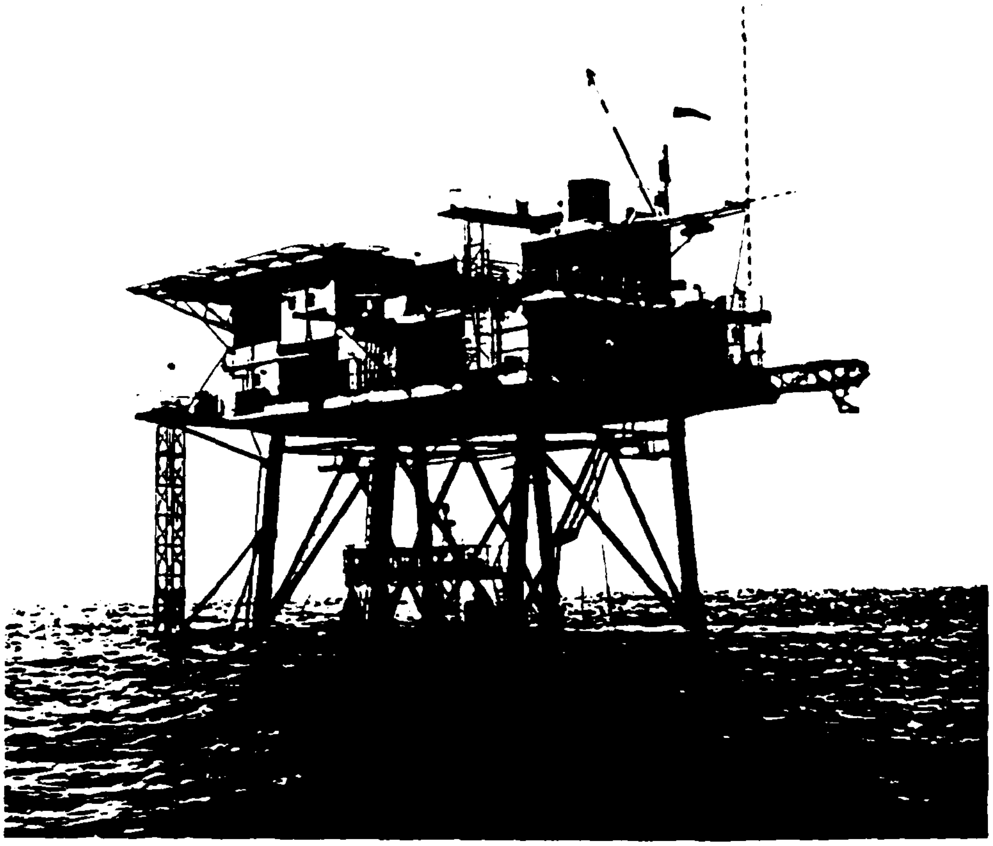

Figure 5.2b
Platform Noordwijk

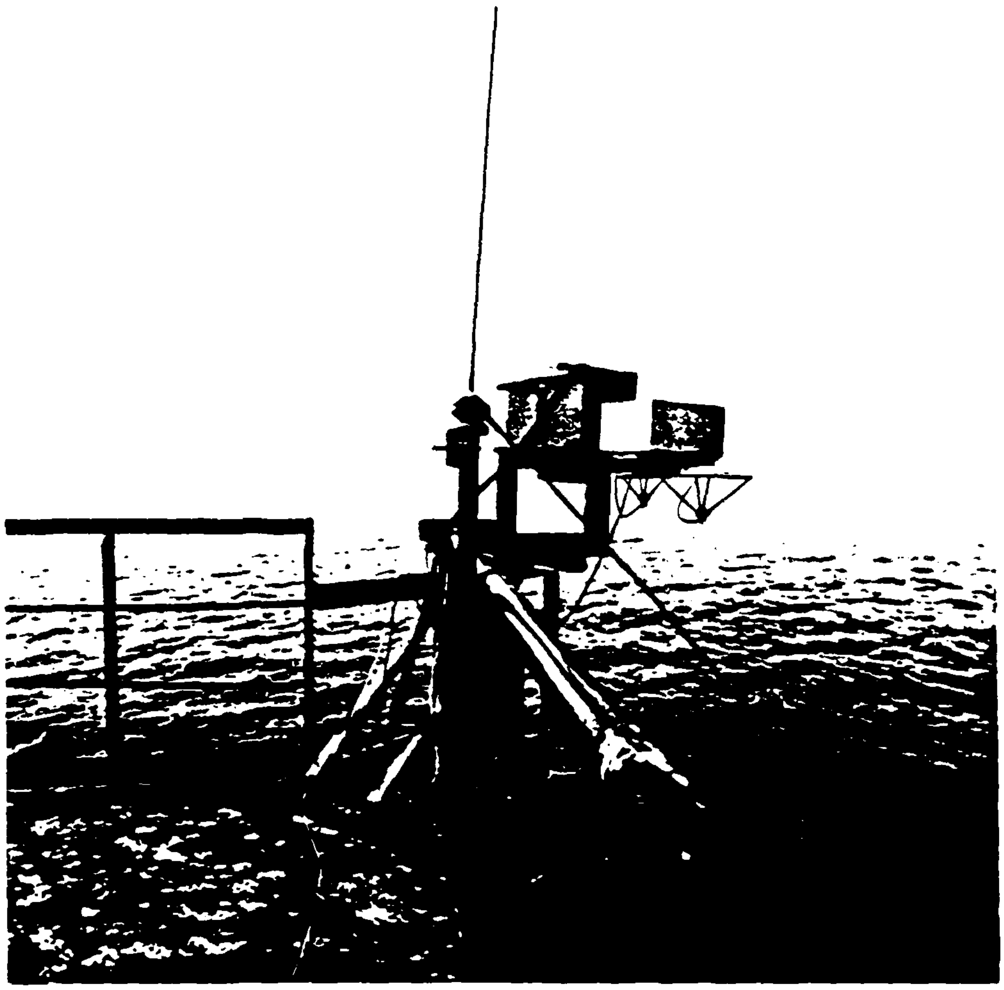

Figure 5.3
Illustration of antenna mounted at the top
of the Noordwijk Tower

essentially unchanged can be represented by

$$P_r = \frac{P_t G_t G_r \lambda^2 \sigma^\circ A_{ill}}{(4\pi)^3 R_t^4} \tag{5.1}$$

where:

P_r = received power

P_t = transmitted power

G_t = transmit antenna gain

G_r = receive antenna gain

λ = wavelength

σ° = scattering coefficient (scattering cross-section per unit area)

A_{ill} = illuminated area

R = slant range to centroid of observation spot

The return power is measured by use of a square-law detector. The power measured by the detector may be related to the returned power at the receive-antenna terminal through an unknown constant K_t, which represents the effects of attenuation and conversion losses between antenna and detector. P_{dt}, the detector power, is therefore related to the returned power by

$$P_{dt} = K_t^2 \left[\frac{P_t G_t G_r \lambda^2 \sigma^\circ A_{ill}}{(4\pi)^3 R_t^4} \right] \tag{5.2}$$

Immediately before and after recording the return from the ocean, a coaxial delay line of loss L is switched into the circuit at the antenna ports to replace the path through the transmit antenna to the surface and back through the receive antenna.

The power (through the delay line) after square-law detection is given by

$$P_{DLT} = K_t^2 P_t L \tag{5.3}$$

Taking the ratio of equations (5.2) and (5.3)

$$\frac{P_{dt}}{P_{DLT}} = \left[\frac{G_t G_r \lambda^2 \sigma^\circ A_{ILL}}{(4\pi)^3 R_t^4 L}\right] \tag{5.4}$$

To complete calibration of the system, the returns from a standard target of a known radar cross-section are measured. The Luneberg lens of the Dutch group was used as a standard target. The returned power of standard radar targets is given by

$$P_{LENS} = K_c^2 \left[\frac{P_t G_t G_r \lambda^2 \sigma_{SRT}}{(4\pi)^3 R_c^4}\right] \tag{5.5}$$

where:

K_c = system constant k at time of calibration

R_c = range to standard radar target

σ_{srt} = scattering coefficient of standard target

The power detected through the coaxial delay line at the time of calibration using the standard radar target is given by

$$P_{DLL} = K_c^2 P_L L \qquad (5.6)$$

The ratio of equations (5.5) and (5.6) is given by:

$$\frac{P_{LENS}}{P_{DLL}} = \frac{G_t G_r \lambda^2 \sigma_{SRT}}{(4\pi)^3 R_c^4 L} \qquad (5.7)$$

Combining equation (5.4) with (5.7) and solving for :

$$\sigma^\circ = \frac{P_{dt} P_{DLL} R^4 \sigma_{SRT}}{P_{DLT} P_{LENS} R_c^4 L} \qquad (5.8)$$

Note that the radar cross-section of the Luneberg lens was supplied by the manufacturer, but a recalibration was performed at the University of Kansas [Kim, 1982].

The illuminated area was calculated using the geometry shown in Figure 5.4. The projection of the radar beam as seen on the flat

surface is a skewed ellipse. The area of the ellipse was calculated using

$$A = \frac{\pi}{4}\left(M_{axis}\right)\left(m_{axis}\right)$$

where M_{axis} is the major axis and m_{axis} is the minor axis.

From the geometry of Figure 5.4, the expressions for the major and minor axes were derived.

$$M_{axis} = R \cos\theta \left[\tan\left(\theta + \frac{\beta_E}{2}\right) - \tan\left(\theta - \frac{\beta_E}{2}\right)\right] \quad (5.9)$$

$$m_{axis} = 2\left[R \tan\left(\frac{\beta_A}{2}\right)\right] \quad (5.10)$$

where:

M_{axis} = major axis

m_{axis} = minor axis

R = range to center of target

θ = pointing angle of antennas off vertical

β_E = effective gain-product (for receiving and transmitting antennas) beamwidth in elevation plane

β_A = effective gain-product beamwidth in the azimuthal plane

For a given target at range R, the time that returned signals are delayed is

$$\Delta t = \frac{2R}{c} \quad (5.11)$$

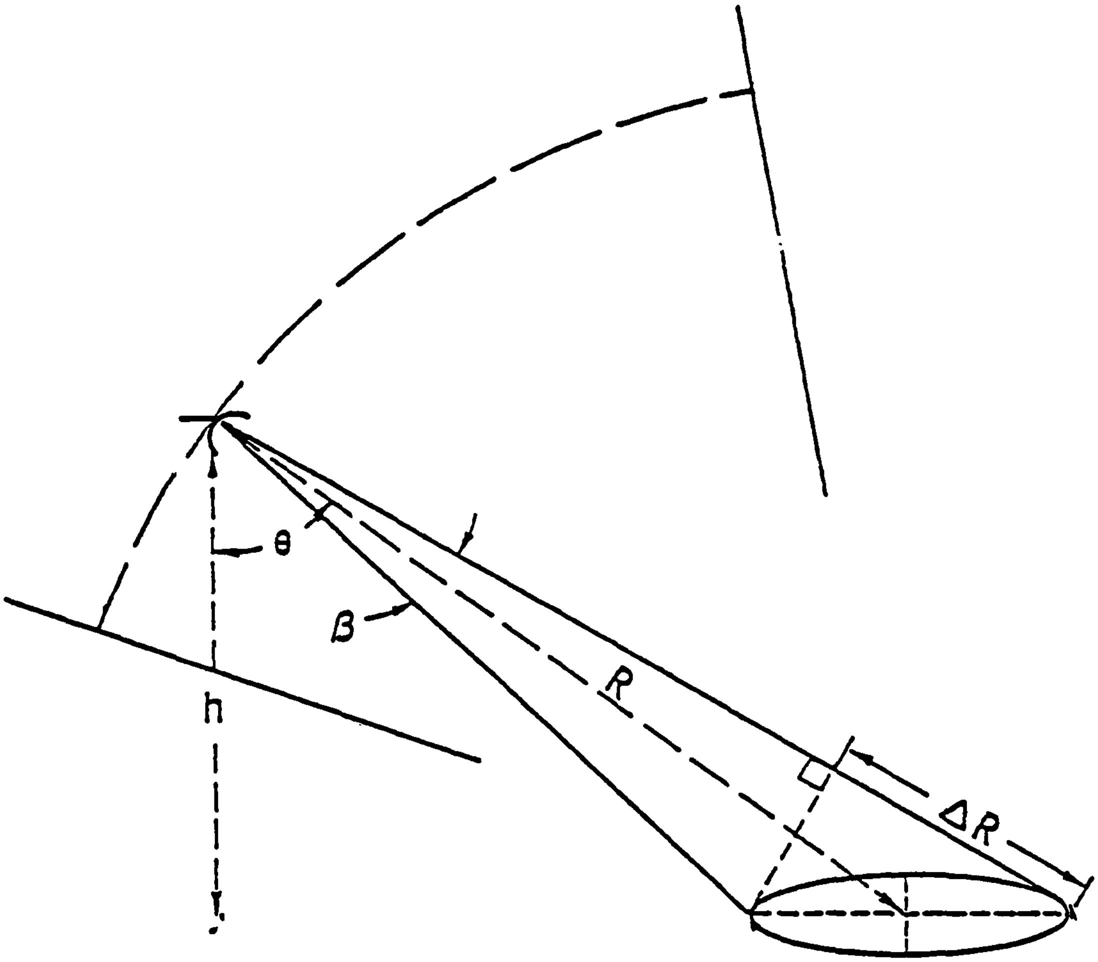

Figure 5.4
Parameters used in determining illuminated area.

An illustration of the frequency relationship between the transmitted and received signal is shown in Figure 5.5. It can be shown that

$$\frac{\Delta t}{F_{IF}} = \frac{1/4 F_M}{\Delta f/2} \tag{5.12}$$

so

$$R = \frac{F_{IF}\, c}{4(\Delta f) F_M} \tag{5.13}$$

where:

c = speed of light

F_{IF} = intermediate frequency

F_M = sweep rate

Δf = sweep frequency width

In this system, F_{IF} was fixed at 50 kHz and Δf was fixed at 1 GHz. F_M is adjusted by a tracking loop to center the target return at 50 kHz.

5.3 Measurement Techniques

Measurements were made at angles of incidence, θ, from 10° to 80° (Figure 5.6), with both vertical and horizontal polarizations. Frequencies for the measurements were at 1 GHz intervals from 9 to 17 GHz. Measurements were made at various angles relative to the wind direction with a large number of measurements in the upwind and downwind direction, a smaller number of measurements in the cross-wind

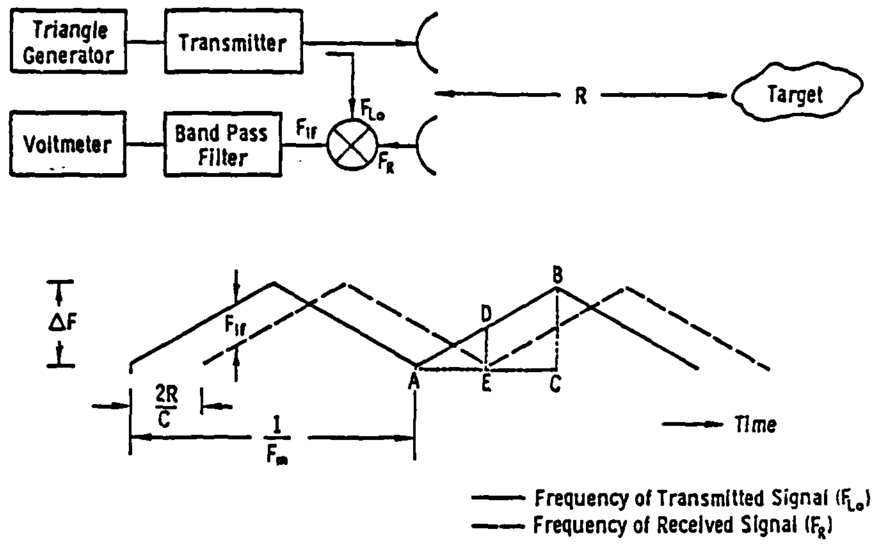

Figure 5.5
Frequency relationship between the transmitted and received signal for an FM radar

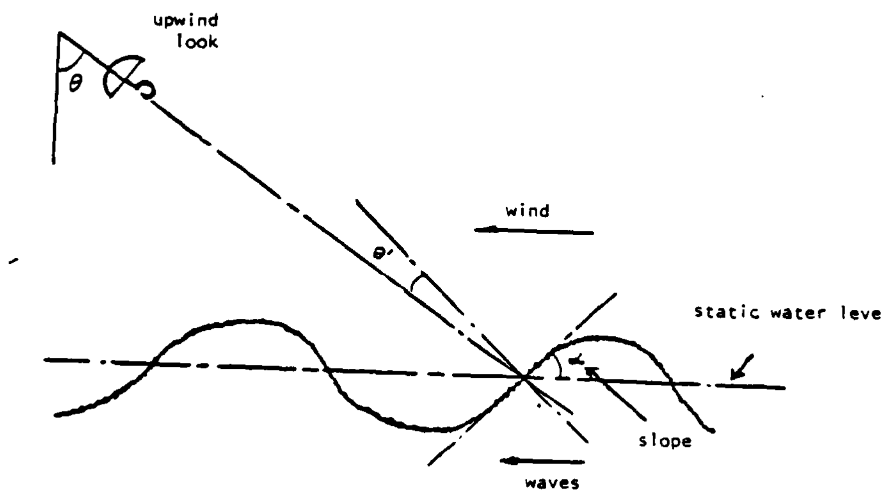

Figure 5.6
Angle of incidence, θ, varies between 10° and 80°. Note that the local angle of incidence θ' is modified by the slope α of the large-scale wave.

direction and a few measurements in which the azimuth angle was varied during collection of a single set of data.

Sampling rate was 1 Hz (one sample per second) so the maximum frequency one expected to see was 0.5 Hz. For both convenience and assurance that aliasing would be prevented, the wave height time series were low-pass filtered to a cutoff frequency of 0.35 Hz. This should not eliminate significant information in the wave height time series, since one expects about 95 percent of signal energy to be distributed between 0.1 and 0.2 Hz in normal climate conditions for wind speed less than 20 m/sec. Each set of experiments usually took 10-15 minutes. At the start of a set, the wind speed, polarization and azimuth were recorded and, in each set, the instantaneous slant range (actually F_M), wave gauge record, and power return were recorded on the cassette tape.

Examination of the reduced data showed that a very large number of successful measurements was made, but that many of the measurements contained errors due to such causes as lack of proper tracking of the illuminated area by the range-tracker circuitry and poor signal-to-noise ratio.

Although measurements were made at frequencies separated by only 1 GHz, many of the data sets were obtained at only two frequencies -- 10 and 15 GHz. This was done to permit longer sampling intervals than would have been possible if both angle of incidence and frequency had been changed over the entire range of parameters. Because of the variation of the Bragg-resonant wavelength with angle of incidence, a nearly complete set of the possible Bragg-resonant conditions was obtained with the two-frequency measurements.

5.4 'Specular Events' Observation

Interesting phenomena that were observed in the time history of radar return records were designated 'specular events'. Study of the time history of radar returns indicates that most of the time the signal fades about a mean level associated with the local angle of incidence. Occasionally certain 'events' occur in which the signal is much larger. This has been noted particularly at angles of incidence near grazing [Kalmykov and Pustovoytenko, 1976], but has also been observed at other angles of incidence. An example of this type of behavior is shown in Figure 5.7 that contains six noncontiguous 128-second samples of the time series of scattering coefficient. Notice the generally small fluctuation about the varying mean level with the occasional events, where the signal increases greatly. No corresponding events occur for decreasing signal, so these large signals appear to be caused by different phenomena than the normal fading. These phenomena were observed by Kwoh and Lake [1981] in a wave tank, where they identified two classes of events. In one class, both polarizations gave the same return, and the laser sensor indicated that specular reflection was possible. In the other class, the vertically polarized returns were larger than the horizontal returns. These were attributed to edge diffraction from sharp edges where waves approach the breaking point.

The capillary-wave return power is proportional to the square of the number of scatterers within the footprint, because their backscattered fields add coherently, whereas the mean return from the events is proportional to the average number of events per footprint. Since the events are randomly located, their backscattered fields add

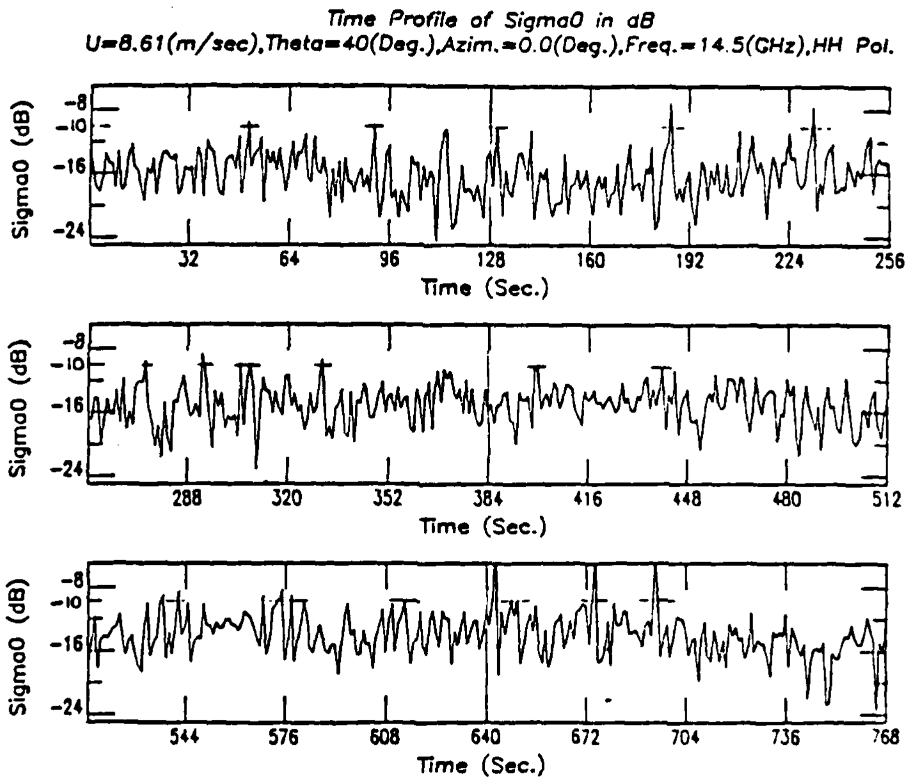

Figure 5.7
Sample of time profile of σ^0 (dB), illustrating the specular events. Each 128-sec record is from a different time.

noncoherently. The significant differences which have been reported between the scattering coefficient of the ocean measured by radars in aircraft and spacecraft and those measured by radars on towers may be explainable with this theory. The larger footprints mean a larger capillary contribution relative to the event contribution. Therefore, the specular and other (perhaps edge diffraction) events cause a much larger modification to the Bragg-scatter signal strength for the low altitude (where the footprint is smaller) than for the high altitude (where the footprint is large). The derivation of this conclusion is shown in Appendix B.

6.0 THE BASIS OF THE CALCULATIONS

6.1 Slope Calculation

The height of the large-scale gravity waves for a finite record length can be written as follows (Section 4.1.5):

$$h(x,t) = \sum_i a_i \cos\left(k_i(x + c_o t) + \varphi_i\right) \qquad (6.1a)$$

$$= \sum_i a_i \cos\left(k_i x + \omega_i t + \varphi_i\right) \qquad (6.1b)$$

where:

a_i = the amplitude of the i^{th} component of the wave

ω_i = angular frequency of the i^{th} component

K_i = i^{th} wave number

The water at Noordwijk is about 20 m deep. This is close enough to the condition for use of a deep-water dispersion relation (Section 4.1.4) that such a relation can be used with little error. Here we used the deep-water form:

$$k_i = \omega_i^2 / g \qquad (6.2)$$

where g is the gravitational constant 9.81 m/sec^2.

Another simplifying assumption made here is that the wave is sufficiently long-crested that its slope may be considered to be in the direction of wave travel in the -x direction. Making this assumption, slope s(x,t) is given by:

$$s(x,t) = \frac{\partial h}{\partial x}(x,t) = -\sum_i a_i k_i \sin(\omega_i t + k_i x + \varphi_i) \qquad (6.3)$$

During the Noordwijk experiment two measurements of H(t) were made (Section 5.3), one with a wave gauge at the tower and the other by measuring the slant range between the radar and the observed spot on the surface. The latter measurement amounts to locating a wave gauge at the centroid of the observed region. If we assume that this point is at x=0, the slope at that point will be, on an instantaneous basis:

$$S(0,t) = -\sum_i a_i k_i \sin(\omega_i t + \varphi_i) \tag{6.4a}$$

$$= -\sum_i a_i \frac{\omega_i^2}{g} \sin(\omega_i t + \varphi_i) \tag{6.4b}$$

This slope, however, is also the tangent of the slope angle so that we write:

$$S(0,t) = \tan(\alpha(0,t)) \cong \alpha(0,t) \tag{6.5}$$

where the approximation has been made that the slopes are small. The maximum slopes observed are on the order of 12°, at least for the lower wind speeds, so that this is a reasonable assumption. Figure 8.8 (Section 8.0) shows sample slope distribution. Combining (6.4b) and (6.5) the slope angle can be approximated by:

$$\alpha(0,t) \cong -\sum_i a_i \frac{\omega_i^2}{g} \sin(\omega_i t + \varphi_i) \tag{6.6}$$

6.2 Scattering Coefficient Calculation

The Bragg-resonant wavelength is a function of the instantaneous angle of incidence. The angle of incidence, normally assumed to be the pointing angle θ_p for a radar, is modified by the slope of the underlying, large-scale wave (Figure 5.7). Thus we may write for the Bragg-resonant condition:

$$K = 2k \sin(\theta_p - \alpha) \tag{6.7}$$

where k is the radar wave number and θ_p is the pointing angle, measured from vertical for the radar antenna.

Let the local angle of incidence be θ', where

$$\theta' = \theta_p - \alpha \tag{6.8}$$

so the instantaneous theoretical scattering coefficient $\sigma^{\circ}_{Theory}(\theta', \varphi)$ would be (Section 4.3.1):

$$\sigma^{\circ}_{pp}(\theta', \varphi) = 8k^4 |\alpha_{pp}|^2 \sigma_1^2 W(\theta', \varphi) \tag{6.9}$$

where for horizontal polarization

$$\alpha_{hh} = R_h \cos^2(\theta') \tag{6.10a}$$

R_h being the Fresnel reflection coefficient for horizontal polarization:

$$R_h = \frac{\cos\theta - \sqrt{\mu_r(\epsilon' - j\epsilon'') - \sin^2\theta}}{\cos\theta + \sqrt{\mu_r(\epsilon' - j\epsilon'') - \sin^2\theta}} \qquad (6.10b)$$

For vertical polarization

$$\alpha_{vv} = R_v \cos^2(\theta') + (k'^2 - k^2)\, T_v^2 \sin^2(\theta)/2k'^2 \qquad (6.11a)$$

R_v and T_v being the Fresnel reflection and transmission coefficients.

For vertical polarization:

$$R_v = \frac{\mu_r(\epsilon' - j\epsilon'')\cos\theta - \sqrt{\mu_r(\epsilon' - j\epsilon'') - \sin^2\theta}}{\mu_r(\epsilon' - j\epsilon'')\cos\theta + \sqrt{\mu_r(\epsilon' - j\epsilon'') - \sin^2\theta}} \qquad (6.11b)$$

$$T_v = 1 + R_v \qquad (6.11c)$$

In α_{pp}, k is the radar wave number in air, k' is the radar wave number in sea water, and θ' is the local angle of incidence.

$W(\theta', \varphi)$ is the normalized anisotropic sea spectrum, and σ_1^2 is the variance of the small-scale, capillary waves as shown by Fung and Chan [1977].

$$\sigma_1^2 W(\theta', \varphi) = \frac{S(K)}{2\pi K}\left[1 + 2\left(\frac{1-R}{1+R}\right)\cos(2\varphi)\right] \qquad (6.12)$$

where $R = \sigma_{c\tau}^2/\sigma_{u\tau}^2$ is the ratio of slope variance at crosswind, $\sigma_{c\tau}^2$, to slope variance at upwind, $\sigma_{u\tau}^2$, and $K = 2k\sin(\theta')$.

Determination of S(K), the spectrum of the small capillary wave is based on a modification of Pierson and Stacy's [1973] sea spectrum (Section 4.3.2). The region of their spectral model that we are

interested in is the capillary region, $S_4(K)$, where

$$S_4(K) = 0.438\,(2\pi)^{\rho_1 - 1}\,\frac{g + 3gk^2/13.1769}{(gk + gk^3/13.1769)^{\rho_1 + 1/2}} \tag{6.13}$$

The parameters which have been used in this model have been described in Section 4.3.2. Even though the model looks very cumbersome, the instantaneous sea spectrum $S(K(\theta'(t)))$, based on instantaneous local angle of incidence and windspeed, can easily be determined.

In the part of the experiment reported here the antenna pointed to upwind (φ =0°), downwind (φ=180°), or crosswind (φ=90°), so the scattering coefficient would be considered only local-angle-of-incidence, θ', dependent. Hence

$$\sigma_{pp}(\theta') = \frac{2k^3}{\pi \sin(\theta')}\,|\alpha_{pp}|^2\, S(2k \sin\theta')\left[1 + 2\left(\frac{1-R}{1+R}\right)\right] \tag{6.14}$$

It is worthwhile mentioning that the last factor in the numerator, [1+2(1-R/1+R)]is constant for a specific, given windspeed u, so one can state

$$\sigma_{pp}(\theta'(t)) = \frac{2k^3}{\pi}\,|\alpha_{pp}|^2\, S(2k \sin\theta')\,A(u)/\sin(\theta') \tag{6.15a}$$

$$= \beta_{pp}(\theta'(t), u)\,A(u) \tag{6.15b}$$

where:

A(u) is constant at a given windspeed

For determination of instantaneous scattering coefficient, $\sigma^{\circ}_{pp}(\theta'(t))$, we normalized the instantaneous calculated value of $\beta_{pp}(\theta'(t),u)$ to $\bar{\beta}_{pp}/\bar{\sigma}^{\circ}_{pp\,Total}$, where $\bar{\beta}_{pp}$ is mean of $\beta_{pp}(\theta'(t),u)$ and $\bar{\sigma}_{pp\,Total}$ is mean of actual, measured scattering coefficient (Section 5.2). This type of normalization, here called theoretical scattering coefficient calibration, not only takes care of A(u),[1+2(1-R/1+R)] but also compensates for any other scaling factor that we did not take into account (Section 5.4). The theoretical scattering coefficient is therefore defined as $\sigma^{\circ}_{Theory}(\theta'(t))$, with

$$\sigma^{\circ}_{Theory}(\theta'(t)) = \beta_{pp}(\theta'(t),u)/(\bar{\beta}_{pp}/\bar{\sigma}^{\circ}_{pp\,Total}) \qquad (6.16)$$

6.3 Modulation Index Calculation

As discussed in Section 4.3, if no amplitude modulation of the capillaries were present, the only source of modulation in backscatter from the sea surface is tilting, but it has been shown very clearly by several investigators (Section 3.0) that the amplitude modulation of the capillary waves does indeed exist and has very important contributions to actual scattering coefficient. Therefore we may write

$$\sigma_{Total}(\theta'(t)) = \sigma^{\circ}_{Tilt}(\theta'(t)) + \sigma^{\circ}_{mod}(\theta'(t)) \qquad (6.17)$$

where:

$\sigma^{\circ}_{tilt}(\theta'(t))$ is instantaneous scattering coefficient contribution due to tilting effect.

$\sigma^{\circ}_{mod}(\theta'(t))$ is instantaneous scattering coefficient contribution due to capillary wave modulation.

Then

$$\sigma^{\circ}_{total}(\theta'(t)) = \sigma^{\circ}_{tilt}(\theta'(t))\left(1 + \frac{\sigma^{\circ}_{mod}(\theta'(t))}{\sigma^{\circ}_{tilt}(\theta'(t))}\right) \tag{6.18}$$

Note that $\sigma^{\circ}_{tilt}(\theta'(t))$ is the same as $\sigma^{\circ}_{Theory}(\theta'(t))$, the theoretical scattering coefficient (Section 4.3), so

$$\sigma^{\circ}_{total}(\theta'(t)) = \sigma^{\circ}_{Theory}\left(1 + \frac{\sigma^{\circ}_{mod}(\theta'(t))}{\sigma^{\circ}_{Theory}(\theta'(t))}\right) \tag{6.19}$$

Here we define the modulation index

$$\mu(t) = \frac{\sigma^{\circ}_{mod}(t)}{\sigma^{\circ}_{Theory}(t)}$$

So, from (6.19)

$$\mu(t) = \frac{\sigma^{\circ}_{total}}{\sigma^{\circ}_{Theory}} - 1 \tag{6.20}$$

$\mu(t)$ is the ratio of the contribution of backscatter due to amplitude modulation of capillary waves to the contribution of backscatter due to orientation of capillary waves over the large-scale waves.

6.4 Cross-Correlation Calculation

Cross-correlation of modulation index, $\mu(t)$ with wave height, $h(o,t)$ can readily show the phase relationships between the peak of capillary amplitude and the crest of the large-scale wave (Section 8.0). Analytically,

$$d(\tau) = \left[\frac{1}{T}\int_0^T \mu(t)\,h(o,t+\tau)\,dt\right] \Big/ \left(\overline{\mu^2}\,\overline{h^2}\right)^{1/2} \qquad (6.21a)$$

Numerically, Section 8.0

$$d(m) = \frac{1}{2N}\sum_0^{2N} \mu(n)\,h(o,n+m) \Big/ \left(\overline{\mu^2}\,\overline{h^2}\right)^{1/2} \qquad (6.21b)$$

With the cross-correlation of modulation index, $\mu(t)$, with slope, $s(o,t)$ one can determine the phase relationships between peak of capillary modulation and peak of the slope. Analytically

$$\ell(t) = \left[\frac{1}{T}\int_0^T \mu(t)\,S(o,t+\tau)\,dt\right] \Big/ \left(\overline{\mu^2}\,\overline{S^2}\right)^{1/2} \qquad (6.22a)$$

Numerically, Section 8.0:

$$\ell(m) = \frac{1}{2N}\sum_0^{2N} \mu(n)\,S(o,n+m) \Big/ \left(\overline{\mu^2}\,\overline{S^2}\right)^{1/2} \qquad (6.22b)$$

6.5 Modulation Transfer Function Calculation

Consider the backscattered signal to a microwave radar which illuminates an area of sea surface, at least one dimension of which is much smaller than the wavelength of the dominant surface wave. The

backscattered power is found to fluctuate with time and may be represented by Fourier series

$$\mathcal{P}(t) = \sum_{0}^{\infty} \mathcal{P}_n \cos(2\pi n f t + \varphi_n) \quad (6.23a)$$

$$= \mathcal{P}_0 \cos(\varphi_0) + \mathcal{P}_1 \cos(2\pi f_0 t + \varphi_1) + \ldots\ldots \quad (6.23b)$$

In many cases, harmonics of the ocean wave frequency are not found in the return power. Furthermore, it is found that the amplitude of the fluctuation in the power increases with the height of the ocean wave [Plant, 1980]. To incorporate these observations in $\mathcal{P}(t)$, let

$$\bar{\mathcal{P}} = \mathcal{P}_0 \cos(\varphi_0) \quad (6.24a)$$

$$\mathcal{P}_1 = \bar{\mathcal{P}} |R| A \quad (6.24b)$$

$$\varphi_1 = \varphi \quad (6.24c)$$

$$\mathcal{P}_n = 0 \quad (6.24d)$$

where $\bar{\mathcal{P}}$ is mean backscattered power, A is wave amplitude and R is a coefficient describing the power modulations with these definitions.

$$\mathcal{P}(t) = \bar{\mathcal{P}} \left[1 + |R| A \cos(2\pi f_0 t + \varphi)\right] \quad (6.25)$$

Let the surface displacement be $h(x, t)$

$$h(x,t) = A\cos(Kx - 2\pi f_o t) \tag{6.26}$$

The wave slope is given by

$$\frac{\partial h}{\partial x} = -KA\sin(KA - 2\pi f_o t) \tag{6.27}$$

We may therefore write the magnitude of the wave slope as

$$\left|\frac{\partial h}{\partial x}\right| = KA = u_o/C \tag{6.28}$$

where C is the phase speed of the ocean wave, $\frac{2\pi f_o}{K}$, and

$$u_o = \left|\frac{\partial h}{\partial t}\right| \tag{6.29}$$

is the magnitude of the horizontal component of orbital velocity. Thus,

$$P(t) = \bar{P}\left[1 + |m|\frac{u_o}{C}\cos(2\pi f_o t + \varphi)\right] \tag{6.30}$$

where

$$|m| = \frac{|R|}{K} \tag{6.31}$$

If we write this in complex notation, we have

$$P(t) = \bar{P}\left[1 + |m|\left(\frac{u_o}{c}\right)e^{i2\pi f_o t}\right] \tag{6.32}$$

where m is now a complex quantity whose phase is positive if it leads the wave crest. Since m may depend on ocean wave frequency, it is called the modulation transfer function. It is a dimensionless quantity and is related to R, which has dimensions of inverse length, by

$$m = \frac{R}{K} \tag{6.33}$$

The modulation transfer function may be evaluated by cross-correlating with either wave height or horizontal component of orbital velocity. In our case we evaluate MTF by cross-correlating with wave height. Correlating $\varphi(t)$ and $h(0,t)$,

$$\varphi(t) * h^{*}(0,t) = \frac{1}{2}\bar{P} R A^{2} e^{i2\pi f_0 \tau} \tag{6.34}$$

where τ is the time lag. But,

$$h(0,t) * h^{*}(0,t) = \frac{1}{2} A^{2} e^{i2\pi f_0 \tau} \tag{6.35}$$

so

$$\varphi(t) * h^{*}(0,t) = \bar{P} R \left(h(0,t) * h^{*}(0,t) \right) \tag{6.36}$$

Transforming the equation to Fourier domain,

$$P(f) H^{*}(f) = \bar{P} R(f) \left| H(f) \right|^{2} \tag{6.37}$$

so

$$\mathcal{R}(f) = \frac{\langle \mathcal{P}(f) H^*(f) \rangle}{\langle \bar{\varphi} \, | H(f)|^2 \rangle} \tag{6.38}$$

The plots of $R(f)$, MTF and $\mathcal{P}(f)$ and $H(f)$ versus frequency are shown in Figures 8.22 through 8.27 (Section 8.0).

6.6 Coherence Function Calculation

The last quantity that we have calculated is coherence function, defined by

$$C^2(f) = \frac{\left\{ E\left[\mathcal{P}(f) H^*(f) \right] \right\}^2}{E\left[|\mathcal{P}(f)|^2 \right] E\left[|H(f)|^2 \right]} \tag{6.39}$$

The coherence function has a maximum of one at any given frequency.

Values less than one indicate either: (1) noisy signal, (2) $\mathcal{P}(f)$ and $H(f)$ are not linearly dependent, or (3) $\mathcal{P}(f)$ is due to sources in addition to $H(f)$. The discussion about coherence function is in Section 8.0. Figures 8.28 and 8.29 (Section 8.0) show the plot of coherence vs frequency.

7.0 TRANSFORMATION FROM TEMPORAL TO SPATIAL DOMAIN

7.1 Problem Description

Measurement of wave height was made with both the wave gauge and the FM radar capability of TRAMAS (Section 5.3). These point measurements of time history are interesting, but many of the features of the waves that are desired are spatial rather than temporal, i.e., distribution of capillary wave amplitude over large-scale wave. In the following we discuss the means to convert the temporal information into spatial information on the assumption that waves are long-crested (Section 4.0), and that observations are made in an upwind or downwind direction. If we know the spectrum of the capillary waves S(K), and the slope of the large-scale waves, as a function of distance, the theoretical scattering coefficient may also be established as a function of distance. Furthermore, if one could prove that the transformation of information from temporal to spatial domain is a linear process, the direct conversion of the scattering coefficient or any other quantity of interest from temporal to spatial domain would be possible.

Since the capillary wave amplitudes are not the same at all points on the large-scale wave (Section 3.0), one of the major goals is to establish their distribution. To establish the spatial distribution of capillary wave amplitude over the large-scale wave, one must convert the waveheight-time profile to a waveheight-distance profile. Because of the nonlinear relationship between the wave number K and the angular frequency , this is not as trivial a task as one might suppose. In the following, we undertake to lay the basis for the calculation.

7.2 Discrete Form

Consider a wave traveling in the -x direction. It may be represented by a series of the form (Section 4.1.5):

$$h(x,t) = \sum_i a_i \cos(\omega_i t + k_i x + \varphi_i) \tag{7.1a}$$

or

$$h(x,t) = R_e \sum b_i e^{j(\omega_i t + k_i x)} \tag{7.1b}$$

where b_i is a complex amplitude.

$$b_i = a_i e^{j\varphi_i} \tag{7.2a}$$

In deep water the relation between K and ω is (Section 4.1.4)

$$k_i = \frac{\omega_i^2}{g} \tag{7.2b}$$

In the radar or wave-gauge measurement, we observe the height h(0,t) where it is assumed that the measurement is made at x=0 (Section 5.3). To express this in terms of Fourier series for a measurement of duration T, we may write

$$b_i = \int_{-T/2}^{T/2} h(o,t)\, e^{-j\omega t}\, dt \tag{7.3}$$

where

$$\omega_i = \frac{2\pi i}{T} \tag{7.4}$$

Recovering the time variation of height from the Fourier series then consists merely of evaluating

$$h(o,t) = \mathcal{R}e \sum_i b_i e^{j\omega_i t} \tag{7.5}$$

If somehow we could observe, at a single instant, the height as a function of distance h(x,0) we would obtain the Fourier coefficient for this function by

$$b_n = \int_{-X/2}^{X/2} h(x,o)\, e^{-jK_n x} \tag{7.6}$$

where

$$K_n = \frac{2\pi n}{X} \tag{7.7}$$

We could regain the function of height by

$$h(x,o) = \mathcal{R}e \sum_n b_n e^{jk_n x} \tag{7.8a}$$

where

$$k_n = \left(\frac{2\pi}{T}\right)^2 / g \tag{7.8b}$$

also

$$h(x,0) = R_e \sum b_i \, e^{j\frac{(n\omega)^2}{g}x} \tag{7.8c}$$

Note, however, that the terms in (7.8) are uniformly spaced in K, whereas the terms in (7.5) are uniformly spaced in ω. The Fourier coefficients are different even though the values b_i and b_n are samples of the same continuous spectra. It is this difference that causes problems in using the coefficients obtained by (7.3) to evaluate (7.8a).

The slope might be obtained easily by differentiating the series of (7.1), that is

$$\frac{\partial}{\partial x} h(x,t) = \sum_i j b_i K_i \, e^{j(\omega_i t + K_i x)} \tag{7.9}$$

so either $\frac{\partial h(0,t)}{\partial x}$ or $\frac{\partial h(x,0)}{\partial x}$ can be recovered by multiplying terms in the appropriate series by jK.

7.3 Continuous Form

It is instructive to consider what happens with continuous frequency and K functions rather than Fourier series, particularly since the FFT algorithms, although actually involving Fourier series, are addressed as if they were for continuous functions.

In continuous form we may write the time series as

$$h(0,t) = \int_{-\infty}^{\infty} H(\omega) \, e^{j\omega t} \frac{d\omega}{2\pi} \tag{7.10}$$

or the spatial series as

$$h(x,0) = \int_{-\infty}^{\infty} H(\omega(K))\, e^{jKx} \frac{dK}{2\pi} \tag{7.11}$$

where

$$\omega = \sqrt{Kg}$$

so

$$h(x,0) = \int_{-\infty}^{\infty} H(\sqrt{Kg})\, e^{jKx} \frac{dK}{2\pi} \tag{7.12}$$

The two integrals (7.10) and (7.12) obviously are not the same because K and ω are related by $\omega = \sqrt{Kg}$. Note that H(u) and H($\sqrt{Kg}$) are generally not equal.

One can also find the slope in either the time or the frequency domain by differentiating the appropriate functions obtaining

$$\frac{\partial}{\partial x} h(0,t) = \int_{-\infty}^{\infty} j\frac{\omega^2}{g} H(\omega)\, e^{j\omega t} \frac{d\omega}{2\pi} \tag{7.13}$$

$$\frac{\partial}{\partial x} h(x,0) = \int_{-\infty}^{\infty} jK\, H(\sqrt{Kg})\, e^{jKx} \frac{dK}{2\pi} \tag{7.14}$$

7.4 Numerical Evaluation

The difficulty with converting the formal solution into a numerical one has to do with the way in which the FFT provides the values for the function H(ω). Clearly the inverse FFT requires samples of H($\sqrt{Kg}$) spaced uniformly in K, but the uniform spacing in ω means that the values are non-uniformly spaced in K. Thus, one cannot directly feed the outputs of the FFT of h(0,t) into an inverse FFT in K

to get h(x,0).

If the function were smoothly varying in both amplitude and phase, one could use an interpolation routine to obtain values of the function at uniformly spaced points on the K axis, but unfortunately the values of the Fourier coefficients fluctuate widely. So the interpolation is not possible.

The straightforward way to evaluate the function is simply to sum the series of (7.1a) with t=0 and K given by (7.2b). This can be done in the computer, but not with the inverse FFT routine. Hence, the nonuniformly spaced trigonometric functions themselves must be evaluated, which is time-consuming. For handling masses of data, this means that a table must be generated of the appropriate trigonometric values, so that multiplication can be substituted for the repeated evaluation of numerous trigonometric functions by selecting a standard record length, such as 128 or 256 samples.

Before considering the setting-up of such a table, we must consider the apropriate ranges of X and T. We can write the phase for a component of the surface as

$$\phi = \omega t + \frac{\omega^2}{g} x \tag{7.15}$$

If we are to use values of X and T that correspond to comparable maximum phase shifts, we have

$$T = 2\pi f_m X / g \tag{7.16a}$$

where T is the sample length in time domain and f_m is the maximum

frequency used. Since we start with a time record of limited duration, X must be expressed in terms of

$$X = gT/2\pi f_m \tag{7.16b}$$

which means that we should not try to reproduce h(x,0) over a larger range than this. That is, we must keep

$$X \leq gT/2\pi f_m \tag{7.17}$$

Reasonable record lengths to use with the MARSEN data are 64, 128 and sometimes 256 seconds. If we continue to limit the maximum frequency used to .35 Hz, this means that x should be less than 225, 570 or 1140 m, *respectively. The predominant* wavelength is of the order of 54.0 m, so a 64-second record would only have 5 cycles of this wave and even fewer cycles of the low-frequency components, so correlation achieved with individual records would be very noisy. Accordingly, the minimum record length that should be used is 128 seconds. An analytical experiment was performed to determine the validity of this procedure.

8.0 PRELIMINARY RESULTS

A very large data set (about 115 cassette tapes) was collected during the experiment. The raw cassette-tape data were converted into files in the University of Kansas Honeywell computer system. The files were edited to insert headers and eliminate bad runs. Software was written to produce scattering coefficients, radar wave heights and other quantities of interest. Preliminary calculations have been made on all the basic quantities.

Figures 8.1 and 8.2 illustrate some processed 'raw data' records. Figure 8.1 shows a sample set of versus time, and Figure 8.2 shows the measured wave height both from slant-range measurement and wave staff. The power spectrum for the wave height profile has been calculated both from radar and wave-staff measurements. Figures 8.3 and 8.4 illustrate samples of these spectra. They agree very well. Both have a single peak at about 0.17 Hz. This agreement gave some confidence for further analysis. The sampling rate of the experiment was 1.0 Hz. For slope determination, wave height data set has been low-pass filtered with maximum frequency of 0.35 Hz. This reduces the possibility of aliasing. Figure 8.5 shows a sample histogram of calculated slope for a wind of 12.5 m/sec, obtained from a filtered wave-height measurement. The standard deviation is about 10 degrees. For wind speed cases, say, between 8 and 10 m/sec, one would not expect such a high value of standard deviation. Figure 8.6a illustrates a sample set of measured scattering coefficients with an average windspeed 8.61 m/sec. Note that any point which is greater than 6.0 dB above the mean is called specular 'event' (Section 5.4). Figure 8.6b illustrates the same sample set of scattering coefficients, replacing

the specular events by a seven-point triangularly-weighted average of the adjacent samples. The expected dependence of scattering coefficient on the windspeed has been observed, and is illustrated in Figure 8.7. This dependence is due to the fact that the capillary wave amplitude depends on windspeed (Section 4.3.2) and the amplitude of the capillary spectrum directly governs the backscattered power (Section 4.3.1).

Two samples of measured scattering coefficient for VV- and HH-polarization as a function of incidence are shown in Figure 8.8. The scattering coefficient is inversely proportional to the incidence angle. If the effect of the large-scale wave slope on capillary-wave amplitude could be neglected, the Bragg-wave number, K, would be completely governed by the angle of incidence. Figure 8.9 shows a sample preliminary estimate of the measured spectrum in the Mitsuyasu-Honda range, $S_4(K)$, based on average incidence angle (the pointing angle). The measured values are compared with theoretical K spectra (lines on the figure). Note that the K-spectrum decreases rapidly with increasing Bragg-wave number, K. Since the scattering coefficient is directly governed by K-spectrum, one would expect the smaller value of scattering coefficient for larger incidence angle. Note that Bragg-wave number K is proportional to angle of incidence.

One of the major goals of this analysis is to estimate the modulation of the capillary waves over the large-scale waves, both temporally and spatially. If the capilary wave spectrum S(K) and the instantaneous slope of the large-scale wave are known, one can calculate the theoretical instantaneous scattering coefficient based on uniform capillary distribution (Section 4.3). The RMS value of

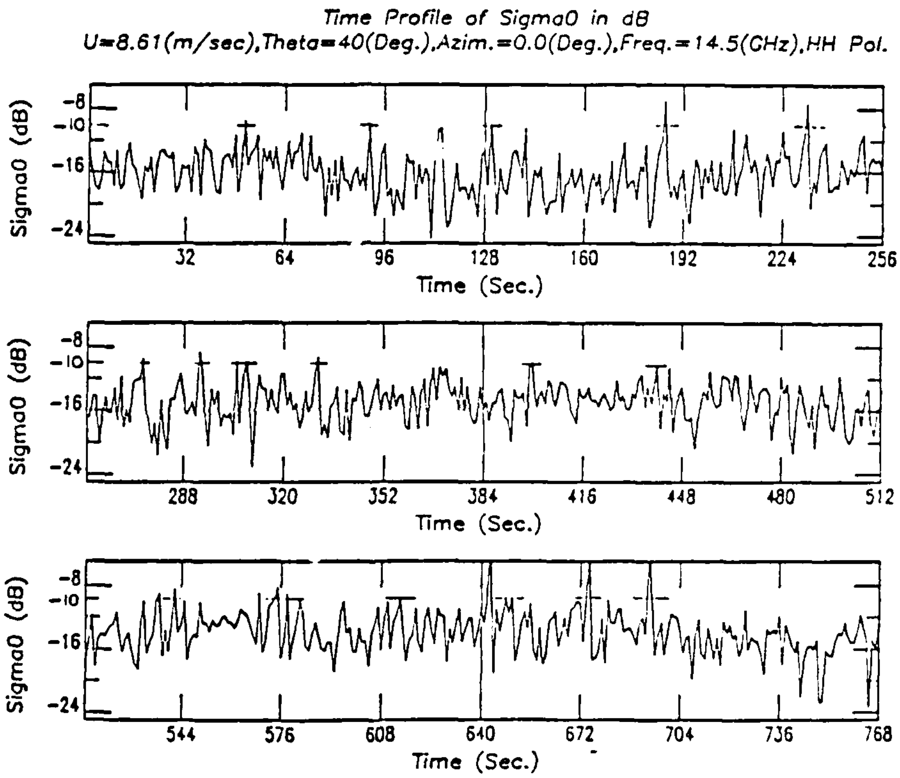

Figure 8.1
Sample of processed σ^{0} (dB), from the radar return, showing the "event" threshold. Each 128-sec record is from a different time.

AD-A129 690 INTERACTION OF THE RADAR WAVES WITH THE CAPILLARY WAVES 2/3
ON THE OCEAN..(U) KANSAS UNIV/CENTER FOR RESEARCH INC
LAWRENCE REMOTE SENSING L.. S BARKESHLI ET AL. MAY 83

UNCLASSIFIED CRINC/RSL-TR-419-1 N00014-79-C-0533 F/G 17/9 NL

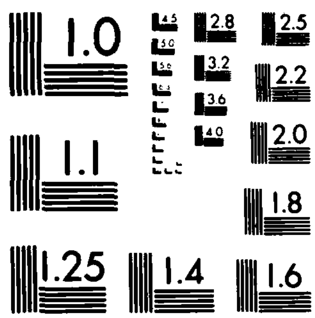

MICROCOPY RESOLUTION TEST CHART
NATIONAL BUREAU OF STANDARDS-1963-A

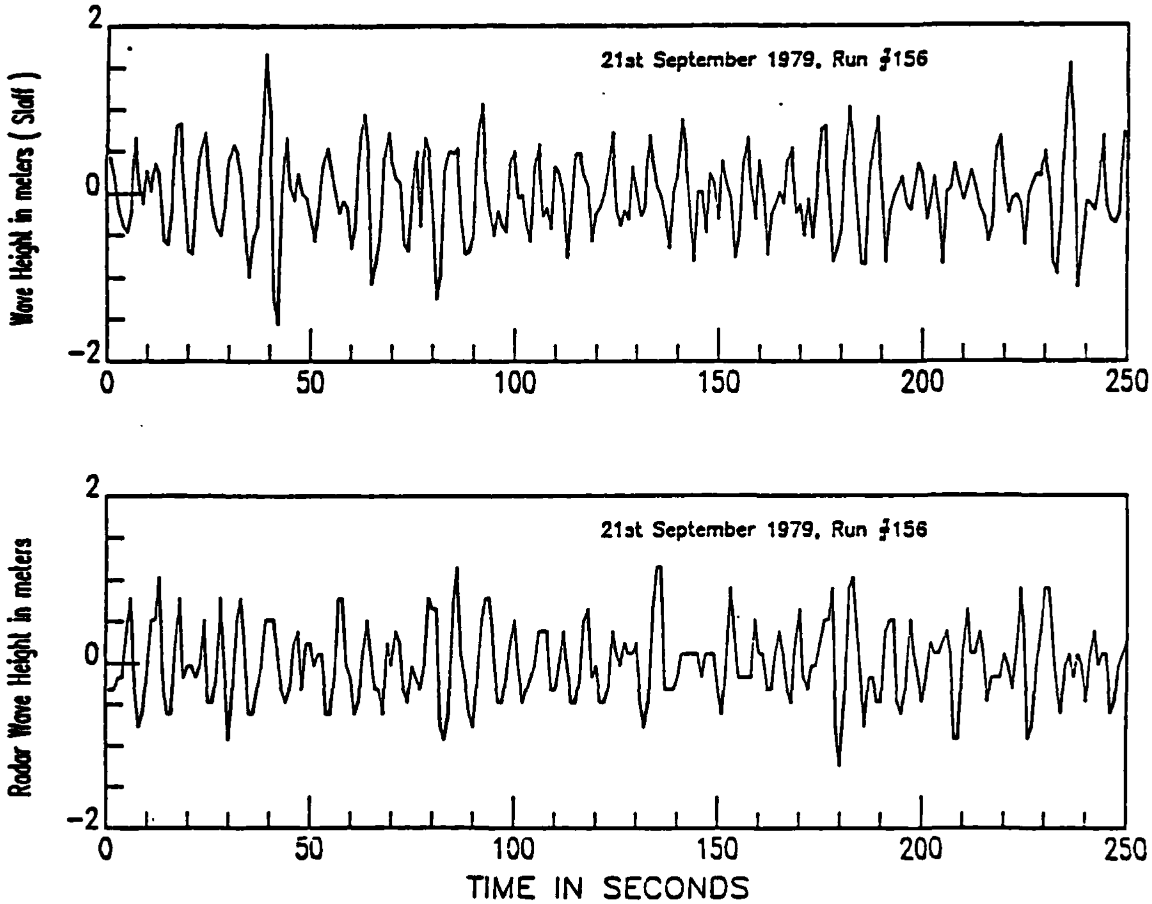

Figure 8.2
Sample comparison of wave staff and radar wave heights.
Wave staff was separated about 11 meters from
Radar Observation.

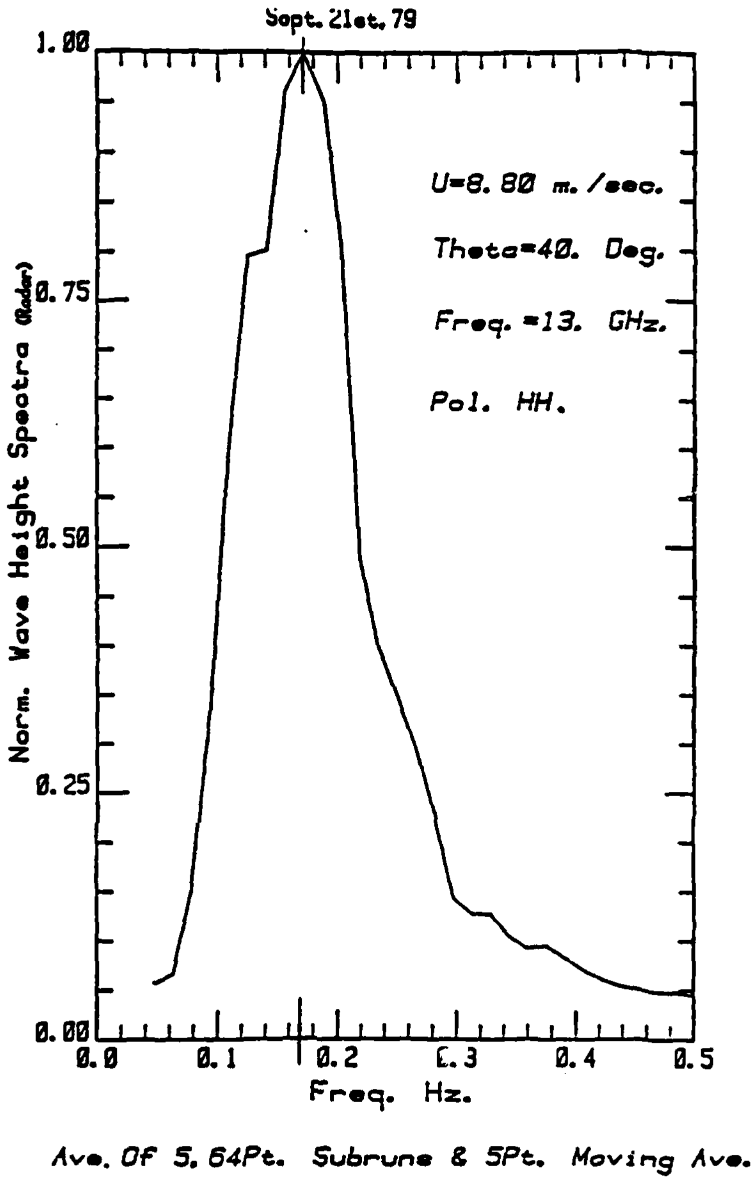

Figure 8.3
Normalized wave-height spectrum (radar);
single peak at 0.17 Hz.

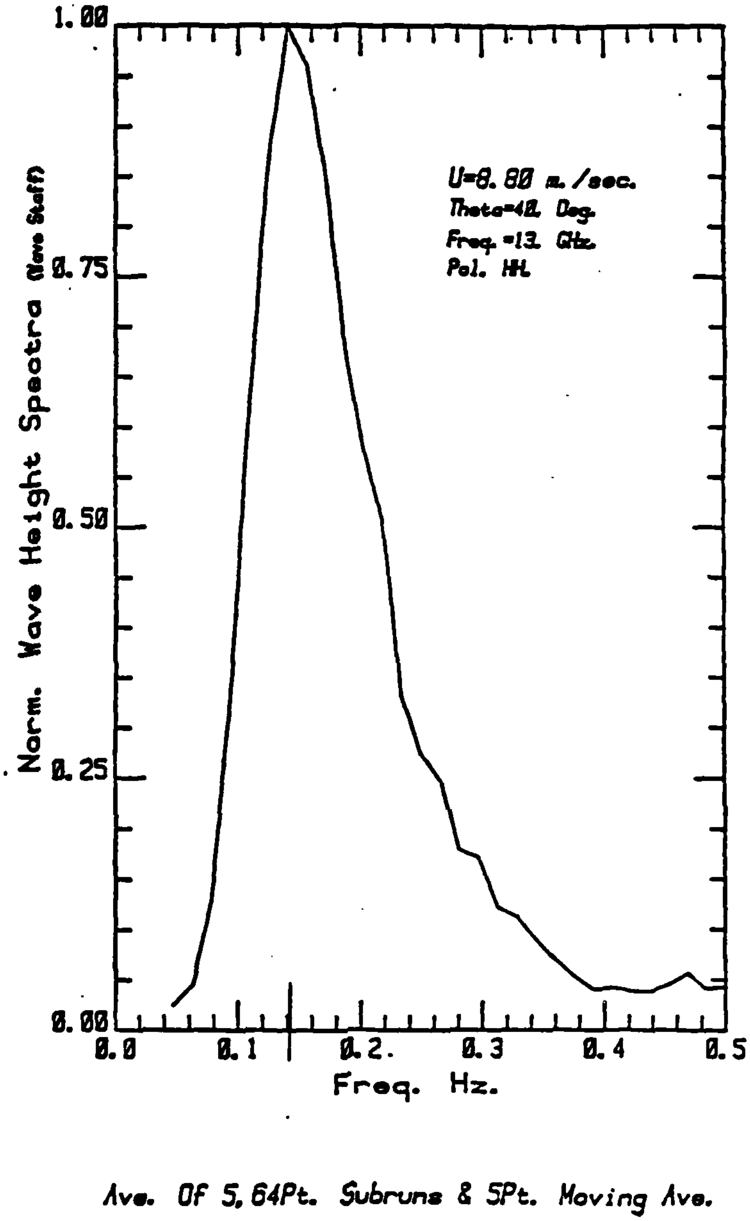

Figure 8.4
Normalized wave-height spectrum (wave staff);
single peak at 0.16 Hz.

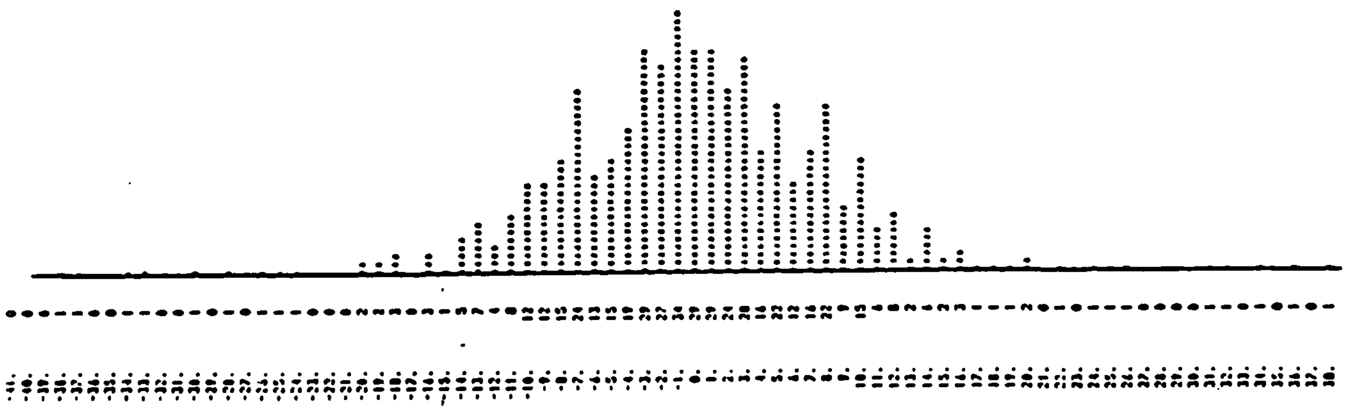

Figure 8.5
Sample slope distribution obtained from instantaneous slopes derived from radar wave-height measurement. Standard deviation 10°. Wind speed 12.5 m/s. Scale on Figure: Number of observations (upper list of numbers).
Slope in degrees (lower list of numbers).

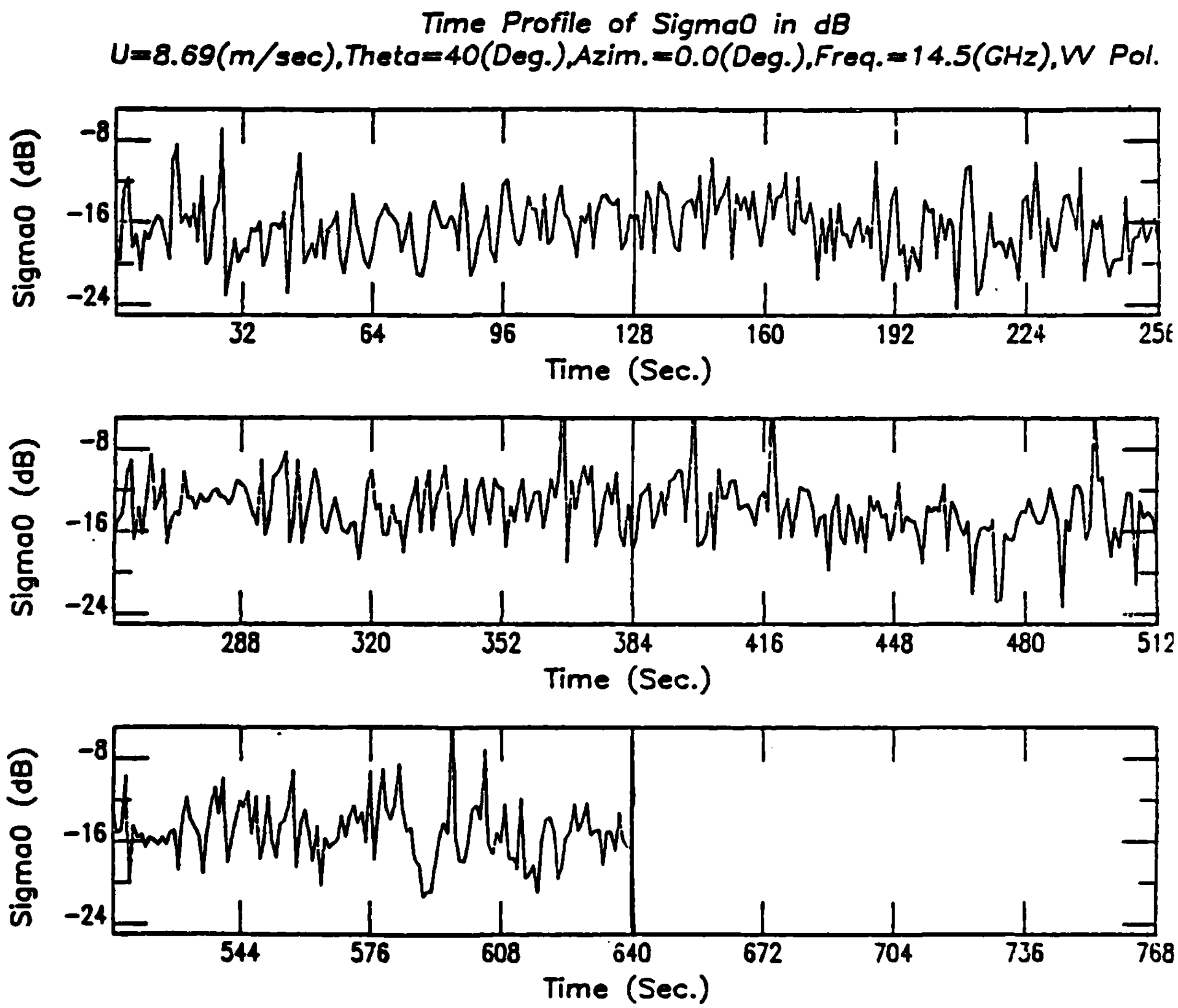

Figure 8.6a
Sample of σ^0 (dB), illustrating numerous specular events.
Each 128-sec record is from a different time.

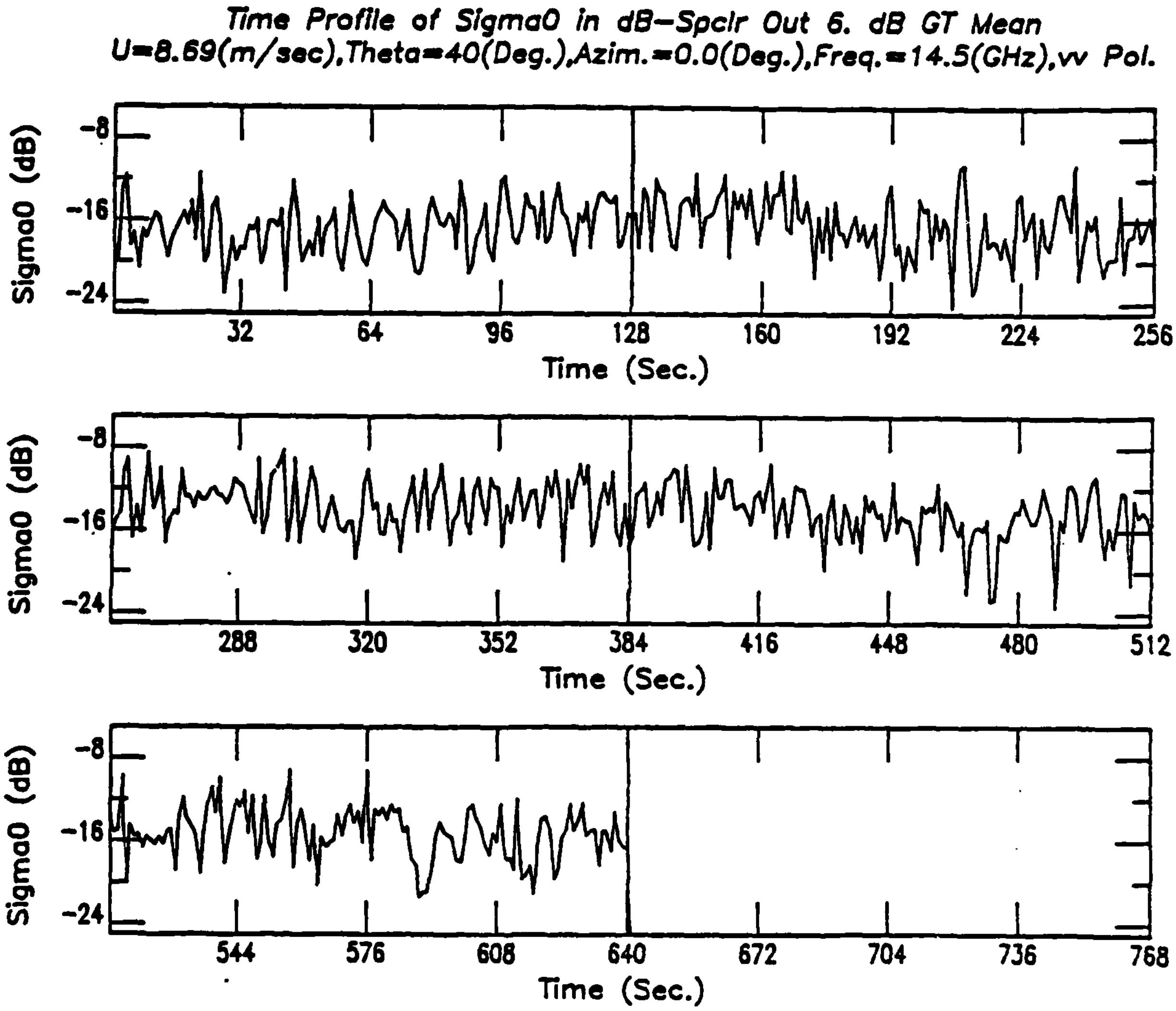

Figure 8.6b
Sample of σ^o (dB) replacing the specular events by 7 point average of an adjacent sample. Each 128-sec record is from a different time.

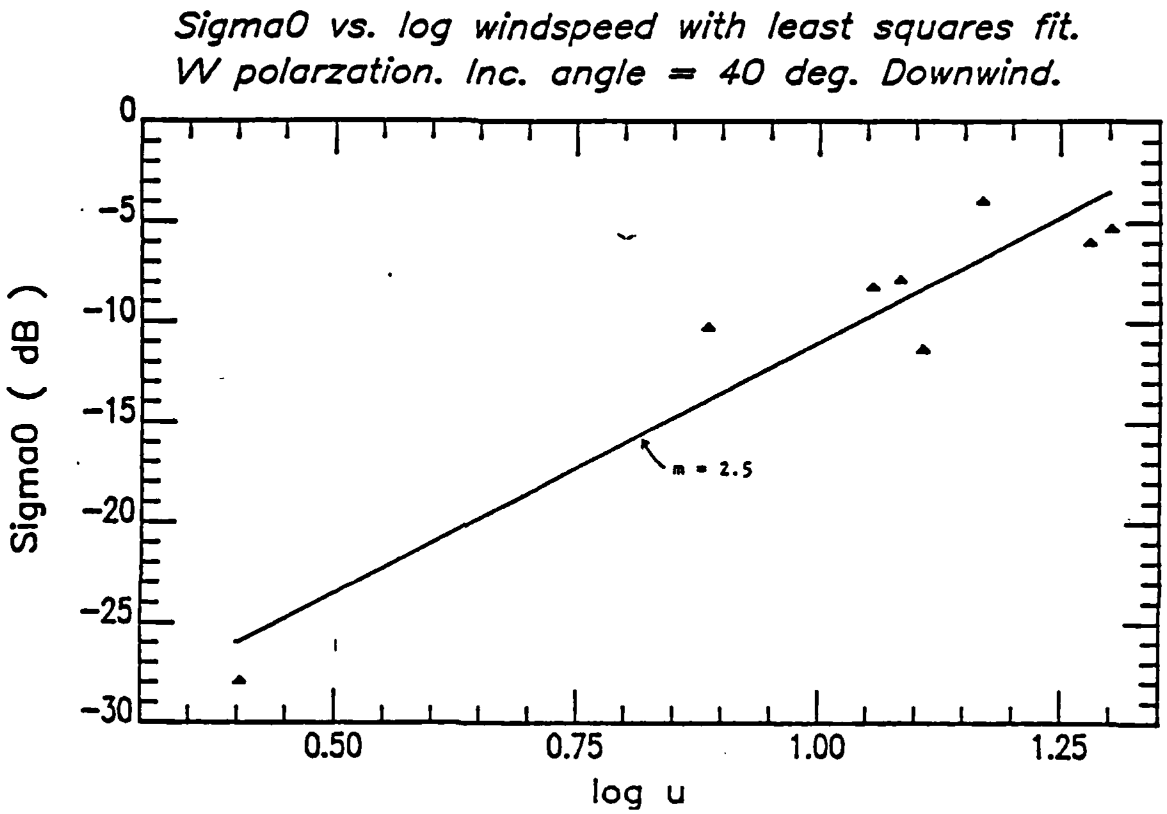

Figure 8.7
Sample preliminary estimate of wind speed response of σ^0 from 3 days of data

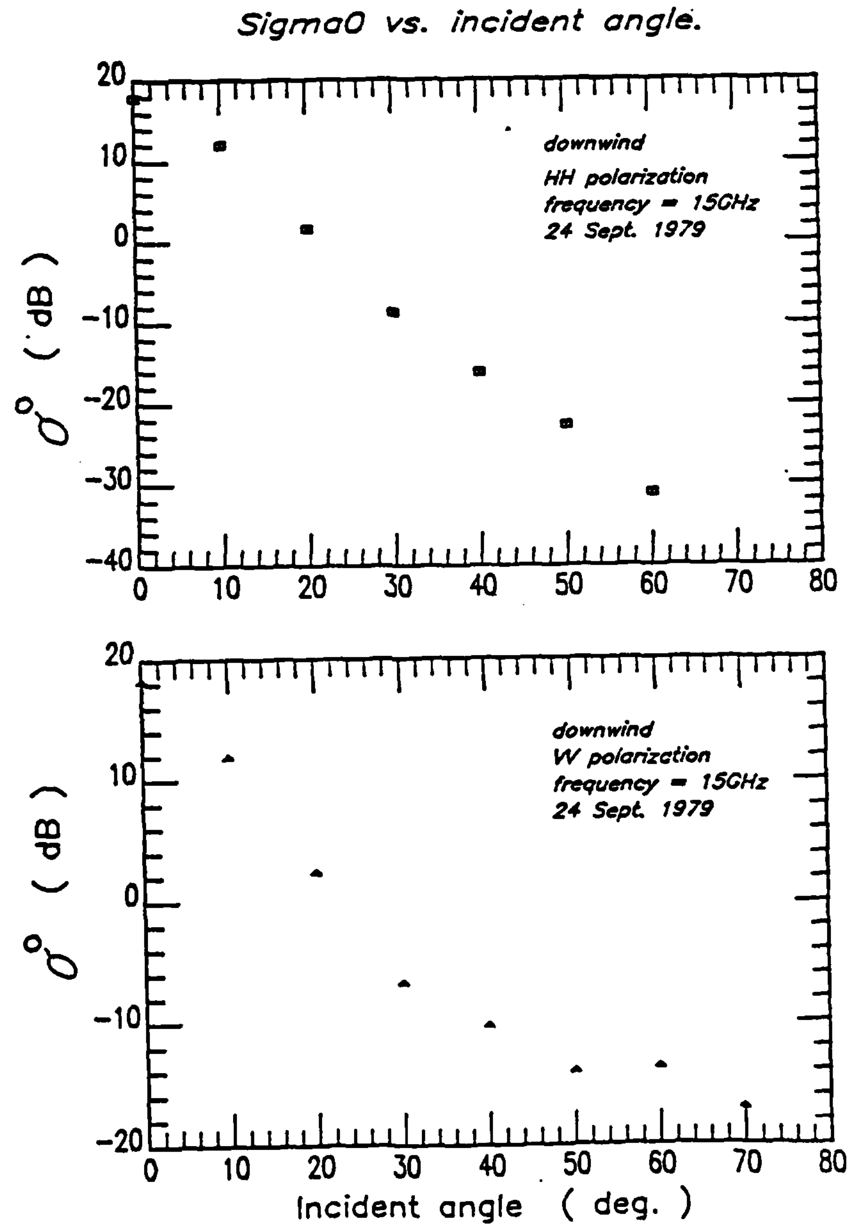

Figure 8.8
A sample preliminary estimate of σ^0 vs angle of incidence based on 10 GHz calibration used at 15 GHz.

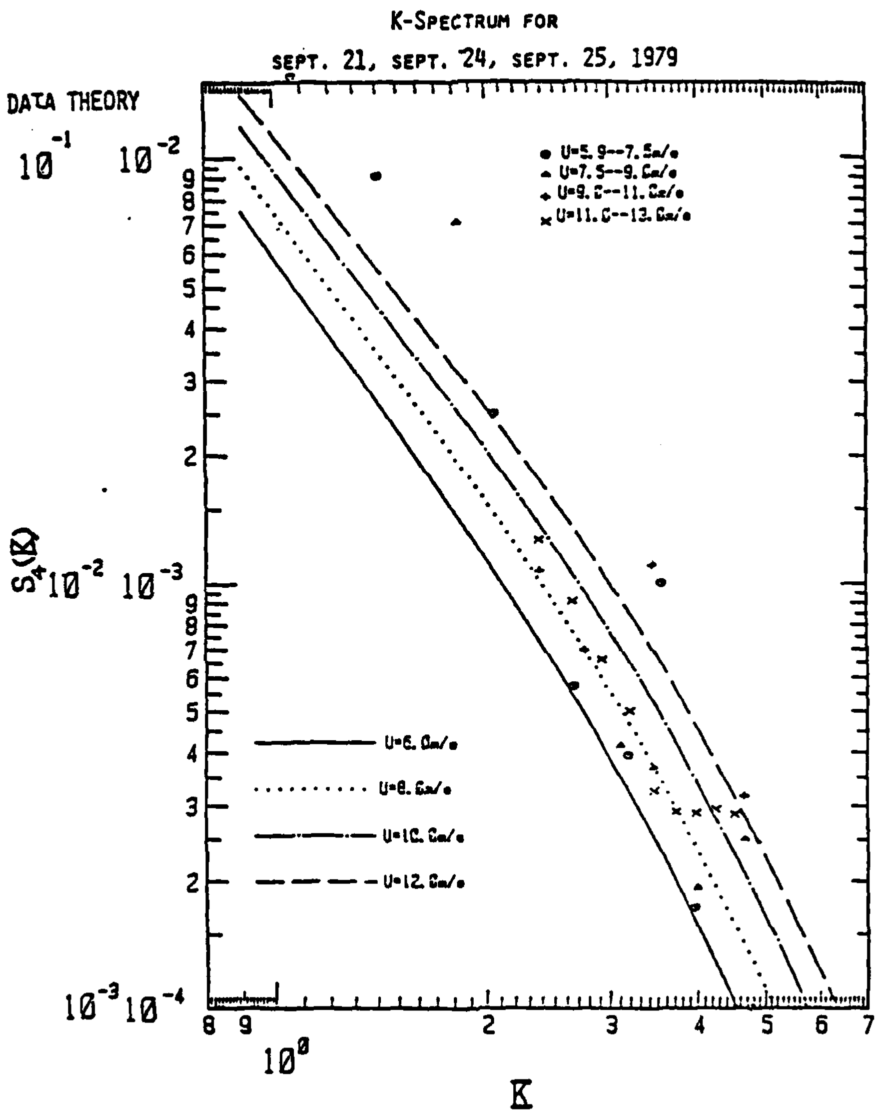

Figure 8.9
Sample preliminary estimate of measured Mitsuyasu-Honda range of wave spectrum. Some of scatter may result from use of 10 GHz reference calibration for both 10 GHz and 15 GHz data.

modulation index μ or $\Delta\sigma$ (Section 4.4.2) can show the modulation effect and tilting effect on total scattering coefficient. Having the cross-correlation between the $\mu(t)$ and slope one can estimate the phase relation of the peak of the modulation with respect to peak of the slope. The phase relation of the peak of the modulation with respect to crest of the wave can be found by the same means.

The ensemble-average RMS value of modulation index has been calculated both for HH- and VV-polarization. The average RMS modulation index is 0.876 with standard deviation of 0.34 for HH-case and is 0.673 with standard deviation of 0.044 for VV-case.

Figures 8.10a and 8.11 illustrate the autocorrelation of wave height and slope. The wave height autocorrelations show that the wave height is a quasi-periodic type of function with a period between 5.5 to 6.5 seconds, which corresponds to a dominant wave with frequency of about 0.15 - 0.17 Hz. The slope autocorrelation function shows that the slope is the same type of the quasi-periodic function, but with shorter periods, about 3.5 seconds, which corresponds tc a dominant frequency of 0.29 Hz. The higher dominant frequency in slope is expected because the slope spectrum components are calculated by multiplication of wave-height spectrum components with the square of corresponding angular frequency, ω_i, divided by g, the gravitational acceleration. This would definitely shift the spectrum peak to the higher frequency. Figure 8.10b shows the cross-correlation of slope and wave height and cross-correlation of theoretical scattering coefficient and slope. As is shown, the slope leads the wave height by about 1.0 second. The cross-correlation of theoretical scattering coefficient and slope has a maximum at zero lag, as it should.

AVE. OF 10 RUNS Sept. 21st/70 - (FILT. .35 Hz)

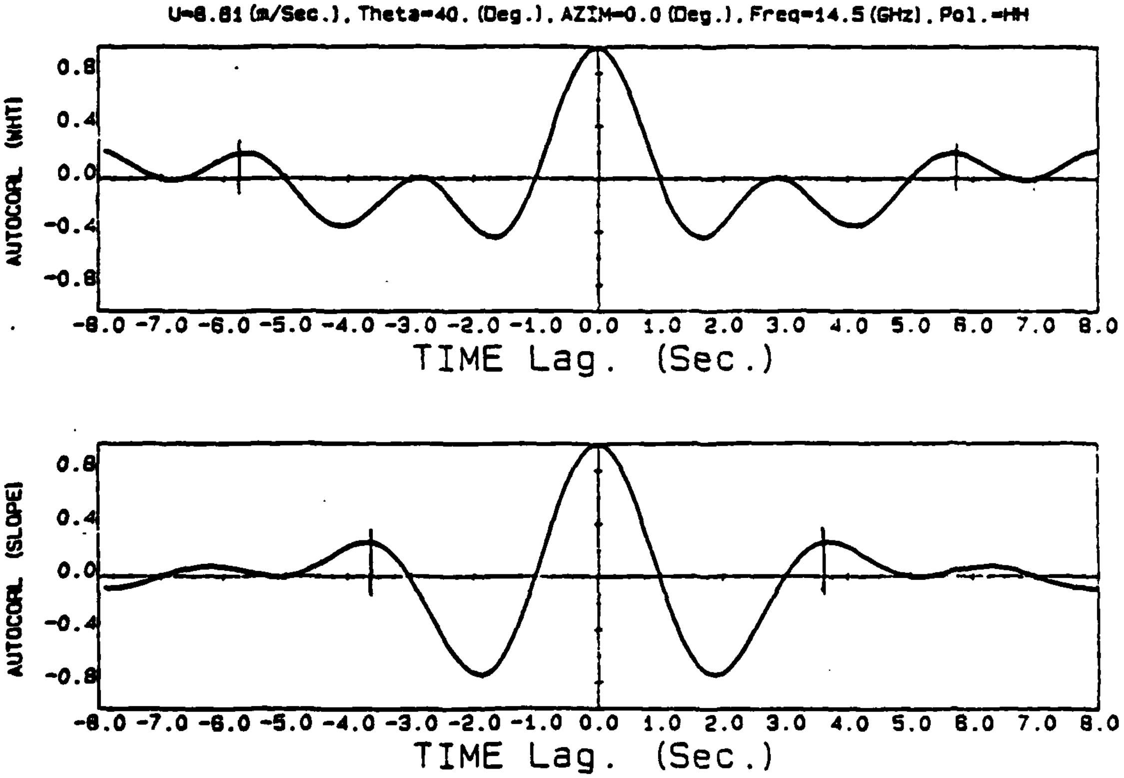

Figure 8.10a

Temporal autocorrelation of wave-height. Dominant period is 5.8 sec.
Temporal autocorrelation of slope. Dominant period is 3.5 sec.

Ave. of 10 Runs Sept.21st/70 (SPCLR OUT 6. dB GT MEAN) - (FILT .35 Hz)

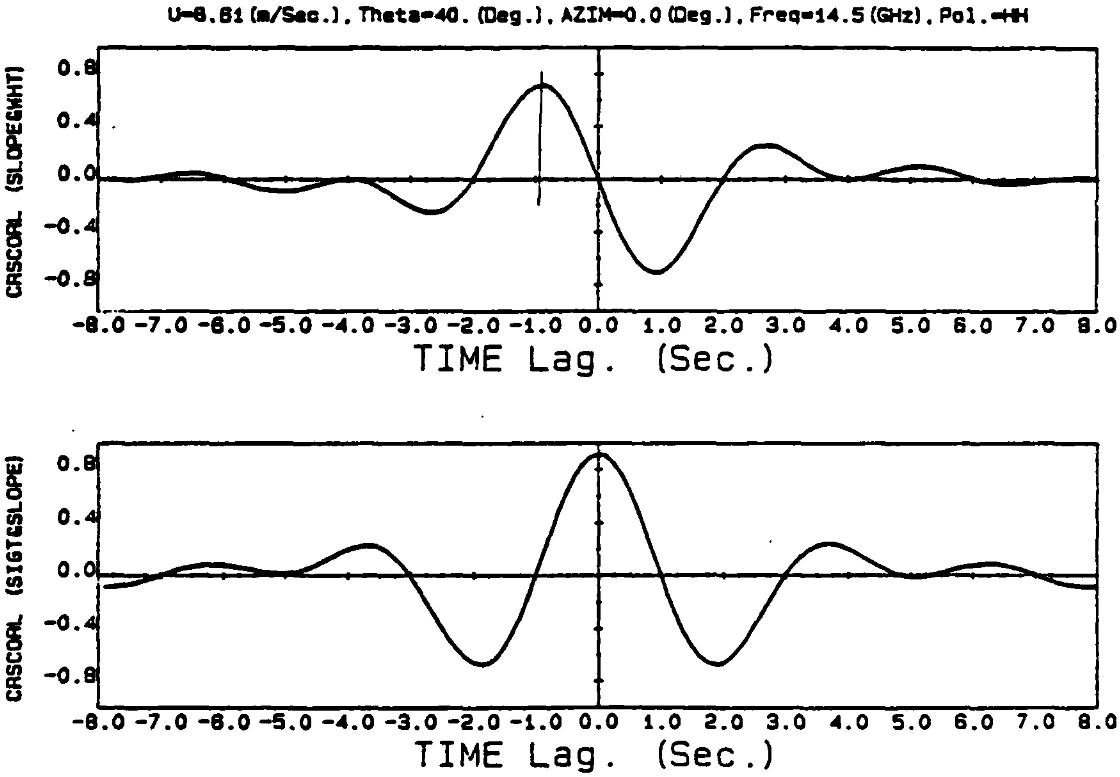

Figure 8.10b
Cross-correlation of slope and wave-height. Slope leads the wave-height by about 1.0 sec. Cross-correlation of theoretical σ^0 and slope. Maximum peak at zero lag.

Ave of 5 Runs Sept. 21st/79 - (FILT .35 Hz)

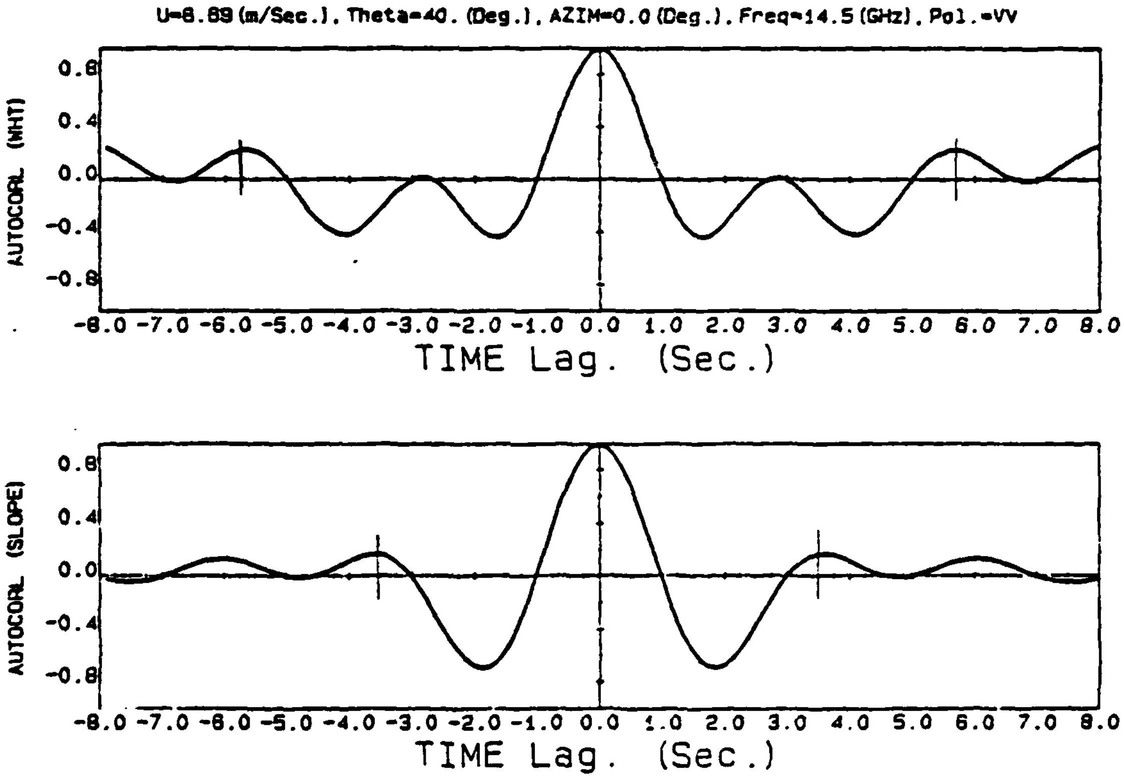

Figure 8.11
Autocorrelation of wave-height. Dominant period is about 5.8 sec.
Autocorrelation of slope. Dominant period is about 3.5 sec.

Figures 8.12 and 8.13 illustrate the cross-correlations of the scattering coefficient and the wave height and also the scattering coefficient and the slope, for both HH- and VV-polarization cases. The values of cross-correlation are not large, since the graphs are the result of averaging ten runs for HH-cases and five runs for VV-cases. Even though much larger correlations have been observed for single cases at different lags, the most significant result is that consistent values were observed for the two polarizations, based on observations at different times. The scattering coefficient leads the slope by about 0.75 seconds or about 1/8 of the dominant large-scale wave period (45°) or 1/4.7 of the dominant slope period, 77°. The scattering coefficient leads the wave height even more, about 1.7 seconds or about 104° ahead of the crest of the dominant wave. Another peak, smaller than the dominant one, can be observed for both cross-correlation functions. The phase difference between the two peaks is about a full period of the dominant slope quasi- periodic component, 3.5 seconds. This obviously shows that the scattering coefficient is dominated by the slope effect, which one would expect from the theory (Section 4.3.1). Note that the cross-correlation function of theoretical scattering coefficient and slope peaks to maximum at zero lag (Figure 8.10b), since maximum theoretical scattering coefficient occurs at maximum slope. We believe the 'unexpected' shift of the cross-correlation of scattering coefficient and slope, 1/8 of the dominant large-scale period, is due to the fact that the capillary waves are not uniformly distributed over the large-scale wave.

The modulation index $\mu(t)$ is called $\Delta\sigma$ in the figures. For both HH and VV cases, Figures 8.14 and 8.15 show that $\Delta\sigma$ leads the

Ave. of 10 Runs Sept.21st/79 (SPCLR OUT 6. dB GT MEAN) - (FILT .35 Hz)

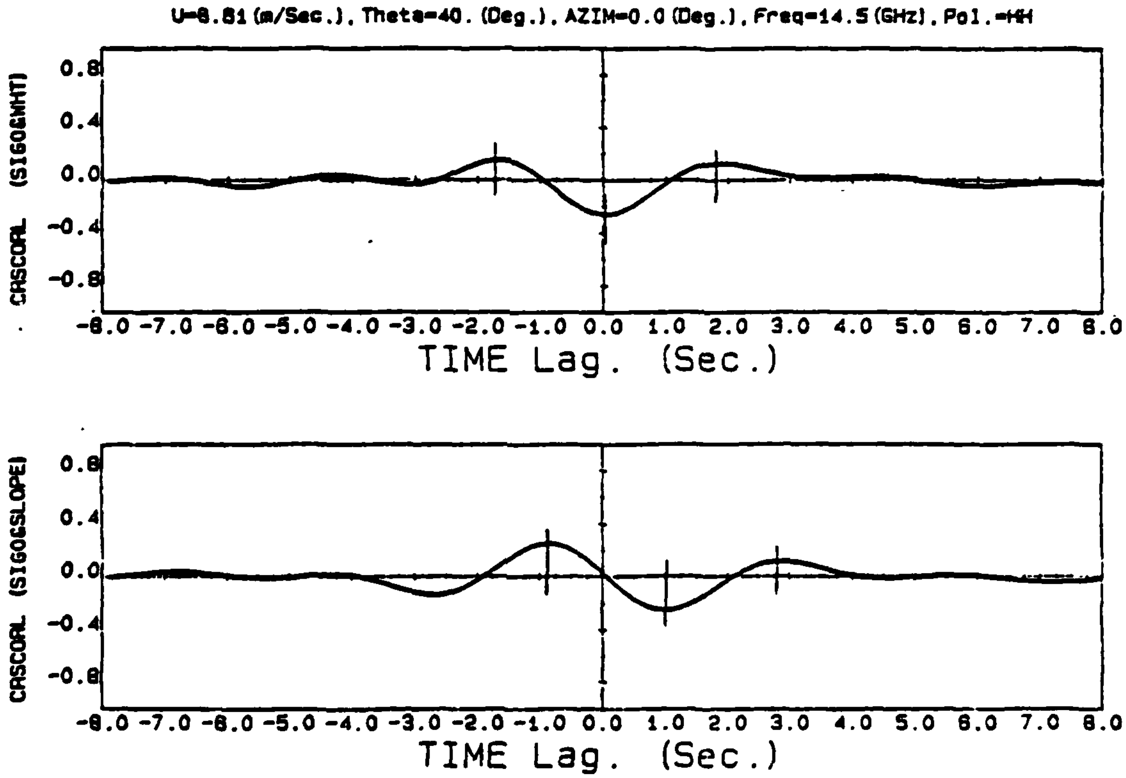

Figure 8.12
Cross-correlation of σ^0 and wave-height. σ^0 leads the wave-height by about 1.7 sec (104°). Cross-correlation of σ^0 and slope. σ^0 leads the slope by about 0.75 sec (90°).

Ave. of 5 Runs Sept.21st/79 (SPCLR OUT 6. dB GT MEAN) - (FILT .35 Hz)

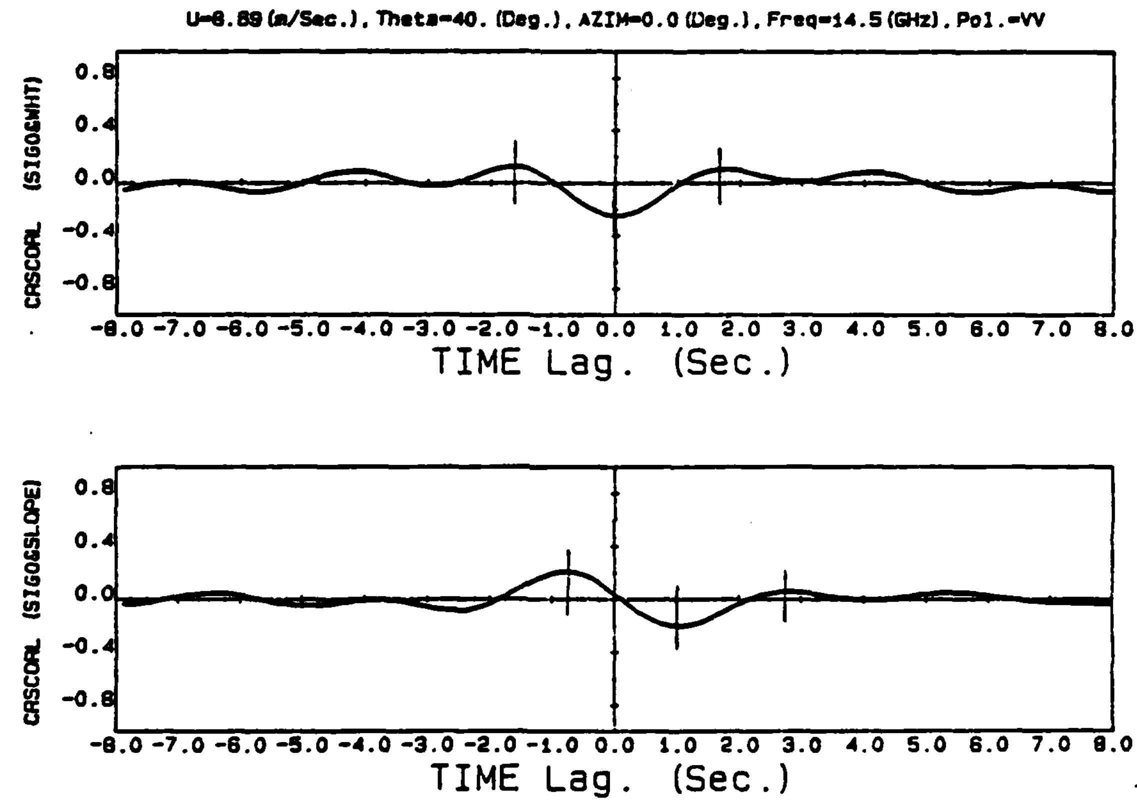

Figure 8.13
Cross-correlation of σ^0 and wave-height. σ^0 leads the wave-height by about 1.7 sec (104°). Cross-correlation of σ^0 and slope. σ^0 leads the slope by about 0.75 sec (90°).

slope by about 1.6 seconds or about 1/3.6 of the dominant period of the large-scale wave (about 1/2.19 of the dominant period of the slope (about 165°)). The cross- correlation of $\Delta\sigma$ and wave height, Figures 8.14 and 8.15, shows that $\Delta\sigma$ leads the wave height by about 2.5 seconds which is about 1/2.35 of dominant period of the large-scale wave or about 153 degrees ahead of the crest of the wave. Note that the cross-correlation of the $\Delta\sigma$ and wave height for HH is stronger than for VV, but the locations of the peaks are reasonably consistent.

Since the spatial cross-correlation functions should be studied for an estimation of the spatial distribution of the capillary waves over the large-scale waves, a set of spatial profiles has been determined using the method described in Chapter 7. Figure 8.16 shows the profiles of the wave height for a sample record in the temporal and spatial domains and Figure 8.17 shows the comparable slope profiles. These spatial slope profiles were used to compute a theoretical scattering coefficient profile in the spatial domain as shown in Figure 8.18. The relationship between the scattering coefficient and the wave height is very nonlinear. Consequently, the assumptions of Chapter 7 regarding transformation from temporal to spatial domain probably are not sufficiently good to justify a direct transformation of the scattering coefficient to the spatial domain. Accordingly, a transformation has been made of the values of $\Delta\sigma$. For relatively small values of $\Delta\sigma$ the relation should be sufficiently close to linear that the transformation has a reasonable chance of success. A sample is shown in Figure 8.19. For larger values of $\Delta\sigma$ the values presented in the spatial domain probably are not very accurate. A simple set of spatial autocorrelations is presented in Figure 8.20 for

Ave. of 10 Runs Sept.21st/79 (SPCLR OUT 6. dB GT MEAN) - (FILT .35 Hz)

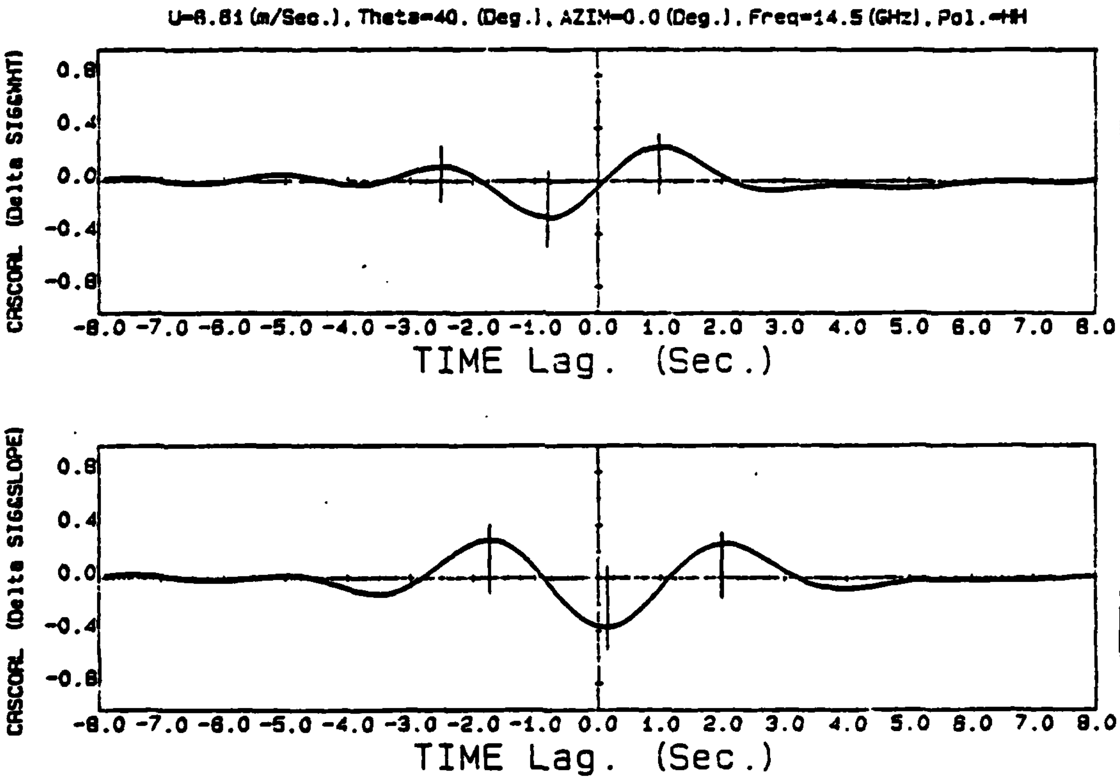

Figure 8.14
Cross-correlation of $\Delta\sigma$ and wave-height. $\Delta\sigma$ leads the wave-height by about 2.5 sec (153°). Cross-correlation of $\Delta\sigma$ and slope. $\Delta\sigma$ leads the slope by about 1.6 sec (165°).

Ave. of 5 Runs Sept. 21st/79 (SPCLR OUT 6. dB GT MEAN) - (FILT .35 Hz)

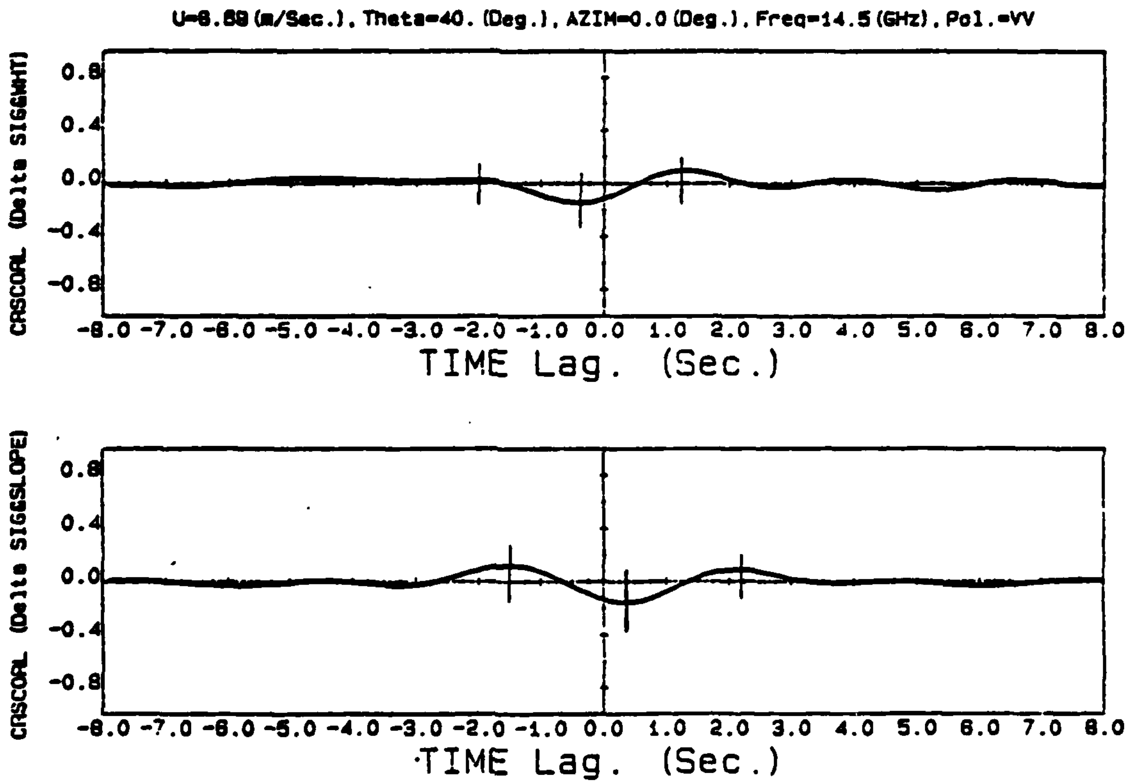

Figure 8.15

Cross-correlation of $\Delta\sigma$ and wave-height. $\Delta\sigma$ leads the wave-height by about 2.5 sec (153°). Cross-correlation of $\Delta\sigma$ and slope. $\Delta\sigma$ leads the slope by about 1.6 sec (165°).

wave height and slope. It seems the dominant spatial wave length is about 70 m and the dominant slope wave length is about 42 m. Figure 8.21 shows the spatial cross-correlations between $\Delta\sigma$ and wave height and slope for the same data set.

Spatial analysis has just started and requires considerably more study before conclusions can be drawn. Hence, the above presentations of results must be considered as very preliminary.

The final quantity of interest is the modulation transfer function, MTF (Section 6.5). Figures 8.22 and 8.23 illustrate the MTF for HH and VV polarization cases. Both the Alpers form R(f) and the NRL form m(f) are shown. Below 0.35 Hz the MTFs have more or less the same characteristics. R(f) has a minimum at about 0.1 Hz, and m(f) decreases monotonically. More smoothing and more sample averaging needs to be done for more stable, smooth characteristics. R(f) above 0.35 Hz has more noiselike characteristcs because the wave-height power spectrum, which is in the denominator of the MTF expression, would not have proper information beyond 0.35 Hz (Section 5.3). For both VV and HH polarization cases shown in Figures 8.24 and 8.25, the power spectra have similar characteristics, except for some peaks at 0.22 Hz and 0.35 Hz for VV cases. Note that for VV only 5 sample records were averaged whereas for HH 10 samples have been averaged. Hence, one would expect more smooth and stable characteristics in power spectra and MTF for HH case. The wave height power spectra of both cases have been plotted in Figures 8.26 and 8.27. Both have a single peak around 0.15 Hz.

The average coherence for function for radar power return spectra and wave height spectra have been found both for HH and VV polarization and plotted in Figures 8.28 and 8.29. The average value of coherence

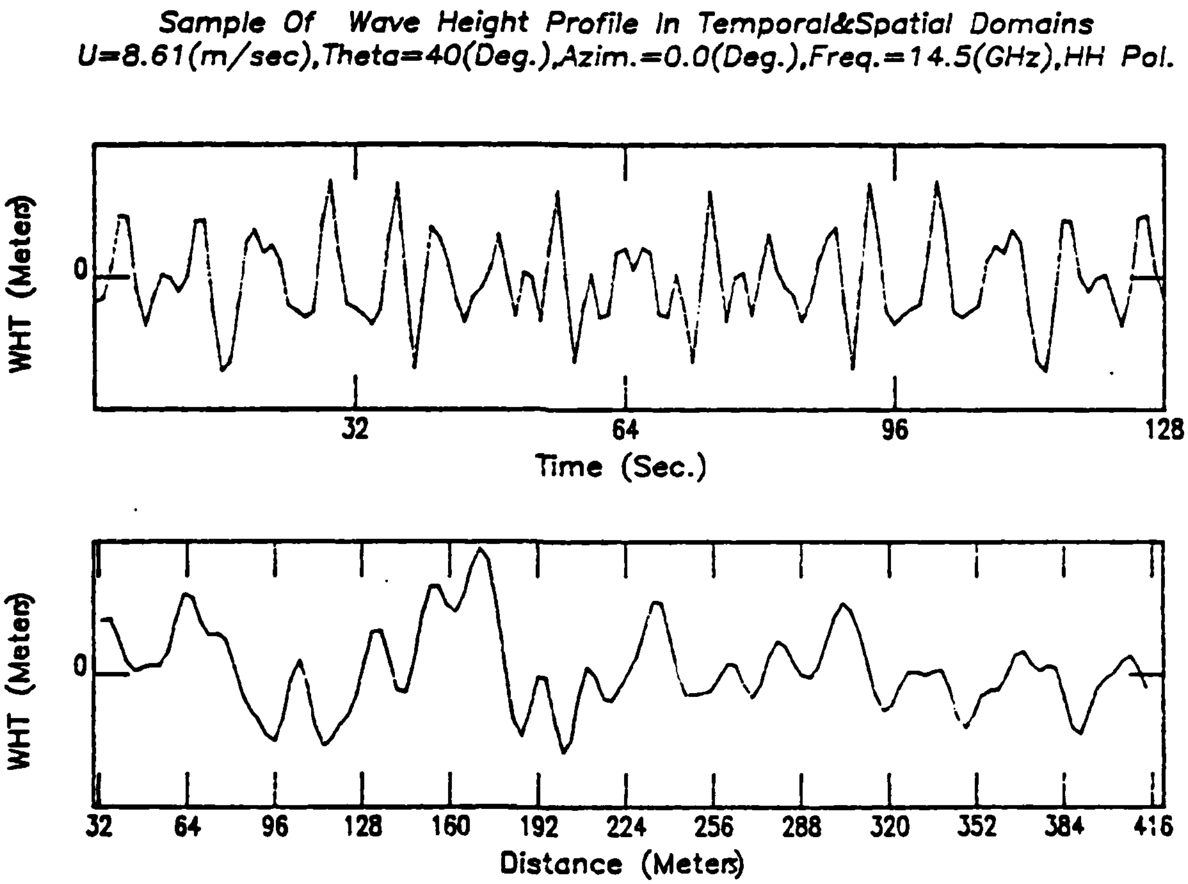

Figure 8.16
Sample of wave-height profiles in temporal and spatial domains

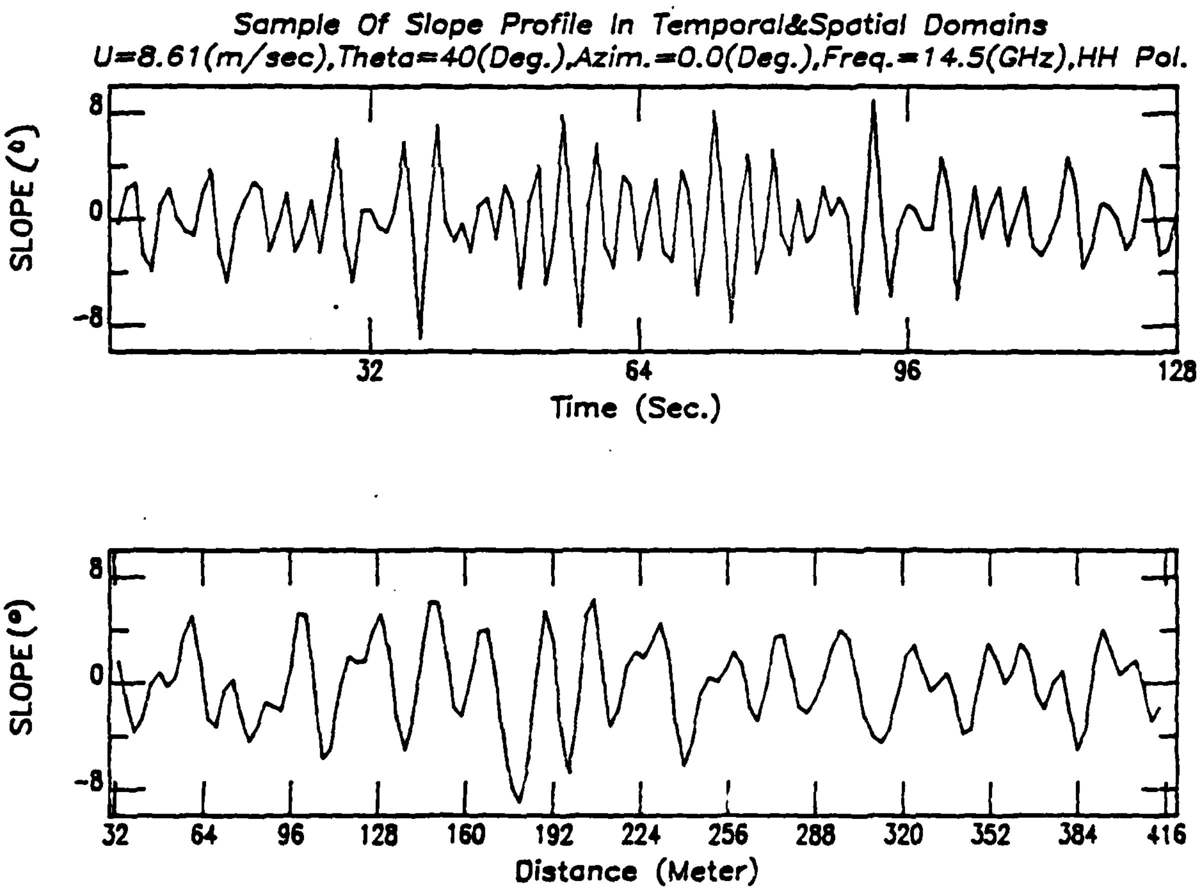

Figure 8.17
Sample of slope profile in temporal and spatial domains

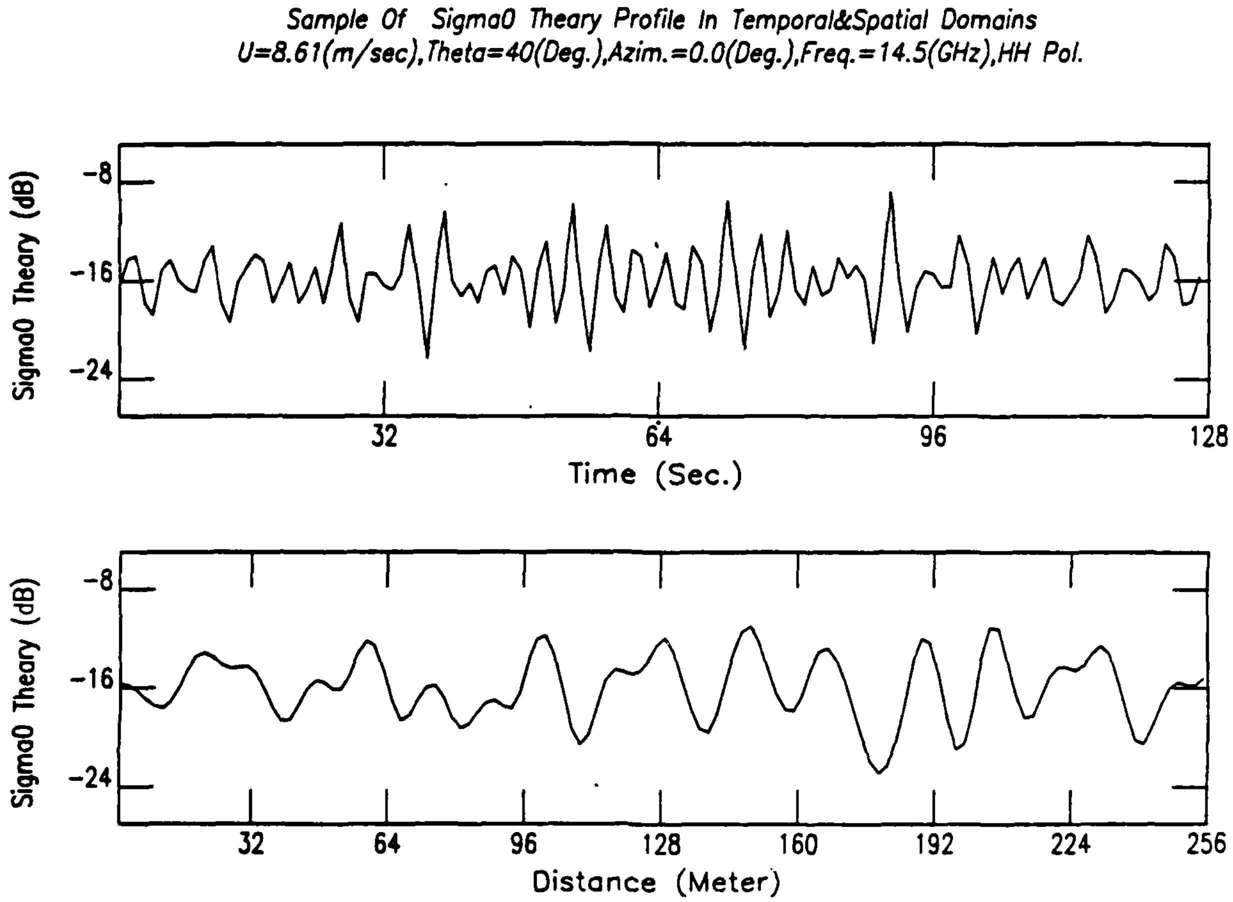

Figure 8.18
Sample of σ^0 theory profile in temporal and spatial domains

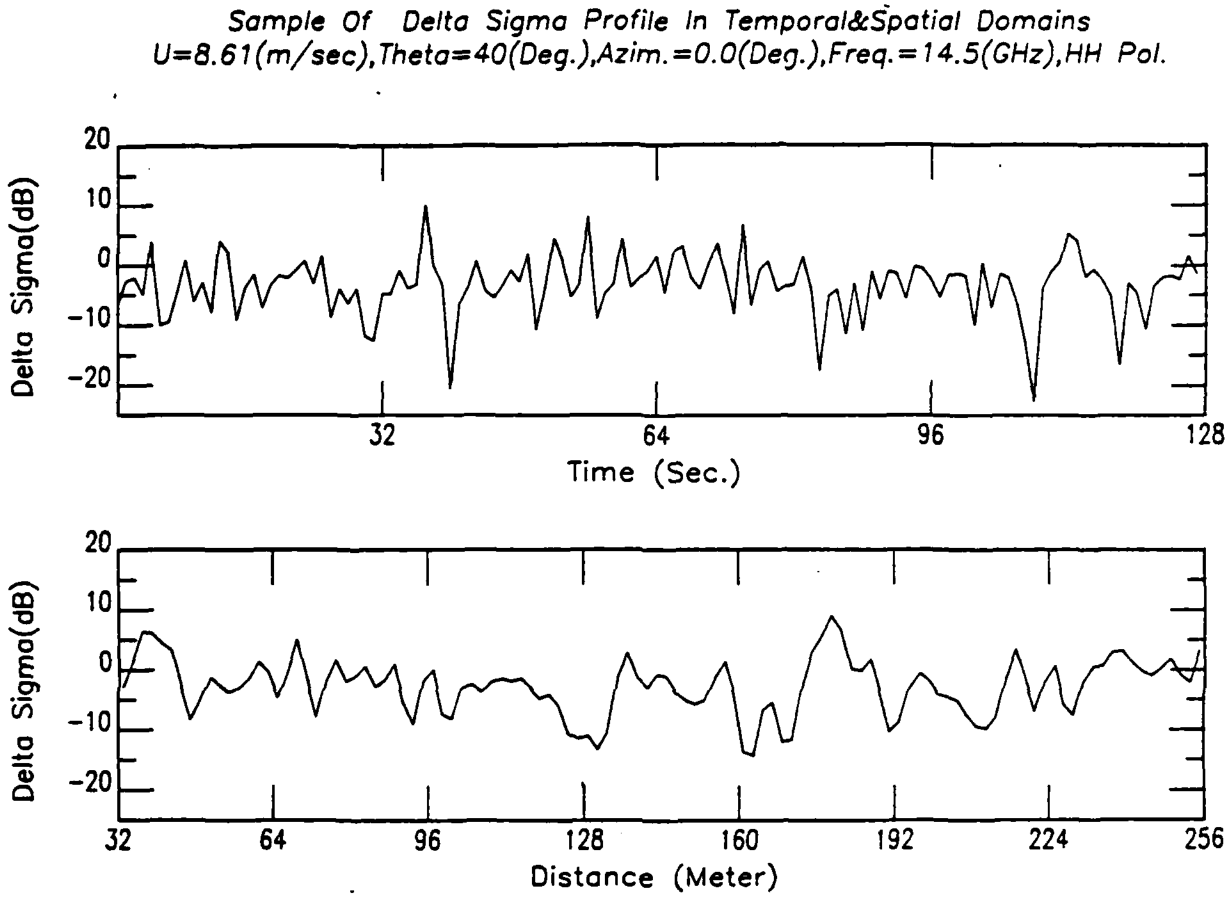

Figure 8.19
Sample of $\Delta\sigma$ profile in temporal and spatial domains

Ave. of 10 Runs Sept. 21st/79 - (FILT .35 Hz)

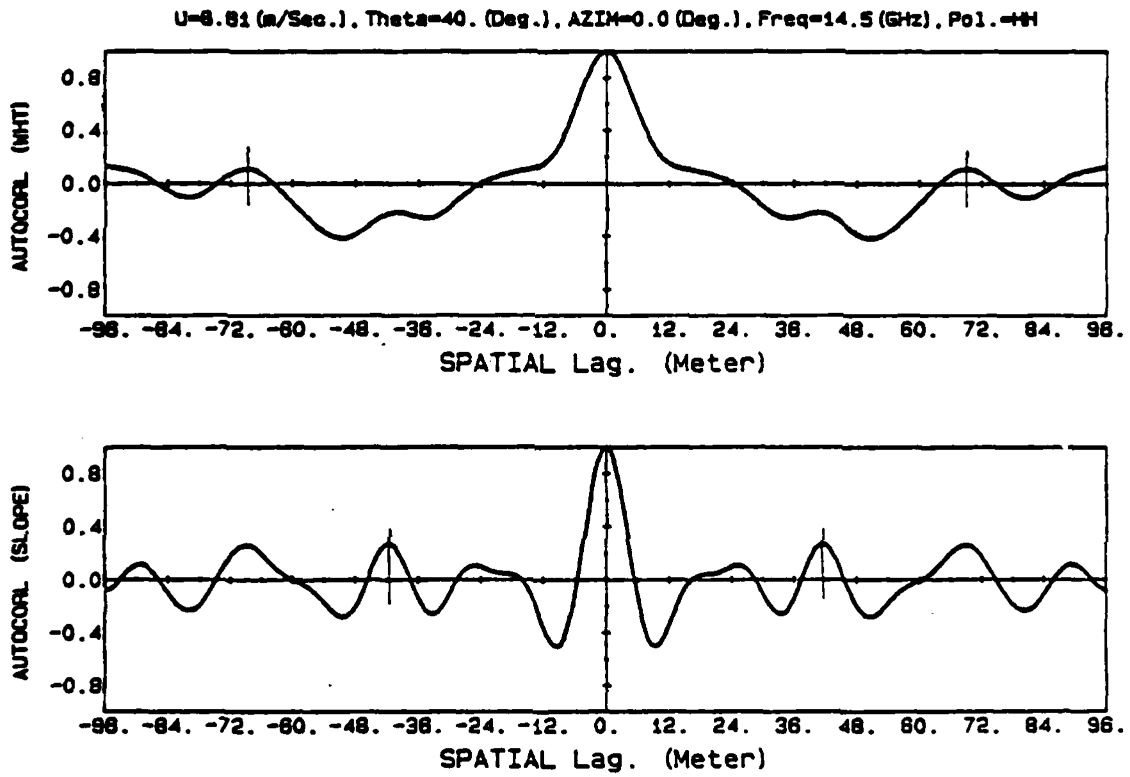

Figure 8.20
Spatial autocorrelation of wave-height. The dominant period is about 72 meters.
Spatial autocorrelation of slope. The dominant period is about 42 meters.

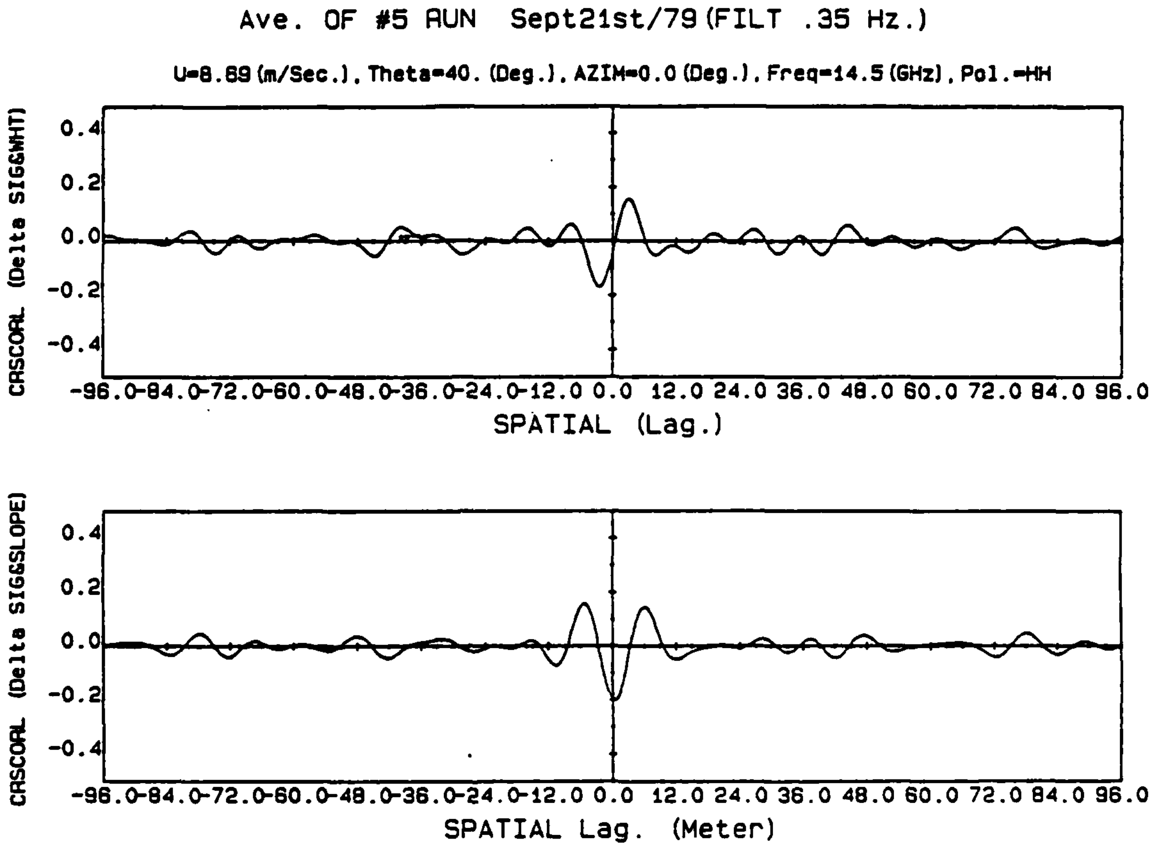

Figure 8.21
Cross-correlation between $\Delta\sigma$ and wave height and slope.

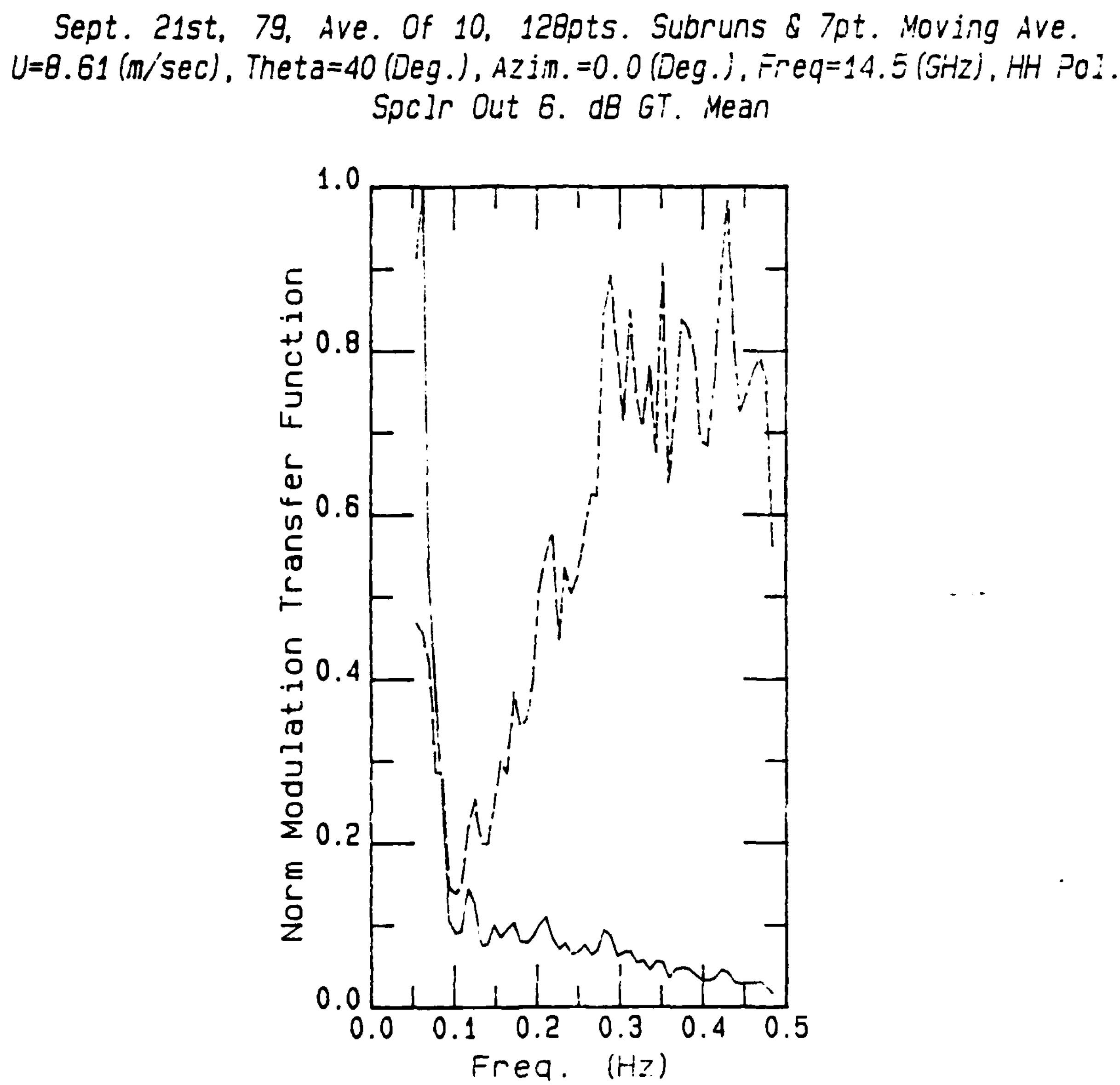

Figure 8.22
Normalized modulation transfer functions R(f) (dash line) and m(f) (solid line).

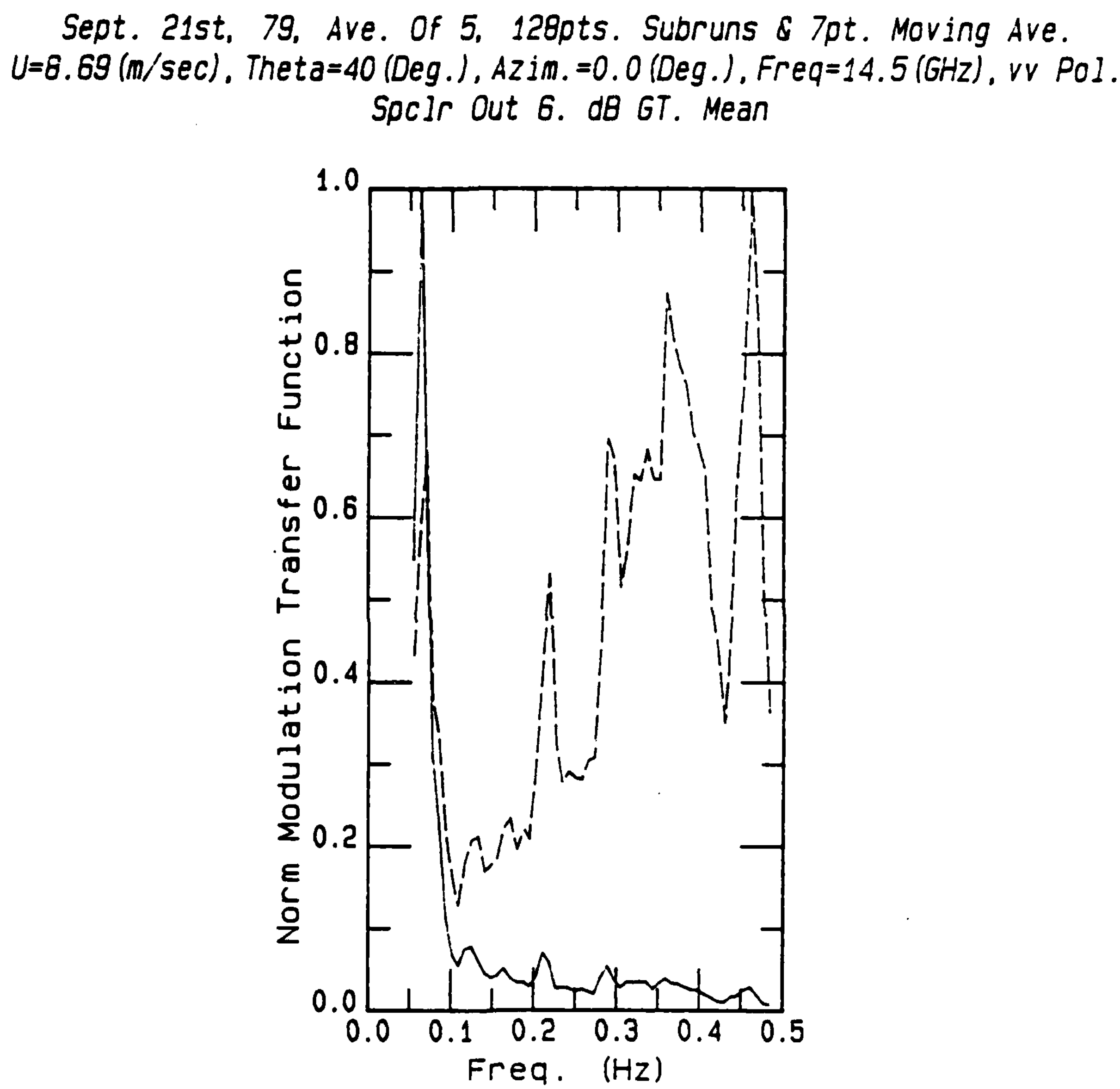

Figure 8.23
Normalized modulation transfer functions R(f) (dash line) and m(f) (solid line). Note it is not as smooth and stable as the HH MTF.

Sept. 21st, 79, Ave. Of 10, 128pts. Subruns & 7pt. Moving Ave.
U=8.61 (m/sec), Theta=40 (Deg.), Azim.=0.0 (Deg.), Freq=14.5 (GHz), HH Pol
Spclr Out 6. dB GT. Mean

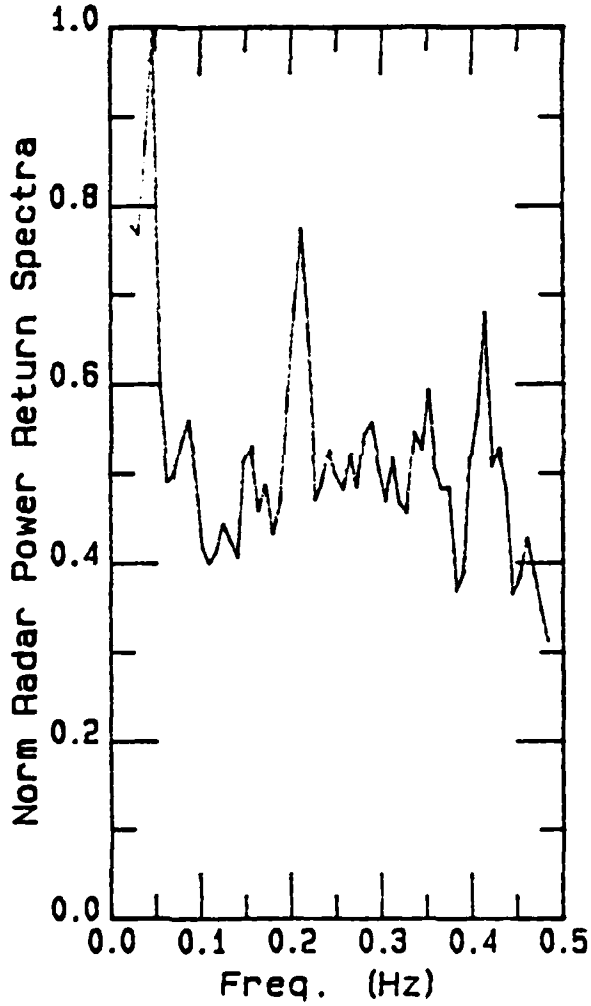

Figure 8.24
Normalized power return power spectra.

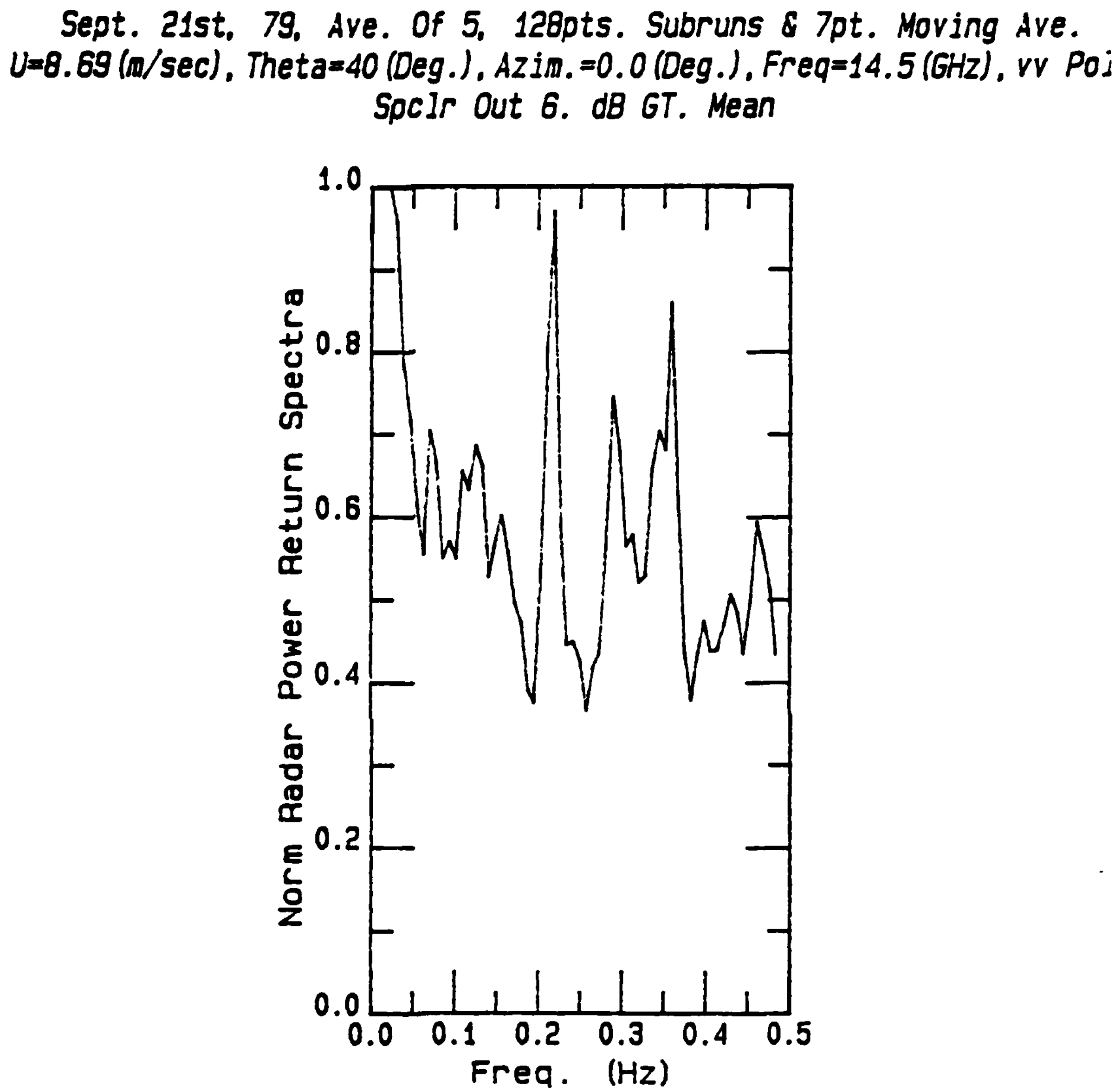

Figure 8.25
Normalized radar power return spectra.

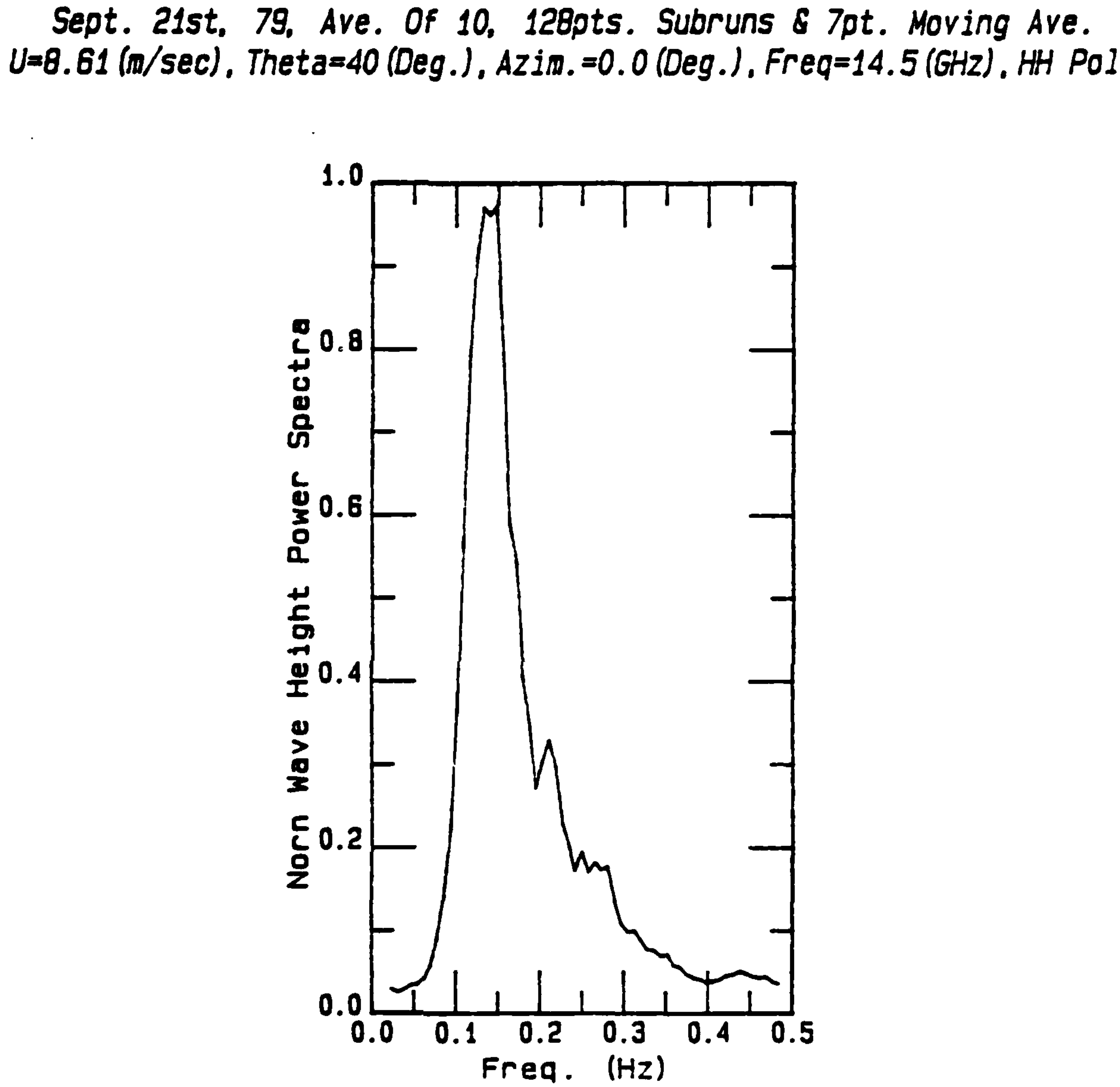

Figure 8.26
Normalized wave-height power spectra;
single peak about 0.15 Hz.

Sept. 21st, 79, Ave. Of 5, 128pts. Subruns & 7pt. Moving Ave.
U=8.69 (m/sec), Theta=40 (Deg.), Azim.=0.0 (Deg.), Freq=14.5 (GHz), vv Pol

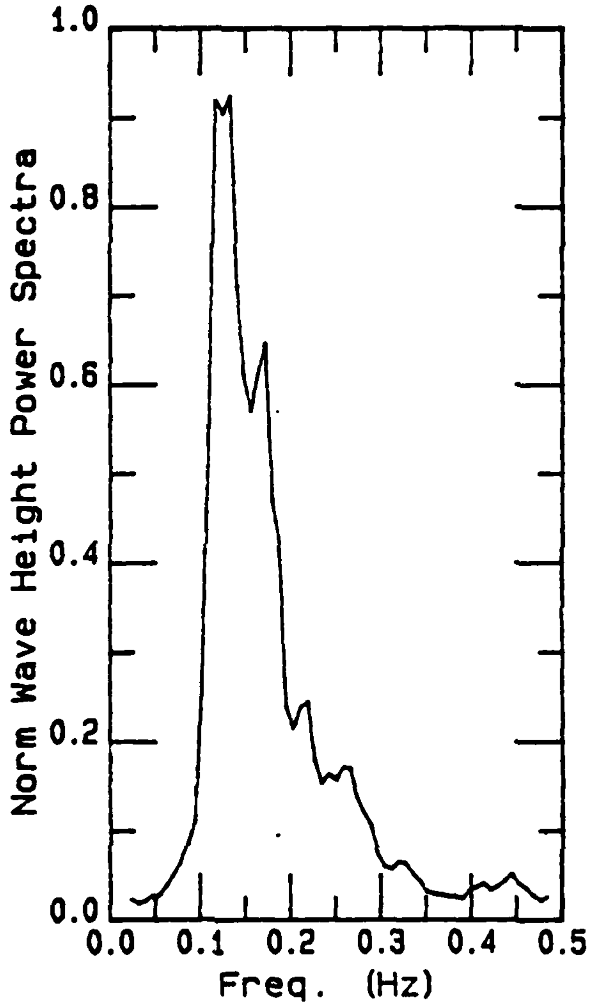

Figure 8.27
Normalized wave-height power spectra;
single peak about 0.14 Hz.

over the frequency for HH is 0.321 with standard deviation of 0.013 and for VV is 0.72 with standard deviaton 0.02. The coherence functions show more dependence between radar power return spectra and wave height for VV than for HH. Further study is needed to explain the difference. Plant [1980] stated that a useful, though arbitrary, convention in analyzing the MTF is to use only data for which the coherence is greater than 0.3. One result of a low value of coherence function is that the corresponding values of MTF have large variances.

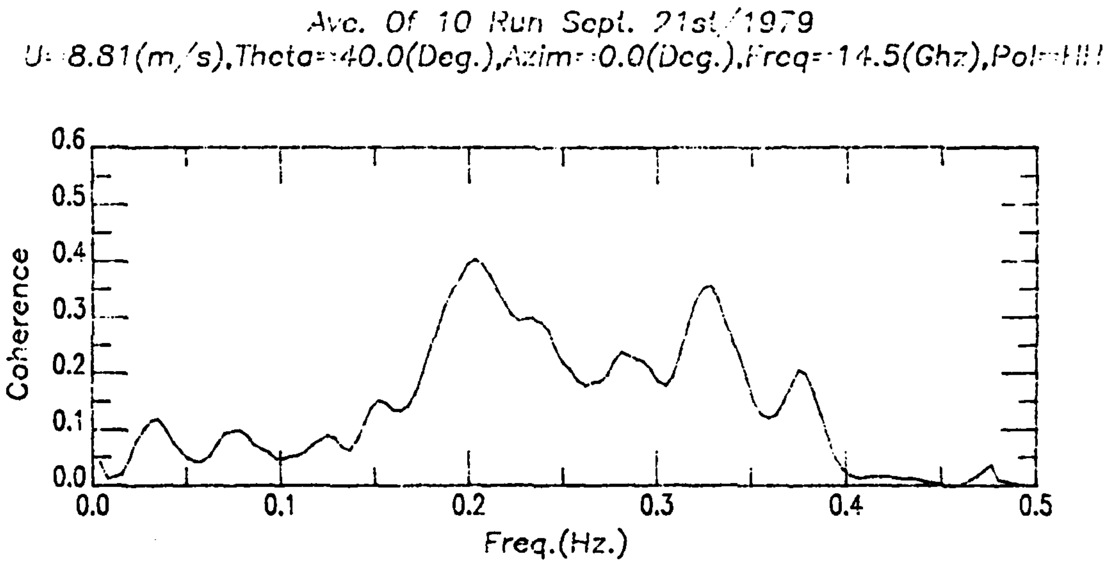

Figure 8.28
Coherence function for horizontal polarization

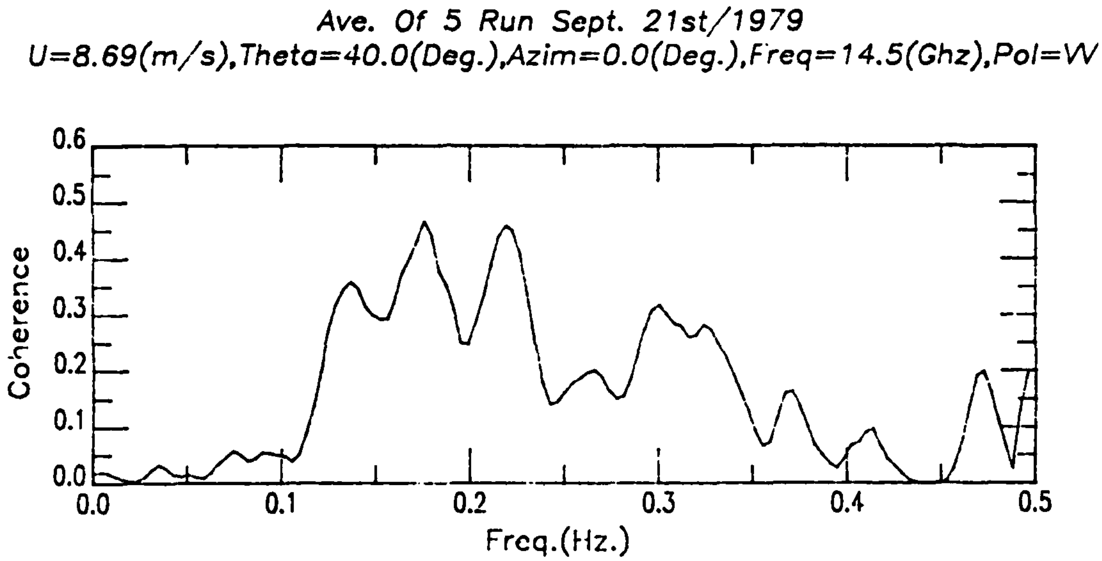

Figure 8.29
Coherence function for vertical polarization

9.0 DISCUSSION AND CONCLUSIONS

9.1 General Discussion

Methods have been developed for analysis of the University of Kansas measurements of radar cross-section and wave height as a function of time that were made as part of Project MARSEN from the Noordwijk platform in the North Sea off the Dutch coast during September through November 1979. The radar spectrometer was unique in two ways:

1. It could operate over a band of frequencies from 8 to 18 GHz, whereas most previous measurements have been made at single frequencies or groups of widely separated spot frequencies.
2. The range-tracker in the system permitted determination of the instantaneous wave height at the centroid of the radar footprint, whereas previous measurements have depended upon wave gauges located some distance from the radar footprint or upon integration of the velocity obtained by Doppler-frequency measurement to obtain the instantaneous wave height.

The first capability permits observations over a range of Bragg-resonant ocean wave numbers (K) not previously studied. The second permits development of cross-correlations between radar cross-section and wave height not previously possible.

The overall experiment provides information that permits determination of the apparent wave spectrum S(K) in the capillary region, as well as empirical observations of the radar scattering coefficient over a wide range of controlled conditions. These studies are the subject of other reports in this series. This report concentrates on the methodology and preliminary results of the study of

modulation of the radar cross-section, and consequently of the Bragg-resonant capillary-wave components, associated with the structure of the underlying larger waves.

Because of the large number of parameters that could be varied during the experiment (frequency, polarization, angle of incidence, look direction relative to the wind), the individual observation runs were relatively short. This means that the statistics of this experiment are somewhat less stable than those for experiments where fewer parameters had to be varied. Typical data runs varied from 3 to 7 minutes. However, on many days observations with the same radar parameters were repeated often enough to improve the stability of the statistical results. Because of the relatively short duration of the individual runs, simplification of data processing (involving numerous FFT operations) was achieved by standardizing on 128-second sequences. For the case analyzed as an example in this report (21 September 1979, 40° angle of incidence) this meant that averages could be obtained for 5 vertically polarized (VV) and 10 horizontally polarized (HH) 128-second samples.

Algorithms were developed to compute the modulation transfer functions (MTFs) used by other investigators, so that comparisons are facilitated. Because the instantaneous wave heights were measured, it is possible to calculate the instantaneous slopes for the underlying larger waves, on the assumption that these waves are long-crested. One can then calculate the scattering coefficient variations that would be observed if there were no modulation of the capillary waves by using the capillary wave spectrum S(K) in the theoretical expression for scattering—and the S(K) used can be that derived from the experiments

themselves. The difference of the observed radar scattering coefficient and the one that would be observed without modulation is therefore a measure of the modulation, here called the modulation index.

This instantaneous modulation index is then, in our analysis, cross-correlated with the instantaneous record of wave height and that of wave slope to obtain new measures of the variation of the modulation over the underlying larger waves (previously only frequency-domain measures have been used). Furthermore, the RMS value of this index represents a new measure of the size of the modulation of the capillary waves. Preliminary interpretations for the correlation with wave height have been made here for the sample case studied. The interpretation of the correlation with wave slope remains to be developed.

In the course of the analysis it became obvious that ''specular events'' or ''sea spikes'' were present in most of the measurements. A technique was developed for removing these from the data used in analysis of the modulation phenomenon, but a study of these anomalies themselves will be important as the data analysis proceeds.

The observations used in this preliminary study were for the radar looking in the upwind direction. The same methods can be used for the downwind direction. For the crosswind direction the analysis can be simplified, since the long-crested assumption (and the available point measurement of wave height) precludes assuming any slopes relative to the radar look direction. Crosswind data analyses will be presented in future reports in the series.

An algorithm has been developed to convert the time histories of

the waves into spatial descriptions of appropriate parts of the wave trains. This technique can be used readily with the wave-height and wave-slope records, but its use with the radar cross-section has more doubtful validity. The wave height can be described by a series with terms of the form $exp(j\omega t + Kx))$, but the radar signal is nonlinearly related to this series. Further study is required to determine whether the difference between the observed radar signal and that due to uniformly distributed capillary waves is sufficiently small that a linear approximation can be made that would validate the spatial Fourier-like series for this quantity.

The remainder of the discussion in this section relates to the preliminary results obtained by analysis of the sample data set for 21 September at 40° angle of incidence.

9.2 Discussion of Results for Sample Data Set

The preliminary analysis of the Noordwijk 1979 data has shown that the measured scattering coefficient leads the wave height by about 1.8 sec. The full period of the dominant wave is about 5.8 sec so 1.8 sec corresponds to about 104°. The measured scattering coefficient leads the maximum slope by 1.0 sec. Note that the full period of the dominant slope component is about 3.5 sec, so 1.0 sec corresponds to 103° for both HH- and VV-polarizations.

These phase differences, especially the phase difference of the scattering coefficient with respect to slope, brought up the idea of modulation index, $\mu(t)$ or $\Delta\sigma$, the ratio of total scattering coefficient (based on the instantaneous footprint of the radar antenna beam) to the theoretical scattering coefficient that would be found if

capillary wave amplitude were uniform over the large-scale waves. The theoretical value is also based on $S_4(K)$, where K is the instantaneous Bragg-resonant wave number. The RMS value of modulation index is 0.876 with a standard deviation of 0.349 for HH-polarization and 0.623 with standard deviation of 0.044 for VV-polarization.

The apparent phase relations between the modulation and the dominant wave and slope components are illustrated in Figure 9.1. An apparent discrepancy exists between the relations with the dominant ''slope wave'' and the dominant ''waveheight wave'' because of the higher frequency of the dominant slope (associated with the larger influence of the high-frequency components of the wave on the slope than on the height). Interpretation of this point remains to be established.

Figure 9.1a shows that the largest modulation appears 62° back from the crest of the wave, on the upwind side, but a relatively strong modulation peak appears to be 153° ahead of the crest. These do not appear to be artifacts of the data handling procedure, so one must assume that they are real, pending analysis of other data sets.

Figure 9.1b is a similar illustration indicating the location of the modulation peaks relative to the dominant slope component. These appear to be symmetrical and near the point of minimum slope. This is consistent with the location of the maximum modulation on the back face of the dominant wave, but since the dominant wave and slope have different periods, one must use caution in this interpretation.

As indicated, the interpretation of the locations of the modulation peaks is confused because one cannot simply use the ideas that come from a very-narrow-band process. Furthermore, the 1-second

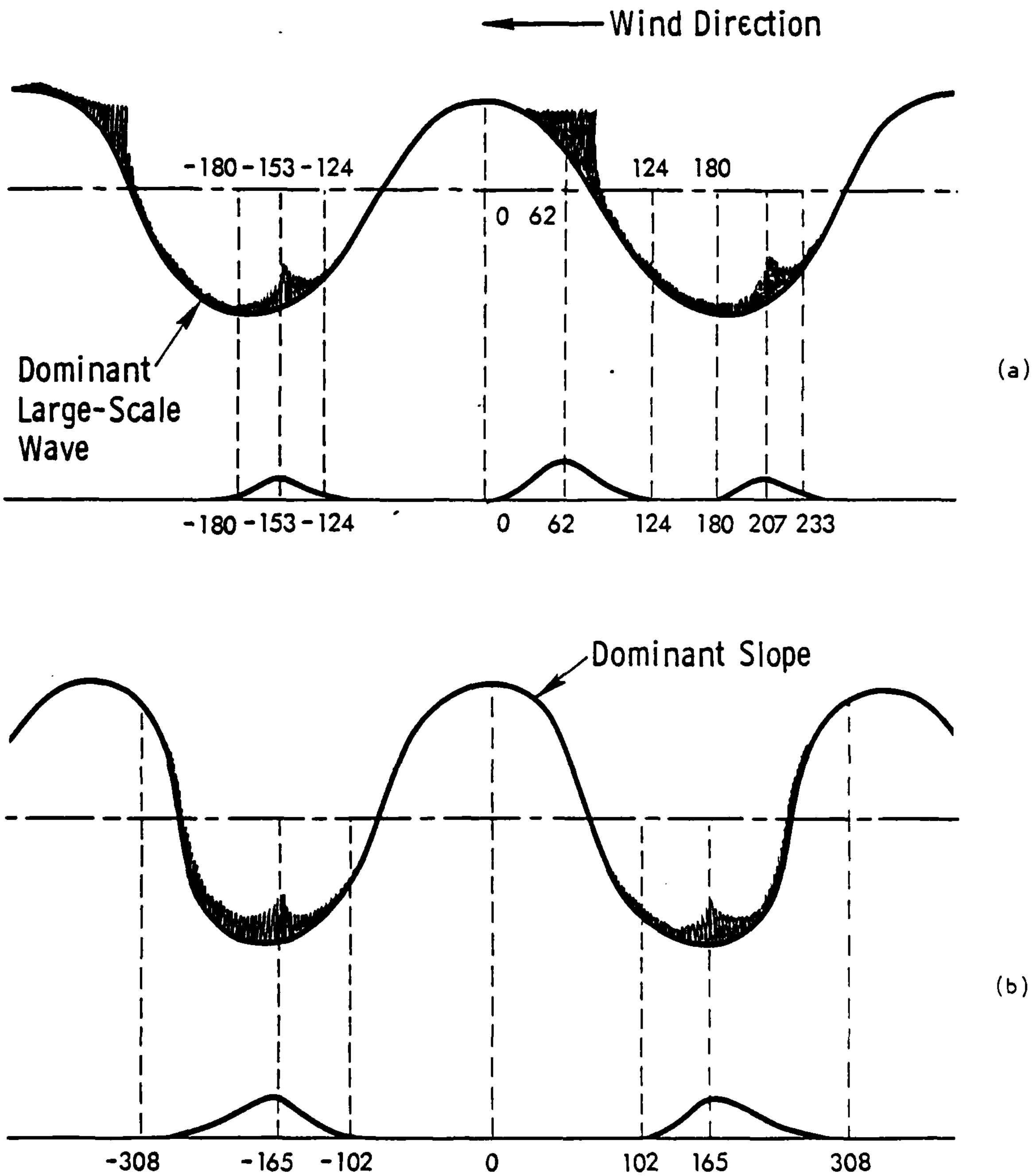

Figure 9.1
Graphic illustration of the nature of the results of the correlation study. The locations of the maximum correlations between apparent capillary amplitude (from $\Delta\sigma$) and wave height on the dominant component are shown in (a) and the locations relative to the dominant slope component are shown in (b). The apparent locations of maximum capillary-wave amplitude are sketched on large sinusoids representing dominant large-wave components. The sketches below show more quantitatively the apparent distribution of capillary amplitudes, but these sketches should not be considered accurate as to amplitude --they are intended only to illustrate the nature of the waves.

sampling interval used to measure the wave height may have been too great to give a good estimate of the slope spectrum, i.e., the latter may be corrupted by aliasing since its components are multiplied by 2, thereby enhancing the effect of the higher-frequency components of the measured spectrum that are more subject to corruption by aliasng. Clearly more study is needed.

The study of modulation in the spatial domain has just started, and more attention to the basic assumptions underlying it should be given before quantitative results are presented in the spatial domain.

9.3 Discussion

9.3.1 The Validity of the Analysis

The validity of this analysis is directly related to the goodness of the theoretical scattering coefficient estimation. Two different problems arise in estimating the theoretical scattering coefficient: first, the validity of the estimate of the K-spectrum of the capillary wave region $S_4(K)$, and second the effect the computer calibration factor which differs from run to run (Section 6.2) has on the true value of the theoretical scattering coefficient. The $S_4(K)$ which has been used in preliminary analysis was based on an average of three days of data in the windspeed range of 8.0 - 10.0 m/sec. The average calibration factor (ratio of the mean of the measured scattering coefficient to the mean of the theoretical scattering coefficient) is 17.5 with standard deviation of 4.8 for HH-polarization and 3.04 with standard deviation of 0.66 for VV-polarization.

9.3.2 Further Study Needed

The preliminary results have shown that the idea of modulation index can describe the phenomenon of capillary modulation over the large-scale wave. For further analysis a more accurate model of the K-spectrum $S_4(K)$ is needed. Note that in preliminary analysis, each set of theoretical scattering coefficient profile has been normalized to the ratio of the average of measured scattering coefficient to the average of theoretical scattering coefficient. This should be checked to make sure that this is the best approach for further analysis.

The next phase of the analysis is to test the idea of modulation index for different conditions (wind speed and pointing angle) to find out how the modulation index varies as a function of different parameters. The third phase of the analysis is to see if the modulation index can be expressed as a 'simple' function. At the end, one not only can estimate the amount of modulation and the location of the peaks of the modulation with respect to the slope, but also can give a idea about the 'dominant' shape of this modulation as a function of wind speed.

Comparison with cross-wind observations should be especially interesting. The slope, under the long-crested-wave assumption is always zero at crosswind. Viewing the capillary wave components normal to the predominant waves may also provide useful insights into the capillary distribution process.

APPENDIX A

Calculation of the Goodness of Estimation

Based on 90 Percent of Confidence Interval

The cross-correlation of two proper finite functions, x(t),y(t), can be represented as

$$C(\tau) = \sum_n (ac + bd)\cos(\omega_n \tau) + (bc - ad)\sin(\omega_n \tau) \quad \text{(A.1a))}$$

$$= \sum_n p_n^2 \cos\left(\frac{2\pi n}{N}\tau\right) + q_n^2 \sin\left(\frac{2\pi n}{N}\tau\right) \quad \text{(A.1b)}$$

where a,b c,d are Fourier components of two functions:

$$X(t) = \sum_n a_n \cos\left(\frac{2\pi n}{N} t\right) + b_n \sin\left(\frac{2\pi n}{N} t\right) \quad \text{(A.2)}$$

$$y(t) = \sum_n c_n \cos\left(\frac{2\pi n}{N} t\right) + d_n \sin\left(\frac{2\pi n}{N} t\right) \quad \text{(A.3)}$$

The Fourier coefficients are unique for each set of records.

The quantities p_n^2 and q_n^2 have a probability density functions given approximately by [Donelan and Pierson, 1981]

$$f(p_n^2)\,dp_n^2 = \exp\left(-\frac{p_n^2}{S_n}\right) d\left(\frac{p_n^2}{S_n}\right) \quad \text{(A.4)}$$

$$S_n = S\left(\frac{N}{n}\right) = \int_{\frac{n}{N} - \frac{1}{2N}}^{\frac{n}{N} + \frac{1}{2N}} S(f)\,df \quad \text{(A.5)}$$

where $S(f)$ is the 'true', but unknown, cross-spectrum of the random

process which is assumed to be approximately a stationary Gaussian process.

Equation (A.4) is a chi-square distribution with two degrees of freedom with an unknown parameter, .

Given just one set of time profiles the values of p_n^2 must be smoothed over frequency as in

$$p_n^2 = \frac{1}{2R+1} \sum_{n-R}^{n+R} p_s^2 \tag{A.6a}$$

or more generally

$$\overline{p_n^2} = \sum_{n-R}^{n+R} \delta_s p_s^2 \tag{A.6b}$$

where

$$\Sigma \delta_s = 1 \tag{A.7}$$

so as to obtain a smoother function for the cross-spectrum estimate by means of the assumption, which may not always be correct, that the true spectrum is slowly varying. If the cross-spectrum is slowly varying, then the values of $\overline{p_n^2}$ will be approximately distributed according to a chi square distribution with 2(2R+1) degrees of freedom. Successive estimates will not be independent. Those elemental frequency bands that are 2R+1 bands apart will be independent. With five pooled

samples and a triangular moving window, the value of $\overline{p_n^2}$ could be shown as

$$\overline{p_n^2} = \frac{1}{3}\left\{\frac{1}{3}\left(p_{n-2}^2 + p_{n+2}^2\right) + p_n^2 + \frac{2}{3}\left(p_{n-1}^2 + p_{n+1}^2\right)\right. \qquad \text{(A.8)}$$

If one gets an average of 10 individual sample records of $\overline{p_n^2}$ then equation (A.5) can be estimated by 100 degrees of freedom.

For a chi-square distribution with 2 degrees of freedom, it can be shown that

$$P\left(0.103 < 2\,\frac{\overline{p_n^2}}{S_n} < 5.99\right) = 0.90 \qquad \text{(A.9)}$$

and since the value of $\overline{p_n^2}$ is known from the FFT, it follows that

$$P\left(0.334 < \frac{S_n}{p_n^2} < 19.42\right) = 0.90 \qquad \text{(A.10a)}$$

$$P\left(0.334\,p_n^2 < S_n < 19.42\,p_n^2\right) = 0.90 \qquad \text{(A.10b)}$$

Given just one value of p_n^2 , the value of the cross-spectrum is not known to within a factor of 58 at the 90 percent confidence level. For the 5 point, triangle moving average, 10 different sample

records, the estimate of $\bar{p}_n^2$ has 100 degrees of freedom so that

$$P\left(77.93 < \frac{100\,\bar{p}_n^2}{S_n} < 124.34\right) = 0.90 \qquad \text{(A.11a)}$$

so that

$$P\left(\frac{100}{124.34} < \frac{S_n}{\bar{p}_n^2} < \frac{100}{77.93}\right) = 0.90 \qquad \text{(A.11b)}$$

$$P\left(0.804\,\bar{p}_n^2 < S_n < 1.283\,\bar{p}_n^2\right) = 0.90 \qquad \text{(A.12)}$$

The true cross-spectrum is known to within about $\pm$ 23.9 percent or a range of 47.9 percent at 90 percent confidence level.

APPENDIX B

Theoretical Development of 'Events' Effect (based on Moore, 1981)

For the theoretical development a simplified model involving a uniform capillary-wave distribution is assumed (Section 5.4). It further is assumed that *randomly located specular points occur.* The waves are assumed to be one-dimensional traveling in the direction of the wind.

The Bragg-scatter component is made up of a coherent sum of the voltages associated with scatter from each individual capillary wavelet. The voltage received from an individual capillary wavelet is V_c. The voltage associated with the scatter from an individual specular point is V_p. The total number of capillary wavelets in a footprint is n_c and the total number of specular points is n_p.

Assume a resolution cell with length L and width W. The radar is at a height h and has both vertical and horizontal beamwidths .

The transverse dimension of the footprint is

$$W = \beta R \tag{B.1}$$

and the longitudinal dimension is

$$L = \frac{\beta R}{\cos\theta} = \frac{\beta h}{\cos^2\theta} \tag{B.2}$$

since

$$h = R\cos\theta \tag{B.3}$$

Consequently the footprint area is

$$A = \frac{\beta^2 h^2}{\cos^3\theta} \tag{B.4}$$

The total voltage received from the capillary waves is proportional to the number of them because of the coherent additions, that is,

$$V_{rc} = n_c V_c \tag{B.5}$$

Consequently, the square of the received voltage is

$$V_{rc}^2 = n_c^2 V_c \tag{B.6}$$

Note that the scattering coefficient is an ensemble average that is proportional to V_{rc}^2. Consequently the scattering coefficient is given by

$$\sigma_{rc}^2 = M \langle V_{rc}^2 \rangle / A = M n_c^2 \langle V_c^2 \rangle / A \tag{B.7}$$

Where M is a constant including the various radar parameters and the other quantities have been designated above.

Since the 'events' occur at random, the voltage due to them do not add coherently. Rather, the power must be added. Thus, the mean-square received voltage for the events is given by

$$\langle V_{rp}^2 \rangle = n_p \langle V_p^2 \rangle \tag{B.8}$$

where n_p is the mean number of events per footprint. This may be less than 1 since many footprints must be averaged to obtain the ensemble average of (B.8). Using this expression we may determine a scattering coefficient for the events:

$$\sigma^{\circ}_{rp} = \frac{M\langle V_{rp}^2\rangle}{A} = \frac{M n_p}{A}\langle V_p^2\rangle \tag{B.9}$$

The total scattering coefficient is the sum of those due to the capillary waves from (B.7) and those due to the events from (B.8). Thus

$$\sigma^{\circ} = \sigma^{\circ}_{rc} + \sigma^{\circ}_{rp} = \frac{M}{A}\left(n_c^2\langle V_c^2\rangle + n_p\langle V_p^2\rangle\right) \tag{B.10}$$

For a given length L of the illuminated area, one may obtain n_c and n_p. n_c is simply the length divided by the Bragg-resonant wavelength on the surface.

$$n_c = \frac{L\sin\theta}{\lambda/2} \tag{B.11}$$

n_p is the ratio of the length L of the footprint to the mean spacing s_p between events

$$n_p = \frac{L}{s_p} \tag{B.12}$$

Substituting these values into (B.8) gives

$$\frac{\sigma^{\circ}A}{M} = \frac{4L^2\sin\theta}{\lambda^2}\langle V_c^2\rangle + \frac{L}{s_p}\langle V_p^2\rangle \tag{B.13}$$

which may be rewritten in terms of the capillary wave scattering coefficient and a correction term as

$$\sigma^{\circ} = \frac{4(\langle V_c^2 \rangle M L^2 \sin^2\theta}{\lambda^2 A}\left(1 + \frac{\langle V_p^2 \rangle \lambda^2}{4 \langle V_c^2 \rangle S_p L \sin^2\theta}\right) \qquad \text{(B.14a)}$$

or

$$\sigma^{\circ} = \sigma^{\circ}_{rc}\left(1 + \frac{\langle V_p^2 \rangle}{\langle V_c^2 \rangle S_p} \frac{\lambda^2}{4h\beta} \cot^2\theta\right) \qquad \text{(B.14b)}$$

The first factor in the second term is an unknown quantity because we do not know the ratio of the mean power returned for an event to the mean power returned from an individual component of the Bragg scattering capillary waves. The quantity S_p is also an unknown at the present time, although it may be possible to find a value for S_p. At present, however, these unknown quantities are simply combined into a single unknown factor Q. The second factor in the second term involves parameters of the system, and is readily determined. The third factor depends, of course, on the angle of incidence. Thus, we may write this equation as

$$\sigma^{\circ} = \sigma^{\circ}_{rc}\left(1 + Q\left(\frac{\lambda^2}{4h\beta}\right)\cot^2\theta\right) \qquad \text{(B.15)}$$

Although the value of Q is unknown, we can compare results for tower and aircraft. Examples are shown in the tables. Table B.1 gives the variation of the ratio of the scattering coefficient including the

effect of the events to that ignoring the events and including only capillary-wave Bragg scatter for the tower experiment. Values of Q of 100 to 50,000 are presented. If Q is only 100 the events have little effect on the scattering. However, a value of Q of 10,000 gives a difference of over 10 dB with and without the events at 20 degrees, falling off to a negligible value at 80_{0}.

Table B.2 gives a comparable set of calculations for an aircraft at 3000 m altitude except that the minimum value of Q is 1000 and computations are carried out up to $Q = 5 \times 10_{-6}$. If one assumes that Q is somewhere between 10,000 and 20,000, in accord with the observation that tower experiments give 20 degree measurements between 11.7 and 14.5 dB higher than aircraft experiments, we can check Tables B.1 and B.2 to see if this is really the case. For Q = 10,000 at 20 degrees with the aircraft the difference is only .23 dB between considering and ignoring the events. Yet, this was the case where there was more than a 10 dB difference at two heights. For Q = 20,000 the effect of the events is still less than 0.5 dB for the aircraft, yet it is more than 13 dB for the tower.

Thus, one can use this to explain the difference between tower and aircraft measurements on the assumption that Q is between 10,000 and 20,000 for the condition of measurement.

Q \ θ°	20 dB	30 dB	40 dB	50 dB	60 dB	70 dB	80 dB
100	0.56	0.23	0.11	0.06	0.03	0.01	0.002
1000	3.77	1.90	1.01	0.53	0.26	0.10	0.02
10,000	11.71	8.13	5.57	3.60	2.07	0.94	0.24
20,000	14.58	10.79	7.93	5.54	3.47	1.72	0.47
30,000	16.29	12.43	9.45	6.88	4.52	2.38	0.69
50,000	18.46	14.55	11.47	8.72	6.08	3.45	1.09

TABLE B.1
The variation of the ratio of the scattering coefficient including the effect of the events to that ignoring the events and including only capillary-wave Bragg-scatter for tower experiment

Q \ θ°	20 dB	30 dB	40 dB	50 dB	60 dB	70 dB	80 dB
1000	0.02	0.01	0.004	0.002	0.001	0.0004	0.0061
5000	0.12	0.05	0.02	0.01	0.01	0.002	0.0005
10,000	0.23	0.09	0.04	0.02	0.01	0.004	0.001
20,000	0.46	0.19	0.09	0.04	0.02	0.01	0.002
5×10^5	5.76	3.22	1.82	1.0	0.50	0.21	0.05
5×10^6	14.58	10.79	7.93	5.54	3.47	1.72	0.47

TABLE B.2:
A comparable set of calculations of the ratio of the scattering coefficient including the effect of the events to ignoring the events and including only capillary-wave Bragg-scatter for an aircraft at 3000 m altitude

APPENDIX C

Computer Programs

The main goal of these computations is to calculate the theoretical value of ° based on instantaneous slope, determine the spatial data profile from the time-data profile and ultimately calculate the proper cross-correlations both in the time and spatial domains.

The processing routine consists of a main program (*EEN353*), *two* main sub-routines (CCA3G3 and HH03L3) and a large block of calculation routines. Figure C.1 shows the block diagram of the processing routine.

(a) EEN353 reads the first set of raw data and feeds it through HH03L3, which controls and provides the inputs to the calculation routines. Calculated values will be located in the buffer of EEN353. When the first set of calculations is complete, the second and third will be fed through HH03L3. Calculated results will be averaged by means of CCA3G3 routine. Note that in cross-correlation calculations the results will be smoothed and averaged in the frequency domain and then will be transformed to the time domain (Figure C.2).

(b) Low-pass filtering: FLTRR: This block low-pass filters the wave height time profile by means of an FFT routine. It transforms the h(0,t) from the time domain to the frequency domain, chops all frequency components which are greater than .35 Hz, and transforms the chopped spectrum to the time domain (Figure C.3).

(c) Slope calculation SSLLPP: This block takes the filtered wave height and computes the spatial derivatives by means of an FFT routine

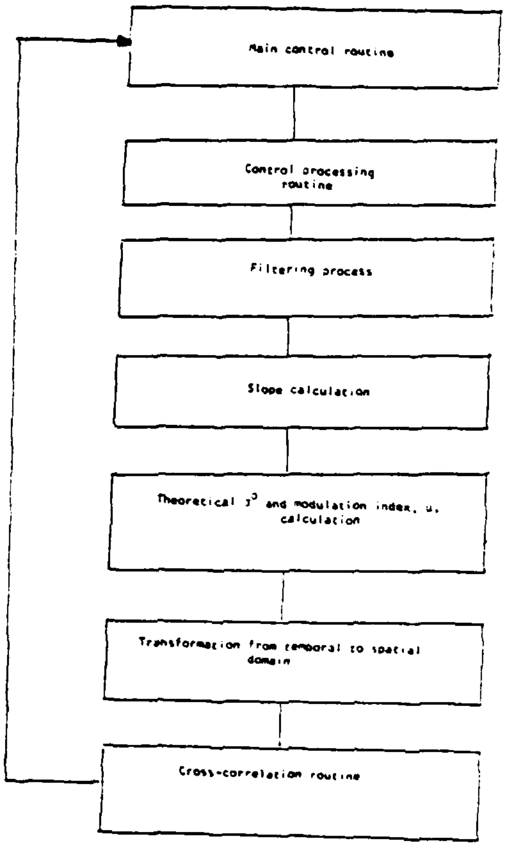

Figure C.1
Overall block diagram of processing

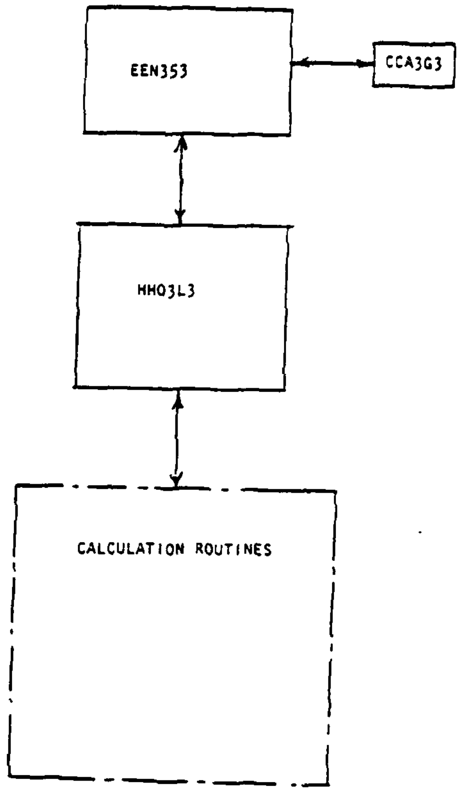

Figure C.2
Block diagram of control processing routine.
EEN353 is main controller; HH03L3 is the controller of the calculation routines; CCA3G3 transforms the averaged cross-spectra to cross-correlation.

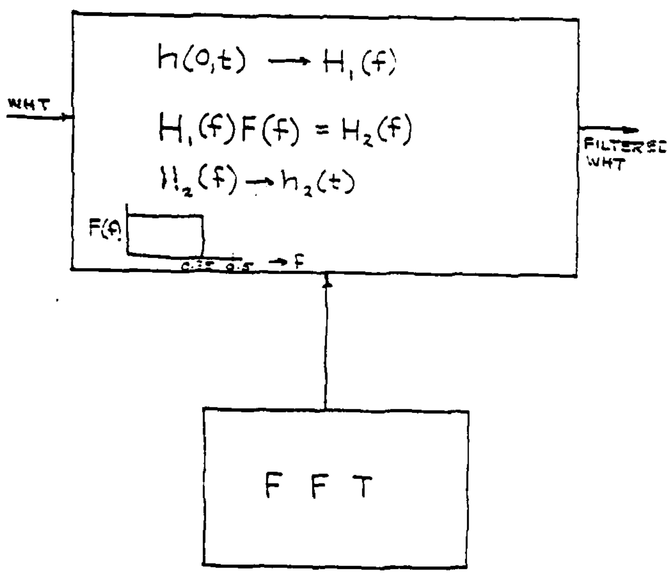

Figure C.3
Block diagram of lowpass filtering process (FLTRR)

(Figure C.4). Note that

$$h(x,t) = Re \sum_i b_i e^{j(\omega_i t + \omega_i^2 x/g)} \tag{C.1}$$

$$\frac{\partial h(x,t)}{\partial x} = Re \sum_i j b_i \frac{\omega_i^2}{g} e^{j(\omega_i t + \frac{\omega_i^2}{g} x)} \tag{C.2}$$

$$\frac{\partial h(0,t)}{\partial x} = Re \sum_i j b_i \frac{\omega_i^2}{g} e^{j(\omega_i t)} \tag{C.3}$$

$$\alpha = \tan^{-1}\left(\frac{\partial h(0,t)}{\partial x} \right) \tag{C.4}$$

(d) Theoretical σ° Calculation: This block consists of three different routines, DIECO, DDSTPP, and PWRSK. DIECO is a standard routine which calculates the sea-water dielectric constant, $\epsilon = \epsilon' - j\epsilon''$, and R_p, T_p, Fresnel reflection and transmission coefficients from θ, (antenna pointing angle), α, (sea slope), f, (frequency), p (polarization HH or VV), s_x (salinity) and T (water temperature) (Figure C.5).

PWRSK is a routine which calculates the value of S(K), based on $\overline{u}$, (average windspeed), f, (frequency) and θ', (local angle of incidence).

DDSTPP is a routine which computes the theoretical scattering coefficient based on Chan and Fung's model [1977]

$$\sigma^{\circ}_{Theory}(t) = 8 k^4 |\alpha_{pp}|^2 S(k) \tag{C.5}$$

and also $\Delta\sigma$, $\frac{\sigma^{\circ}_{total}}{\sigma^{\circ}_{Theory}}$ (measured σ° over theoretical σ°). Finally,

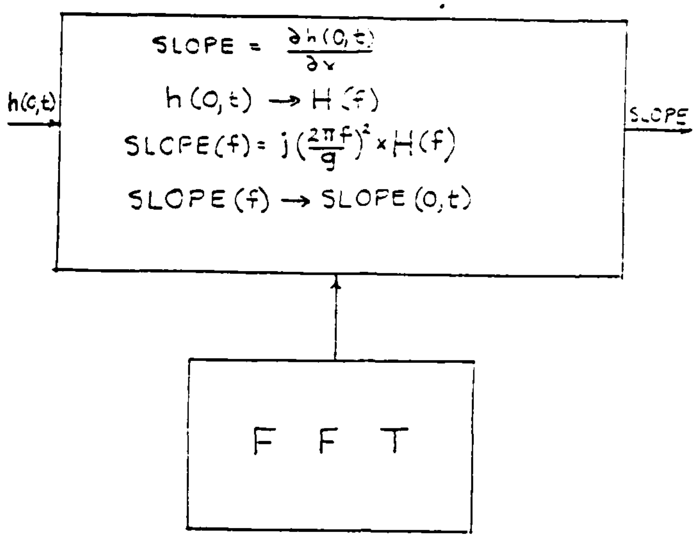

Figure C.4
Block diagram of slope calculation routine
from filtered wave height (SSLLPP)

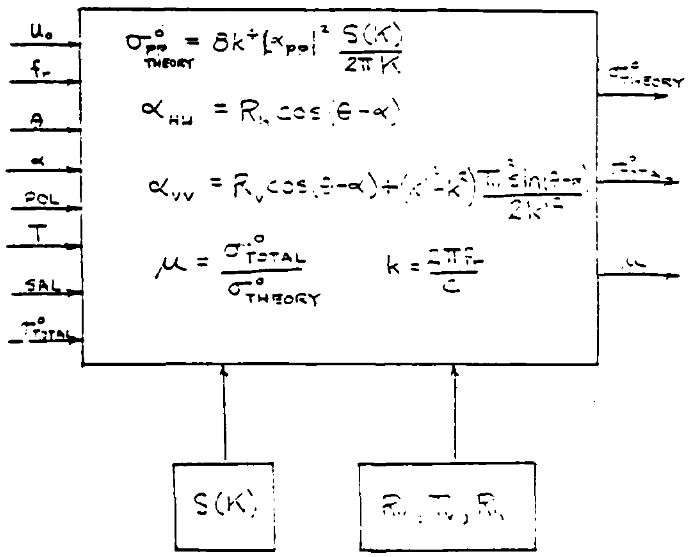

Figure C.5
Block diagram of theoretical σ^0 and modulation index, μ
calculation (DDSTPP)

it calculates the RMS modulation 'index' based upon:

$$\sigma^{\circ}_{total} = (1+\mu(t))\,\sigma_{Theory} \tag{C.6}$$

$$\mu(t) = \frac{\sigma^{\circ}_{total}}{\sigma^{\circ}_{Theory}} - 1 \tag{C.7}$$

$$RMS(\mu) = \left[\sum_{n} \mu_n^2(t)/N\right]^{1/2} \tag{C.8}$$

where N is number of samples per set.

(e) Spatial Transformation *routine:* This block consists of two routines, FRCFGN and XXFFCC. FRCFGN generates the proper Fourier coefficients and makes a table which can be used by XXFFCC.

XXFFCC transforms the time profile data set to a spatial profile (Figure C.6).

$$\eta(0,t) = Re \sum_{i} c_i e^{j(\omega_i t)} \tag{C.9}$$

$$\eta(x,0) = Re \sum_{i} c_i e^{j(\frac{\omega_i^2}{g} x)} \tag{C.10}$$

Note that if the transformation is not made this block can be ignored.

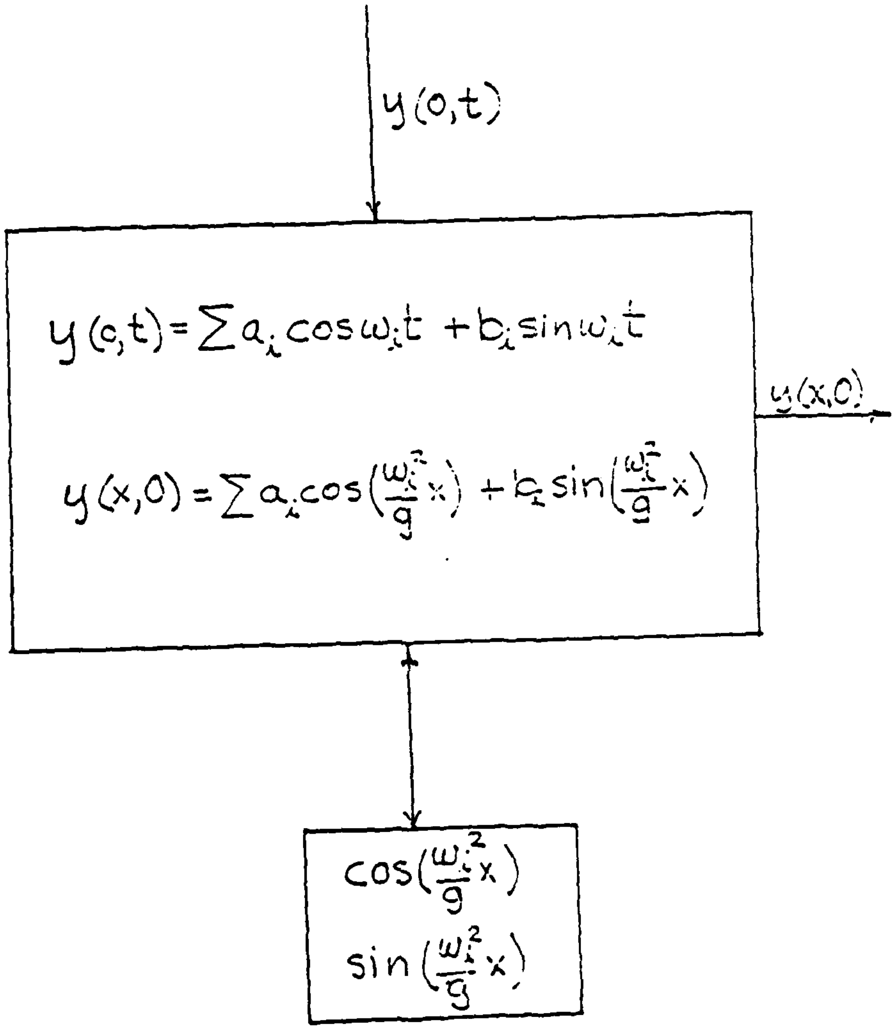

Figure C.6
Block diagram of temporal to spatial domain transformation (XXFFCC)

(f) Cross-Correlation routine: This block consists of four routines: MMOOTT, ZZGGNN, CCS323, and CCL3T3.

MMOOTT subtracts the mean from the sample set (Figure C.7).

$$\bar{p} = \frac{\Sigma p}{N} \tag{C.11}$$

$$p' = p - \bar{p} \tag{C.12}$$

ZZGGNN adds a string of zeroes at the end of each file. This provides an interpolation process when the FFT routine is used for cross-correlation calculation.

CCS3L3 and CCL3T3 process and calculate the cross-spectra by means of FFT. The result of averaged n_1 samples of cross-spectra are saved in EEN353.

(g) The final cross-correlation functions are provided when CCA3G3 smooths the provided values of cross-spectra by means of a five-point moving average and transforms it to the time or spatial domain. The smoothing process, five-point moving average improves the estimation of the 'true' value of cross-spectra, (Appendix B)

<u>Miscellaneus Programs</u>:

(1) <u>Spclout</u>:

This program calculates the upper limit of the maximum value of scattering coefficient which can occur. It calculates the mean of scattering coefficient and adds about 6.0dB to the mean and compares this value to all the sample points of measured scattering coefficient.

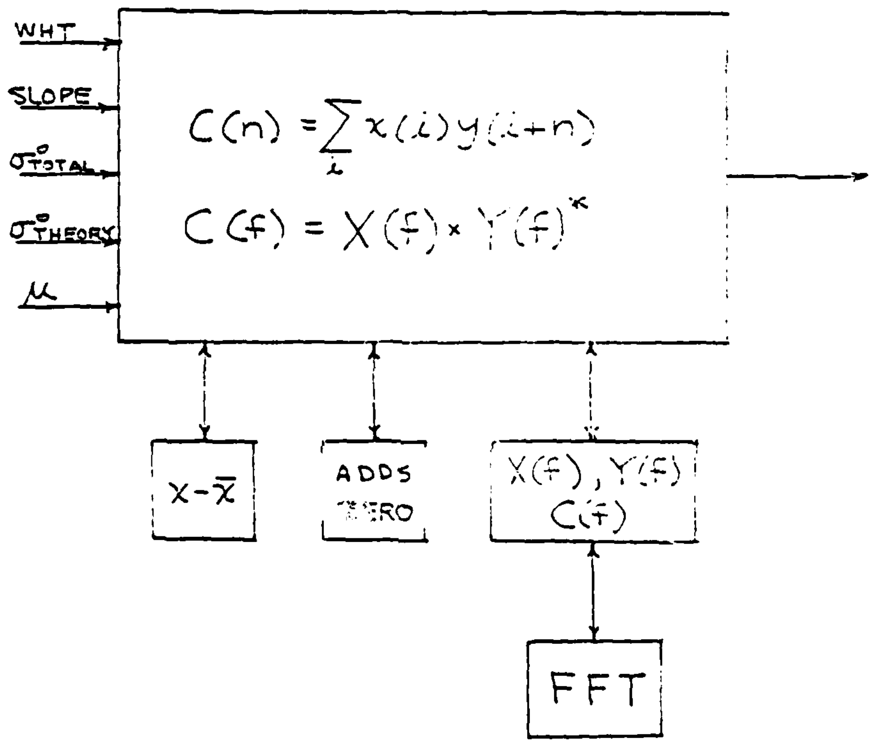

Figure C.7
Block diagram of cross-correlation calculation routine (CCS3L3). Note that the final transform, from frequency to time domain will be completed by means of CCA3G3.

If the value is greater than this 'threshold', a specular event (Section 5.4) will be replaced by a weighted average of its 5 adjacent points. Note that for 90 percent of the time the scattering coefficient over a range from 5.8 dB above the mean envelope level to 11.9 dB below the mean.

(2) MDTRNC

This program calculates MTF, Section 3.0. It simply calculates the smoothed, averaged cross-spectra of wave height and power return over the smoothed averaged power-spectra of wave height and mean of power return. For obtaining the 'stable' and smooth modulation transfer function, the result will be smoothed by means of seven point moving average.

$$R(f) = \frac{\langle P(f)\, H^*(f) \rangle}{\langle \bar{P}\, |H(f)|^2 \rangle} \tag{C.13}$$

(3) Coherence:

This program calculates the coherence function for power return and wave height. It simply finds the average cross-spectrum of wave height and power over the square root average of wave height power spectrum and square root of average power return power spectrum.

$$C^2(f) = \frac{\left\{ E[P(f)\, H^*(f)] \right\}^2}{E[|P(f)|^2]\, E[|H(f)|^2]} \tag{C.14}$$

(4) FOURT

This is an FFT standard Fast Fourier Transform routine. It

takes a data set and will transform it from time to frequency or from frequency to time domain. The direction of the transformation depends on how the variables have been set.

$$Y(m) = \sum_{m} y(n) e^{-j \frac{2\pi}{N} nm} \qquad (C.15)$$

$$y(n) = \sum_{m} Y(m) e^{j \frac{2\pi}{N} nm} \qquad (C.16)$$

Call.FOURT (DATA, Num,a,b,c,d)

where:

Data is the name of the array

Num is the number of Data elements

a,b if a=1, b=-1. The Data will be transformed from time to frequency domain.

a,b if a=1, b=1. The Data will be transformed from frequency to time domain.

c=0 if imaginary part of Data is zero.

c=1 if imaginary part of Data is not zero.

d=0 if No. of element is the power of 2.

d=1 is no. of element is not the power of 2.

PROGRAM LISTS

```
*L EEN3S3

0010   PARAMETER ENS=10,V=[illegible],S1=128,W1=2048,U1=256,Q1=64
0011C           (NOTE THAT V IS 2*S , Q IS S/2)
0013C   PARAMETER FC1=30,FC2=12,FC3=13C,FC4=10,FC5=.1,FC6=14
0014C PARAMETER FC7=06,FC8=09,FC9=16
0015C  PARAMETER FRQ=1[illegible].,POL=1.,THETA=30.,U0=21.[illegible]
0016C   PARAMETER FRQ=13.,POL=1.,THETA=40.,U0=[illegible]
0020  PARAMETER FRQ=14.5,POL =1.,THETA=40.,U0=8.61
0021C    (IF POL=1. POLARIZATION=HH,IF POL=2. POLARIZATION=VV)
0022C  PARAMETER [illegible]
0023  PARAMETER MTL=9
0024 REAL AVE1(V),AVE2(V),AVE3(V),AVE4(V),AVE5(V),AVE6(V),AVE7(V)
0025 REAL AVE8(V),AVE9(V),AVE10(V),AVE11(V)
0025 REAL UK(V),LL(V)
0026 REAL TATA(S1),XATA(S1),FINT(2,Q1),ZCOS(Q1,S1),ZSIN(Q1,S1),FCOS(Q1,S1),
0027&FSIN(Q1,S1)
0027  REAL DATA(2,U1),EATA(2,U1),FILT(2,S1),CATA(U1),RATA(S1)
0028  REAL SLOP(2,S1),FREQ(S1),ALPHA(S1),JUNK(2,S1)
0029  REAL CRSTSL(U1),CRSOSW(U1),CRSTSW(U1),CRSOSL(U1),CRSDSW(U1),CROSS(U1)
0030  REAL CRSDSL(U1),CRSLSW(U1),CRSWW(U1),CRSSS(U1),CRSMM(U1)
0031 REAL SATA(2,U1),ZATA(2,U1),QATA(U1),DUM(U1)
0032  INTEGER GDS,POM1,UUZ
0033 REAL MOP
0034 GDS=U1/(S1*2)
0035 POM1=GDS*MTL
0036 PRINT,"POM1=",POM1
0037  UUZ=2*POM1
0038 MOP=1./FLOAT(ENS)
0039 SLP=0.0
0039 HGT=0.0
0039 SGT=0.0
0039 SGO=0.0
0039 THGD=0.0
0040 DO 17  K=1,U1
0041  CRSTSL(K)=0.0
0042  CRSOSW(K)=0.0
0043  CRSTSW(K)=0.0
0044  CRSOSL(K)=0.0
0045  CRSDSW(K)=0.0
0046  CRSDSL(K)=0.0
0047  CRSLSW(K)=0.0
0048  CRSWW(K)=0.0
0049  CRSSS(K)=0.0
0050  CRSMM(K)=0.0
0051 17 CONTINUE
0051    DO 13 K=1,ENS
0052 PRINT,"NO.#=",K
0053 REWIND 30
0054 DO 89 N=1,S1
0055  READ(33,150)J,AA,BB,CC
0056 WRITE(30,450)J,AA,BB,CC
0057 89 CONTINUE
0058 REWIND 30
0059  CALL BOOM(S1,W1,U1,Q1,POM1,
0060&TATA,XATA,FINT,ZCOS,ZSIN,FCOS,FSIN,
0070&DATA,EATA,FILT,CATA,RATA,
0080&SLOP,FREQ,ALPHA,JUNK,
0090&CRSTSL,CRSOSW,CRSTSW,CRSOSL,CRSDSW,CROSS,
0092&CRSDSL,CRSLSW,CRSWW,CRSSS,CRSMM,
0094&SATA,ZATA,QATA,DUM,
0100&HGT,SLP,SGO,SGT,THGD)
0110C
0115 REWIND 08
0116 REWIND 09
0117 REWIND 10
0132 REWIND 17
0133 DO 332 N=1,S1
0134 READ(17,450)J,GG
0135 AVE11(N)=AVE11(N)+MOP*GG
0136 332 CONTINUE
0137 REWIND 17
0139 13 CONTINUE
0140  PRINT,"[illegible]EEEEEEEE"
0141  CALL CROLTN(DATA,[illegible],CRSWW,[illegible],QATA,[illegible]
```

Copy available to DTIC does not permit fully legible reproduction

EEN353 (cont'd.)

```
GO TO 445
 CALL CRSLTN(DATA,EATA,CRSMM,ZATA,SATA,QATA,DUM,U1,U1)
 CALL CRSLTN(DATA,EATA,CRSTSL,ZATA,SATA,QATA,DUM,U1,U1)
 CALL CRSLTN(DATA,EATA,CRSSS,ZATA,SATA,QATA,DUM,U1,U1)
 CALL CRSLTN(DATA,EATA,CRSLSU,ZATA,SATA,QATA,DUM,U1,U1)
 CALL CRSLTN(DATA,EATA,CRSOSU,ZATA,SATA,GATA,DUM,U1,U1)
 CALL CRSLTN(DATA,EATA,CRSTSU,ZATA,SATA,GATA,DUM,U1,U1)
 CALL CRSLTN(DATA,EATA,CRSOSL,ZATA,SATA,GATA,DUM,U1,U1)
 CALL CRSLTN(DATA,EATA,CRSDSU,ZATA,SATA,GATA,DUM,U1,U1)
 CALL CRSLTN(DATA,EATA,CRSDSL,ZATA,SATA,GATA,DUM,U1,U1)
445 CONTINUE
REWIND 08
REWIND 09
REWIND 16
REWIND17
PRINT,HGT,SLP,SGO,SGT,TMOD
DO 15 K=((U1/2)-PONT+2),((U1/2)+PONT+1)
 J=K-(U1/2)-1
 BB=FLOAT(J)/8.
C BB=FLOAT(J)*3./8.
 WRITE(09,100)BB,CRSDSU(K)/(SQRT(TMOD)*SQRT(HGT)),CRSDSL(K)/(SQRT(SGO)
&*SQRT(SLP)),CRSDSL(K)/(SQRT(TMOD)*SQRT(SLP))
 WRITE(08,100)BB,CRSLSU(K)/(SQRT(SLP)*SQRT(HGT)),CRSOSU(K)/(SQRT(SGO)
&*SQRT(HGT)),CRSTSL(K)/(SQRT(SGT)*SQRT(SLP))
 WRITE(16,100)BB,CRSUU(K)/HGT,CRSSS(K)/SLP,CRSMM(K)/TMOD
C
15 CONTINUE
DO 336 K=1,ST
WRITE(17,450)K-1,AVE11(K)
336 CONTINUE
450 FORMAT(V)
100 FORMAT(V)
STOP
END
*
```

L HH03L3

```
 SUBROUTINE DDON(S,W,U,Q,POM,
&TATA,XATA,FINT,ZCOS,ZSIN,FCOS,FSIN,
&DATA,EATA,FILT,CATA,RATA,
&SLOP,FREQ,ALPHA,JUNK,
&CRSTSL,CRSOSU,CRSTSU,CRSOSL,CRSDSU,CROSS,
&CRSDSL,CRSLSU,CRSWW,CRSSS,CRSMM,
&SATA,ZATA,QATA,DUM,
&HGT,SLP,SGO,SGT,TNOB)
C   INTEGER S=128,W=2048,U=256,Q=64
C            <NOTE THAT W IS 2*S , Q IS S/2>
  PARAMETER FC1=30,FC2=12,FC3=13,FC4=10,FC5=11,FC6=14
 PARAMETER FC7=08,FC8=09,FC9=16
C  PARAMETER FRQ=15.,POL=1.,THETA=50.,U0=21.64
C   PARAMETER FRQ=15.,POL=1.,THETA=40.,U0=20.44
 PARAMETER FRQ=14.5,POL =1.,THETA=40.,U0=8.51
C    <IF POL=1. POLARIZATION=HH,IF POL=2. POLARIZATION=VV>
 PARAMETER LF=0.0,HF=.35
 INTEGER S,W,U,Q,POM,S2,U2,W2,Q2,POM2
 REAL TATA(S),XATA(S),FINT(2,Q),ZCOS(Q,S),ZSIN(Q,S),FCOS(Q,S),FSIN(Q,S)
 REAL DATA(2,U),EATA(2,U),FILT(2,S),CATA(U),RATA(S)
 REAL SLOP(2,S),FREQ(S),ALPHA(S),JUNK(2,S)
 REAL CRSTSL(W),CRSOSU(W),CRSTSU(W),CRSOSL(U),CRSDSU(U),CROSS(W)
 REAL CRSDSL(W),CRSLSU(U),CRSWU(U),CRSSS(W),CRSMM(U)
 REAL SATA(2,W),ZATA(2,W),QATA(W),DUM(U)
 S2=S
 W2=W
 U2=U
 Q2=Q
 POM2=POM
 PRINT,"POM=",POM2
 REWIND FC1
 REWIND FC2
 REWIND FC3
 REWIND FC4
 REWIND FC5
 REWIND FC6
C  GO TO 997
   CALL FILTER(FC1,FC2,S2,LF,HF,RATA,FILT,CATA)
   CALL SLOPE(FC2,FC3,S2,SLOP,FREQ,ALPHA,JUNK)
  CALL DISTRN(FC1,FC3,FC4,FC5,FC6,S2,FRQ,POL,THETA,U0,DATA,EATA)
 GO TO 997
 CALL XFUNC(FC2,S2,Q2,TATA,XATA,ZCOS,ZSIN,FCOS,FSIN,FINT)
C
 CALL XFUNC(FC3,S2,Q2,TATA,XATA,ZCOS,ZSIN,FCOS,FSIN,FINT)
 CALL XFUNC(FC4,S2,Q2,TATA,XATA,ZCOS,ZSIN,FCOS,FSIN,FINT)
 CALL XFUNC(FC5,S2,Q2,TATA,XATA,ZCOS,ZSIN,FCOS,FSIN,FINT)
 CALL XFUNC(FC6,S2,Q2,TATA,XATA,ZCOS,ZSIN,FCOS,FSIN,FINT)
   997 CONTINUE
   CALL ANOUT(FC2,S2,RATA)
   CALL ANOUT(FC3,S2,RATA)
   CALL ANOUT(FC4,S2,RATA)
   CALL ANOUT(FC5,S2,RATA)
   CALL ANOUT(FC6,S2,RATA)
   CALL ZRGEN(FC2,2*S2,CATA)
   CALL ZRGEN(FC3,2*S2,CATA)
   CALL ZRGEN(FC4,2*S2,CATA)
   CALL ZRGEN(FC5,2*S2,CATA)
   CALL ZRGEN(FC6,2*S2,CATA)
C GO TO 998
C PRINT,"POM2",POM2
   CALL CRSSLL(FC2,FC3,FC4,FC5,FC6,FC7,FC8,FC9,U2,W2,DATA,EATA,CRSTSL
&,CRSOSU,CRSTSU,CRSOSL,CRSDSU,CRSDSL,CROSS,CRSLSU,CRSWU,CRSSS,CRSMM,ZATA,
&SATA,DUM,QATA,POM2,
&HGT,SLP,SGO,SGT,TNOB)
 998 CONTINUE
C    STOP
 RETURN
   END
*
```

FLTRR

```
      SUBROUTINE   FILTER(FC1,FC2,S,LF,HF,DATA,FILT,CATA)
      INTEGER FC1,FC2,S
      REAL LF,HF
C      PARAMETER  S=128
      REAL DATA(2,S),FILT(2,S)
     REAL CATA(S)
     REAL SUM,SUN
C
C
C
      REAL NUM
      NUM=S
 PRINT,"NUM=",NUM
 FREQ=.35
  LUM=INT(FREQ*NUM)
 PRINT,LUM
   MUN=1./FLOAT(NUM)
   SUM=0.0
   DO 10 K=1,NUM
   READ(30,100)J,WHT,PWT,SIGO
   DATA(1,K)=WHT
  CATA(K)=WHT
   DATA(2,K)=0.0
   FILT(1,K)=0.0
   FILT(2,K)=0.0
   SUM=SUM+DATA(1,K)
 10 CONTINUE
   AVE=SUM/NUM
   PRINT,"SUM",SUM
   PRINT,"WHT",AVE
   CALL FOURT(DATA,NUM,1,-1,0,0)
  DO 11 K=1,(NUM/2)
 if (k.gt.lum) go to 666
  FILT(1,K+1)=1.
  FILT(2,K+1)=1.
  FILT(1,NUM-K+1)=FILT(1,K+1)
  FILT(2,NUM-K+1)=-FILT(2,K+1)
  11 CONTINUE
 666 CONTINUE
  FILT(1,1)=1.
 FILT(2,1)=0.0
  FILT(1,NUM/2)=0.0
  FILT(2,NUM/2)=0.0
   DO 12 K=1,NUM
   DATA(1,K)=DATA(1,K)*FILT(1,K)*MUN
   DATA(2,K)=DATA(2,K)*FILT(2,K)*MUN
   filt(1,k)=mun*filt(1,k)
   filt(2,k)=mun*filt(2,k)
C   WRITE(14,100)K,DATA(1,K),DATA(2,K)
C write(14,100)k-1,filt(1,k),filt(2,k)
 12 CONTINUE
C
C
   CALL FOURT(DATA,NUM,1,1,1,0)
    CALL FOURT(FILT,NUM,1,1,1,0)
C
   SUM=0.0
   DO 14 K=1,NUM
   SUM=SUM+DATA(1,K)
   WRITE(12,1000)K,DATA(1,K)
C  write(11,100)k-1,FILT(1,k),FILT(2,k)
C   WRITE(13,100)K,CATA(K),DATA(1,K),DATA(2,K),FILT(K)
 14 CONTINUE
  PRINT,"SUM",SUM
    PRINT,"WHTFILT",SUM/NUM
 1000 FORMAT(V)
  100 FORMAT(V)
  RETURN
C   STOP
  END
```

L SSLLPP

```
0005 SUBROUTINE SLOPE(FC2,FC3,S,SLOP,FREQ,ALPHA,JUNK)
0010  INTEGER S,FC2,FC3
0023C DIMENSION FILT(S)
0030  REAL SLOP(2,S),FREQ(S),JUNK(2,S),ALPHA(S)
0050 INTEGER NUM
055 REAL MUN
0060 NUM=S
065 MUN=1./FLOAT(NUM)
0070 PI=3.141519
0100 SUM=0.0
0105 F0=.35
0107 REWIND 12
0110   DO 59 K=1,NUM
0125   READ(12,100)J,WHT
0130 SLOP(1,K)=WHT
0140 SLOP(2,K)=0.0
0150 SUM=SUM+WHT
0160 59 CONTINUE
0170 AVHT=SUM/NUM
0180 PRINT,AVHT
0185 PRINT,"SUM",SUM
0190C
0200 CALL FOURT(SLOP,NUM,1,-1,0,0)
0205 PRINT,"O.K.!!!!!!!"
0210C
0220 DO 101 I=1,NUM
0240 FREQ(I)=FLOAT(I-1)/FLOAT(NUM)
0250 101 CONTINUE
0251C
0252C
0253C DO 112 K=1,NUM/2
0254C FILT(K)=1./(1+(FREQ(K)/F0)**16)
0255C FILT(K)=1.
0256C SLOP(1,K)=FILT(K)*SLOP(1,K)
0258C SLOP(1,NUM-K+1)=SLOP(1,NUM-K+1)*FILT(K)
0260C SLOP(2,NUM-K+1)=SLOP(2,NUM-K+1)*FILT(K)
0262C SLOP(2,K)=FILT(K)*SLOP(2,K)
0264C 112 CONTINUE
0265 JUNK(1,1)=0.0
0266 JUNK(2,1)=0.0
0268C
0270 DO 102 K=1,NUM/2
0280 Z=(2.*PI*FREQ(K+1)*2.*PI*FREQ(K+1))/(9.81)
0285 IF(FREQ(K+1) .GE. 5.) Z=0.0
0290 JUNK(1,K+1)=-Z*MUN*SLOP(2,K+1)
0300 JUNK(2,K+1)=Z*MUN*SLOP(1,K+1)
0310 JUNK(1,NUM-K+1)=JUNK(1,K+1)
0320 JUNK(2,NUM-K+1)=-JUNK(2,K+1)
0331 102 CONTINUE
0332 DO 50 K=1,NUM
0334 SLOP(1,K)=MUN*SLOP(1,K)
0336 SLOP(2,K)=MUN*SLOP(2,K)
0338 50 CONTINUE
0340 JUNK(2,(NUM/2)+1)=0.0
0343 DO 107 K=1,NUM
0347C WRITE(15,400)FREQ(K),SLOP(1,K),SLOP(2,K),Z(K),JUNK(1,K),JUNK(2,K)
0349 107 CONTINUE
0360C
0370 CALL FOURT(SLOP,NUM,1,1,1,0)
0380C
0390 CALL FOURT(JUNK,NUM,1,1,1,0)
0400C
0410 DO 103 I=1,NUM
0420 ALPHA(I)=ATAN(JUNK(1,I))
0430 ALPHA(I)=(180./PI)*ALPHA(I)
0440 103 CONTINUE
0450 DO 104 K=1,NUM
0460C WRITE(08,200)K-1,SLOP(1,K),JUNK(1,K),ALPHA(K),FREQ(K)
0464  WRITE(13,300)K,ALPHA(K)
0470 104 CONTINUE
0475 100 FORMAT(V)
0480 900 FORMAT(I4,4X,F9.3,4X,F9.3)
0485 400 FORMAT(F9.3,4X,F9.3,4X,F9.3,4X,F9.3,4X,F9.3,4X,F9.3)
0490 200 FORMAT(I4,4X,F9.3,4X,F9.3,4X,F9.3,4X,F9.3,4X,F9.3)
[illegible] 300 FORMAT([illegible])
[illegible] 500 FORMAT([illegible],4X,F9.3)
[illegible] 600 FORMAT(I4,4X,F9.3,4X,F9.3,4X,F9.3)
[illegible]
```

Copy available to DTIC does not permit fully legible reproduction

C DDSTHA

```
SUBROUTINE DISTRA(FC1,FC3,FC4,FC5,FC6,S,FRQ,FOL,THETA,U0,GAMA,DATA)
INTEGER FC1,FC3,FC4,FC5,FC6,S
REAL FRQ,FOL,THETA,U0
COMPLEX DIECO,RV,RH
  REAL  RI(2),EMISS(2)
REAL DATA(2,S),ENTA(2,S)
REAL SS,X,U0
REAL LAMDA
 T=286.
 SAL=35.
C  FREQ=10.
C  THETA=40.
C  U0=5.76
C U0=8.6
C U0=?.?5
C  U0 ?.77
C LAMDA=2.307e923
LAMDA=30./FRQ
PRINT,FRQ,LAMDA,THETA,FOL,U0
PI=4.*ATAN(1.)
NUM=S
ZEG=0.0
 SUM=0.0
REWIND 13
REWIND 30
     DO 10 K=1,NUM
 READ(13,100)WW,ALPHA
  READ(30,600)J,WMI,FMI,SIGO
 BETA=THETA-ALPHA
GAMA=BETA
 ALPHA=ALPHA*PI/180.
BETA=PI*BETA/180.
C PRINT,BETA
X=4.*PI*SIN(BETA)/(LAMDA)
 AA=ALOG10((2./PI)*((2*PI/LAMDA)**3))
  CALL EMIOCN(T,SAL,FRQ,GAMA,DIECO,RH,RV,RI,EMISS)
C
 FERS=(CABS(RH))*(CABS(RH))
C PRINT,FERS
BB=ALOG10(FERS)
BB=BB+ALOG10((COS(BETA))**4)
C PRINT,BB
  CALL SK(U0,X,SS)
CC=SS
C  PRINT,CC,X,U0
DD=ALOG10(1./SIN(BETA))
EE=AA+BB+CC+DD
DATA(1,K)=10.**EE
C WRITE(19,100)K-1,AA,BB,CC,DD,EE,FERS,DATA(1,K)
IF(ALPHA.LT.0.0)  ENTA(1,K)=SIGO*COS(ALPHA)
IF(ALPHA.GT.0.0)  ENTA(1,K)=SIGO/COS(ALPHA)
ZEG=ZEG+DATA(1,K)
SUM=SUM+ENTA(1,K)
C WRITE(17,100)K-1,10.*ALOG10(SIGO)
   WRITE(16,700)K-1,THETA,ALPHA*180./PI,GAMA,AA,BB,X,CC,DD,DATA(1,K),DIECO
10 CONTINUE
ZEG=ZEG/FLOAT(NUM)
SUM=SUM/FLOAT(NUM)
RATIO=SUM/ZEG
PRINT,"RATIO=",RATIO,SUM,ZEG
C RATIO=1.
REWIND 17
SUM=0.0
```

DDSTHH (cont'd.)

```
DO 13 K=1,NUM
DATA(I,K)=RATIO*DATA(I,K)
C DATA(I,K)=10.*ALOG10(DATA(I,K)
C EATA(I,K)=10.*ALOG10(EATA(I,K)
 UU=ABS((EATA(I,K)/DATA(I,K))-1.)
SUM=SUM+UU*UU
C UU=EATA(I,K)-DATA(I,K)
 WRITE(10,100)K-1,EATA(I,K)
 WRITE(11,100)K-1,DATA(I,K)
 WRITE(14,100)K-1,UU
WRITE(17,100)K-1,UU
13 CONTINUE
RMS=SQRT(SUM /NUM)
PRINT,"RMS OF H(t)='RMS
 200 FORMAT(V)
300 FORMAT(V)
100 FORMAT(V)
400 FORMAT(V)
700 FORMAT(V)
C 900 FORMAT(I3,3X,F7.4,3X,F7.4,3X,F7.4,3X,F7.4,3X,F7.4,3X,F7.4,3X,F7.4,3X,F7.4,3X,F9.5,3X,F7.4,1X,F11.4)
900 FORMAT(I3,3X,9(F7.4,3X),F9.5,3X,F7.4,1X,F11.4)
 RETURN
   END
```

```
L DDS,VV

0005 SUBROUTINE DISTRN(FC1,FC3,FC4,FC5,FC6,S,FRQ,FOL,THETA,UU,DATA,EATA)
0007 INTEGER FC1,FC3,FC4,FC5,FC6,S
0009 REAL FRQ,FOL,THETA,UU
0010 COMPLEX DIECO,...,AH,RH,GV
0020   REAL  R2(2),EMISS(2)
0030 REAL DATA(2,5),EATA(2,5)
0035 REAL SS,X,UU
0037 REAL LAMDA
0040  T=286.
0043  SAL=33.
0050C  FREQ=10.
0055C  THETA=40.
0056C  UO=5.76
0057C UO=8.8
0058C UO=6.25
0059C  UO=21.77
0060C LAMDA=2.3076923
0061 LAMDA=30./FRQ
0062 PRINT,FRQ,LAMDA,THETA,FOL,UO
0063 PI=4.*ATAN(1.)
0065 NUM=5
0067 ZEG=0.0
0068  SUM=0.0
0070 REWIND 13
0075 REWIND 30
0080      DO 10 K=1,NUM
0090  READ(13,100)UU,ALPHA
0110   READ(30,600)J,WHT,PUT,SIGO
0120  BETA=THETA-ALPHA
0122 GAMA=BETA
0123  ALPHA=ALPHA*PI/180.
0125 BETA=PI*BETA/180.
0126C PRINT,BETA
0127 X=4.*PI*SIN(BETA)/(LAMDA)
0130  AA=ALOG10((2./PI)*((2*PI/LAMDA)**3))
0140C  AA=AA+ALOG10(COS(BETA)**4)
0160   CALL EMIUCN(T,SAL,FRQ,GAMA,DIECO,RH,RV,R2,EMISS)
0170C
0196  GV=RV*((COS(BETA))**2)+.5*((1.+RV)**2)*(1.-(1./DIECO))*((SIN(BETA))**2)
0198 FERS=(CABS(GV))*(CABS(GV))
0199  BB=ALOG10(FERS)
0200   CALL SK(UO,X,SS)
0202 CC=SS
0205C  PRINT,CC,X,UO
0210 DD=ALOG10(1./SIN(BETA))
0220 EE=AA+BB+CC+DD
00223 DATA(1,K)=10.**EE
0225C WRITE(19,100)K-1,AA,BB,CC,DD,EE,FERS,DATA(1,K)
0235 IF(ALPHA.LT.0.0)  EATA(1,K)=SIGO*COS(ALPHA)
0237 IF(ALPHA.GT.0.0)  EATA(1,K)=SIGO/COS(ALPHA)
0240 ZEG=ZEG+DATA(1,K)
0250 SUM=SUM+EATA(1,K)
0255C WRITE(17,100)K-1,10.*ALOG10(SIGO)
0257   WRITE(18,700)K-1,THETA,ALPHA*180./PI,GAMA,AA,BB,RV,X,CC,DD,DATA(1,K),DIECO
0260 10 CONTINUE
0270 ZEG=ZEG/FLOAT(NUM)
0280 SUM=SUM/FLOAT(NUM)
0290 RATIO=SUM/ZEG
0292 PRINT, RATIO= ,RATIO,SUM,ZEG
0293C RATIO=1.
0294 REWIND 17
0295 SUM=0.0
```

DDSTVV (cont'd.)

```
 DO 13 K=1,NUM
 DATA(1,K)=RATIO*DATA(1,K)
C DATA(1,K)=10.*ALOG10(DATA(1,K)
C EATA(1,K)=10.*ALOG10(EATA(1,K)
  UU=ABS((EATA(1,K)/DATA(1,K))-1.)
 SUM=SUM+UU*UU
C UU=EATA(1,K)-DATA(1,K)
  WRITE(10,100)K-1,EATA(1,K)
  WRITE(11,100)K-1,DATA(1,K)
  WRITE(14,100)K-1,UU
 WRITE(17,100)K-1,UU
 13 CONTINUE
  RMS=SQRT(SUM/NUM)
  PRINT,"RMS OF H(t)=",RMS
  200 FORMAT(V)
 600 FORMAT(V)
 100 FORMAT(V)
 400 FORMAT(V)
 700 FORMAT(V)
 900 FORMAT(I3,3X,F7.4,3X,F7.4,3X,F7.4,3X,F7.4,3X,F7.4,3X,F7.4,3X,F7.4,3X,F7.4,3X,F7.3,3X,F7.4,1X,F.1.4)
  RETURN
```

L DIECO

```
      SUBROUTINE EMISSN(TEMP,SAL,FREQ,THETA,  DIECO,RH,RV,
     &        R2,EMISS)

       PURPOSE

        1. THE EMISSN ROUTINE CALCULATES THE DIELECTRIC
           CONSTANT OF SEA WATER AT ANY FREQUENCY IN
           THE MICROWAVE BAND USING THE DEBYE EXPRESSION
           (DEBYE,P., 'POLAR MOLECULES', J.CHEM. PHYS.,
           VOL. 9, 1941).  THE COEFFICIENTS OF THIS
           EXPRESSION ARE FROM THE MOST RECENT EMPIRICAL
           MODELING (MY BUDDIES) L. KLEIN AND C. SWIFT
           (KLEIN,L.A, C.T. SWIFT, 'AN IMPROVED
           MODEL FOR THE DIELECTRIC CONSTANT OF SEA
           WATER AT MICROWAVE FREQUENCIES', IEEE
           TRANS. ANTENNAS AND PROPAGAT., VOL. AP-25(1),1971).

        2. THE FRESNEL REFLECTION COEFFICIENTS ARE
           CALCULATED USING METHOD BY STRAITON
           (STRAITON,J.A, ELECTROMAGNETIC THEORY,
           MC GRAW-HILL BOOK CO., 1941)

        3. THE POWER REFLECTION COEFFICIENTS AND
           EMISSIVITY ARE DETERMINED(MANUAL OF REMOTE
           SENSING, AMER. SOC. OF PHOTOGRAMMETRY, CHAPTER 9).

       INPUT ARGUMENTS

           TEMP            =        SEA SURFACE TEMPERATURE, KELVIN.
           SAL             =        SALINITY, 0/00.
           FREQ            =        FREQUENCY,GHZ.
           THETA           =        NORMAL INCIDENCE ANGLE, DEGREES.

       OUTPUT ARGUMENTS

           DIECO           =        DIELECTRIC CONSTANT (COMPLEX).
           RH,RV           =        FRESNEL REFLECTION COEFFICENTS,
                           =        H- AND V- POLARIZATIONS.
           R2              =        POWER REFLECTION COEFFICENT,
                           =        1 = H-POL, 2 = V-POL.
           EMISS           =        EMISSIVITY, = 1,H-POL.
                           =                    = 2, V-POL.


       CALCULATION OF DIELECTRIC CONSTANT

      DIMENSION R2(2),EMISS(2)

                      COMPLEX VARIABLES

      COMPLEX DIECO,RV, RH
                      COMPLEX DUMMY VARIABLES

       COMPLEX DUMMY1,DUMMY2,TEP1,TEP2,COST,SQ

                       DEFINE DIELCTRIC CONSTANT AT INFINITE FREQUENCY,EFIN.
                       AND PERMITIVITY OF FREE SPACE,E0.

       DATA EFIN,E0/4.9, 8.854E-12/

       DATA PI/3.14159/
```

DIECO (cont'd.)

```
                        INITIALIZE CERTAIN VARIABLES

       T = TEMP - 273.16
      DELTA = 25.0 - T
       W = 2. * PI * FREQ * 1.0 E09

                        EXPRESSION FOR IONIC CONDUCTIVITY OF SEA WATER,COND

       S = SAL * (0.182521 - 1.46192E-3*SAL + 2.09324E-5*SAL**2
      &     -1.28205E-7*SAL**3)
       B = 2.033E-2 + 1.266E-4*DELTA + 2.464E-6*DELTA**2
      &     -SAL * (1.849E-5 - 2.551E-7*DELTA + 2.551E-8*DELTA**2)
       COND = S *EXP(-DELTA*B)

                        EXPRESSION FOR THE STATIC DIELECTRIC CONSTANT,ES.

       F = 87.134 - 1.949E-1*T - 1.276E-2*T**2
      &     +2.491E-4*T**3
       A = 1.0 +1.613E-5*SAL*T - 3.656E-3*SAL
      &     +3.21E-5*SAL**2 - 4.232E-7*SAL**3
       ES = F * A

                        RELAXATION TIME, TAU

       TT = 1.768E-11 - 6.086E-13*T + 1.104E-14*T**2
      &     -8.111E-17*T**3
       BT = 1. + 2.282E-5*SAL*T - 7.638E-4*SAL
      &     -7.760E-6*SAL**2 + 1.105E-8*SAL**3
       TAU = TT * BT

                        SOLVE DEBYE EXPRESSION FOR DIELECTRIC CONSTANT,DIECO.

       DUMMY1 = CMPLX(1.0, W*TAU)
       DUMMY2 = CMPLX(0.0,COND/(W*E0))

       TEP1 = CMPLX(EFIN,0.0)
       TEP2 = CMPLX(ES-EFIN, 0.0)

       DIECO = TEP1 + TEP2/DUMMY1 - DUMMY2

                        CALCULATION OF FRESNEL REFLECTION COEFFICIENT,RH&RV

       COST = CMPLX( COS(THETA/57.296), 0.0)
       SQ = CSQRT(DIECO - CMPLX(SIN(THETA/57.296)**2, 0.0) )
       RH = (COST - SQ) / (COST + SQ)
       RV = (DIECO * COST - SQ) / (DIECO * COST + SQ)

                        CALCULATE POWER REFLECTION COEFFICIENTS,R2(1=H,2=V)
                        AND EMISSIVITY, EMISS(1=H,2=V).

       R2(1) = RH * CONJG(RH)
       R2(2) = RV * CONJG(RV)
       DO 10 I=1,2
       EMISS(I) = 1.- R2(I)
 10    CONTINUE

       RETURN
       END
```

Copy available to DTIC does not permit fully legible reproduction

L XXFFCC

```
0100 SUBROUTINE XFUNC(FC,S,Q,TATA,XATA,ZCOS,ZSIN,FCOS,FSIN,FINT)
0200 INTEGER S,Q,FC
0250C PARAMETER S=128,Q=64
0300  REAL TATA(S),XATA(S),ZCOS(Q,S),ZSIN(Q,S),FINT(2,Q)
0310  REAL FCOS(Q,S),FSIN(Q,S)
0320  REAL MUN
0330  PI=4.*ATAN(1.)
0335  G=9.81
0337  A0=0.0
0340   NUM=S
0350  MUN=1./FLOAT(NUM)
0355 W=2.*PI*MUN
0356 PRINT,W
0357 PRINT,NUM,FC,S,Q
0359 REWIND FC
0360   DO 12 K=1,NUM
0365C   AA=COS(W*1.*K)
0366C   AA=SIN(2.*PI*.17*K)+COS(2.2*K)+SIN(2.6*K)
0368  READ(FC,1000)VV,AA
0370   TATA(K)=AA
0371c PRINT,J
0372   A0=A0+TATA(K)*MUN
0373  XATA(K)=0.0
0375 12 CONTINUE
0380   DO 15 K=1,NUM/2
0385   FINT(1,K)=0.0
0390   FINT(2,K)=0.0
0400 15 CONTINUE
0405  REWIND 19
0407C print,"00000009090"
0410      DO 10 K=1,NUM/2
0415C   V=W*K*K/G
0417C   V=FLOAT(K)
0420          DO 20 J=1,NUM
0427C   U=FLOAT(J)
0428C   U=1.5*J
0430C      FCOS(K,J)=COS(W*V*U)
0440C      FSIN(K,J)=SIN(W*V*U)
0444C      ZCOS(K,J)=COS(W*K*J)
0446C     ZSIN(K,J)=SIN(W*K*J)
0447    READ(19,1000)AA,BB,CC,DD
0448    FCOS(K,J)=AA
0449    FSIN(K,J)=BB
0450    ZCOS(K,J)=CC
0451    ZSIN(K,J)=DD
0455C WRITE(03,1000)K,J
0460    20 CONTINUE
0480 10  CONTINUE
0490C print,"999989898989"
0500    DO 30 K=1,NUM/2
0510C
0520      DO 40 J=1,NUM
0530     FINT(1,K)=FINT(1,K)+MUN*TATA(J)*ZCOS(K,J)
0540    FINT(2,K)=FINT(2,K)+MUN*TATA(J)*ZSIN(K,J)
0550     40 CONTINUE
0560C   WRITE(16,200)K,FINT(1,K),FINT(2,K)
0570 30 CONTINUE
0580C
0590   DO 50 L=1,NUM
0600C
0610       DO 60 J=1,(NUM-2)/2
0620      XATA(L)=XATA(L)+2.*FINT(1,J)*FCOS(J,L)+2.*FINT(2,J)*FSIN(J,L)
0630C PRINT,CATA(L)
0635C   print,fcos(j,l),fsin(j,l)
0640  60 CONTINUE
0645C PRINT,"!!!!!!!!!!!!!!!!!!!!...OK"
0650C PRINT,CATA(L)
0660  XATA(L)=XATA(L)+A0
0665 XATA(L)=XATA(L)+FINT(1,(NUM/2))*FCOS((NUM/2),L)
0667 XATA(L)=XATA(L)+FINT(2,(NUM/2))*FSIN((NUM/2),L)
0670C
0680   50 CONTINUE
0690C
```

XXFFCC (cont'd.)

```
      PRINT,"AO=",A0
     REWIND FC
       DO 70 L=1,NUM
C       U=4.+16.*L/FLOAT(NUM)
       U=30.+3.*L
C      READ(12,100)J,X,Z,GG,HH,UU,RR
C       READ(09,1000)U,Y
C       Y=SIN(4.*PI*PI*.17*.17*U/G)+COS(4.84*U/G)+SIN(6.76*U/G)
C       Y=COS(1.44*L)
C        Y=COS(U*U*L)
C       Y=DATA(L)
C        DIF=Y-XATA(L)
C      WRITE(15,100)U,TATA(L),Y,XATA(L),DIF,FINT(1,L),FINT(2,L)
C       WRITE(17,300)L,DATA(L),Y,CATA(L),GG,DIF,HH,ABS(CATA(L)-GG)
       WRITE(FC,1000)U,XATA(L)
     IF(FC.EQ.14)   WRITE(18,1000)U,XATA(L)
     70 CONTINUE
     100 FORMAT(F7.3,4X,F9.5,4X,F9.5,4X,F9.5,4X,F9.5,8X,F9.7,4X,F9.7)
     300 FORMAT(I3,4X,F9.5,4X,F9.5,4X,F9.5,4X,F9.5,4X,F9.5,4X,F9.5,4X,F9.5)
     200 FORMAT(I3,4X,F9.5,4X,F9.5)
     1000 FORMAT(V)
       RETURN
C    STOP
     END
*
```

L PURSK

```
SUBROUTINE SK(UO,X,SS)
REAL SS,UO,X
   IF((8.LE.UO).AND.(UO.LE.10.)) SS=-4.6115*ALOG10(X)+ALOG10(.1782)
   IF((18.LE.UO).AND.(UO.LE.22.)) SS=-2.0904*ALOG10(X)+ALOG10(.0460)
C
C
C
C
C
  RETURN
  END
```

L FRCFGN

```
  PARAMETER S=128,Q=64
REAL ZCOS(Q,S),ZSIN(Q,S),FCOS(Q,S),FSIN(Q,S)
 REAL MUN
PI=4.*ATAN(1.)
 G=9.81
  NUM=S
 MUN=1./FLOAT(NUM)
W=2.*PI*MUN
PRINT,W
    DO 10 K=1,NUM/2
  V=W*K*K/G
C  V=FLOAT(K)
       DO 20 J=1,NUM
C  U=FLOAT(J)
 U=30.+3.*J
      FCOS(K,J)=COS(U*V*U)
      FSIN(K,J)=SIN(U*V*U)
      ZCOS(K,J)=COS(W*K*J)
      ZSIN(K,J)=SIN(W*K*J)
  WRITE(19,1000)FCOS(K,J),FSIN(K,J),ZCOS(K,J),ZSIN(K,J)
   20 CONTINUE
10  CONTINUE
1000 FORMAT(V)
 STOP
 END
```

```
L MHOOTT
0005 SUBROUTINE MHOUT(FC7,S,RATA)
0010 INTEGER FC7,S
0011 REAL J,RATA(S)
0012 num=s
0015 SUM=0.0
0018 REWIND FC7
0020 do 10 k=1,num
0030 READ(FC7,100)J,BB
0040   SUM=SUM+BB
0075 10 CONTINUE
0077 v=sum/float(num)
0078 PRINT,"MEAN=",V
0079 REWIND FC7
0080 100 FORMAT(V)
0082 DO 12 K=1,NUM
0084 READ(FC7,100)J,BB
0086 RATA(K)=BB-V
0088 12 CONTINUE
0089 REWIND FC7
0090 DO 16 K=1,NUM
0092 WRITE(FC7,100)K-1,RATA(K)
0094 16 CONTINUE
0098 RETURN
0100 END
```

```
L ZZGGNN
0010 SUBROUTINE ZRGEN(FC8,S,CATA)
0020 INTEGER FC8,S
0025 REAL CATA(S)
0027 NUM=S
0030 do 10 k=1,NUM
0040 CATA(K)=0.0
0050 10 CONTINUE
0055 REWIND FC8
0060 DO 12 K=1,NUM/2
0070 READ(FC8,100)J,BB
0080 CATA(K)=BB
0090 12 CONTINUE
0092C
0093 REWIND FC8
0095 DO 14 K=1,NUM
0100 WRITE(FC8,100)K-1,CATA(K)
0105 14 CONTINUE
0110 100 format(v)
0120 RETURN
0130 end
```

*L CCS3L3

```
10 SUBROUTINE CRSSL1(FC2,FC3,FC4,FC5,FC6,FC7,FC8,FC9,S,W,DATA,EATA,CRSTSL
20&,CRSOSW,CRSTSW,CRSOSL,CRSOSW,CRSBSL,CROSS,CRSLSW,CRSWW,CRSSS,CRSMM,ZATA,
30&SATA,DUM,QATA,LON,
31&HGT,SLP,SGO,SGT,TMOD)
32C PRINT,"LON",LON
40  INTEGER FC2,FC3,FC4,FC5,FC6,FC7,FC8,FC9,S,W
50   REAL DATA(2,S),EATA(2,S)
60  INTEGER NUM,LON,LAN
70  REAL CRSTSL(W),CRSOSW(W),CRSTSW(W),CRSOSL(W),CRSBSW(W),CRSBSL(W)
80  REAL CROSS(W),CRSLSW(W),CRSWW(W),CRSSS(W),CRSMM(W)
90  REAL ZATA(2,S),SATA(2,W),QATA(W),DUM(W)
100  LAN=LON
110 REWIND FC2
120 REWIND FC3
130 REWIND FC4
140 REWIND FC5
150 REWIND FC6
163    NUM=S
170    QUM=W
180 PRINT,"LON=",LON,"NUM=",NUM,"QUM=",QUM
190  DO 34 K=1,NUM
200  READ(12,100)J,WHT
210   DATA(1,K)=WHT
220   EATA(1,K)=WHT
230  DATA(2,K)=0.0
240  EATA(2,K)=0.0
242  HGT=HGT+WHT*WHT
245 34 CONTINUE
250C 34 WRITE(18,100)DATA(1,K),EATA(1,K)
260 REWIND 12
270 CALL COROL(DATA,EATA,CROSS,ZATA,SATA,QATA,DUM,NUM,QUM)
280 DO 35 K=1,QUM
290  CRSWW(K)=CRSWW(K)+CROSS(K)
300 35 CONTINUE
0302 DO 334 K=1,NUM
0304 READ(14,100)J,DIFF
0306 DATA(1,K)=DIFF
0307 EATA(1,K)=DIFF
0308 DATA(2,K)=0.0
0309 EATA(2,K)=0.0
0310 TMOD=TMOD+DIFF*DIFF
0311 334  CONTINUE
0312 REWIND 14
0313   CALL COROL(DATA,EATA,CROSS,ZATA,SATA,QATA,DUM,NUM,QUM)
0315 DO   335 K=1,QUM
0316 CRSMM(K)=CRSMM(K)+CROSS(K)
0317 335 CONTINUE
0319 REWIND 11
320 DO 10 K=1,NUM
330    READ(11,100)J,SIGT
340    READ(13,100)J,SLOP
350    DATA(1,K)=SIGT
360    EATA(1,K)=SLOP
370    DATA(2,K)=0.0
380    EATA(2,K)=0.0
0384  SGT=SGT+SIGT*SIGT
0388  SLP=SLP+SLOP*SLOP
390   10 CONTINUE
400  CALL COROL(DATA,EATA,CROSS,ZATA,SATA,QATA,DUM,NUM,QUM)
410  DO 13 K=1,QUM
440 13 CRSTSL(K)=CRSTSL(K)+CROSS(K)
0445 REWIND 11
450 REWIND 13
460 DO 29 K=1,NUM
470 READ(13,100)J,SLOP
480 DATA(1,K)=SLOP
490 EATA(1,K)=SLOP
500 DATA(2,K)=0.0
510 EATA(2,K)=0.0
520 29 CONTINUE
530  CALL COROL(DATA,EATA,CROSS,ZATA,SATA,QATA,DUM,NUM,QUM)
```

CCS3L3 (cont'd.)

```
540  DO 49 K=1,QUM
550 49 CRSSS(K)=CRSSS(K)+CROSS(K)
560 REWIND 13
570C
580  DO 88 K=1,NUM
590  READ(13,100)J,SLOP
600  READ(12,100)J,WNT
610  DATA(1,K)=SLOP
620  EATA(1,K)=WNT
630  DATA(2,K)=0.0
640  EATA(2,K)=0.0
650 88 CONTINUE
660  CALL COROL(DATA,EATA,CROSS,ZATA.SATA,QATA,DUN,NUM,QUM)
670  DO 99 K=1,QUM
680 99 CRSLSU(K)=CRSLSU(K)+CROSS(K)
690 REWIND 10
700 REWIND 12
710 DO 14 K=1,NUM
720 READ(10,100)J,SIGO
730 READ(12,100)J,WNT
740 DATA(1,K)=SIGO
750  EATA(1,K)=WNT
760  DATA(2,K)=0.0
770  EATA(2,K)=0.0
0775   SGO=SGO+SIGO*SIGO
780 14 CONTINUE
790C
800  CALL COROL(DATA,EATA,CROSS,ZATA,SATA,QATA,DUN.NUM,QUM)
810C
820   DO 15 K=1,QUM
830 15 CRSOSU(K)=CRSOSU(K)+CROSS(K)
840C
850 REWIND 11
860 REWIND 12
870C
880 DO 16 K=1,NUM
890 READ(11,100)J,SIGT
900  READ(12,100)J,WNT
910   DATA(1,K)=SIGT
920  EATA(1,K)=WNT
930  EATA(2,K)=0.0
940   DATA(2,K)=0.0
950 16 CONTINUE
960C
970   CALL COROL(DATA,EATA,CROSS.ZATA,SATA.QATA,DUN.NUM,QUM)
980C
990 DO 17 K=1,QUM
1000 17 CRSTSU(K)=CRSTSU(K)+CROSS(K)
1010C
1020REWIND 11
1030 REWIND 12
1040 REWIND 10
1050 REWIND 13
1060 DO 18 K=1,NUM
1070READ(10,100)J,SIGO
1080 READ(13,100)J,SLOP
1090  DATA(1,K)=SIGO
1100  EATA(1,K)=SLOP
1110  DATA(2,K)=0.0
1120  EATA(2,K)=0.0
1130 18 CONTINUE
1140C
1150    CALL COROL(DATA,EATA,CROSS,ZATA,SATA,DATA,DUN,NUM,QUM)
1160C
```

CCS3L3 (cont'd.)

```
 DO 49 K=1,QUM
49 CRSSS(K)=CRSSS(K)+CROSS(K)
REWIND 13
C
 DO 88 K=1,NUM
 READ(13,100)J,SLOP
 READ(12,100)J,WNT
 DATA(1,K)=SLOP
 EATA(1,K)=WNT
 DATA(2,K)=0.0
 EATA(2,K)=0.0
88 CONTINUE
 CALL COROL(DATA,EATA,CROSS,ZATA,SATA,QATA,DUM,NUM,QUM)
 DO 99 K=1,QUM
99 CRSLSW(K)=CRSLSW(K)+CROSS(K)
REWIND 10
REWIND 12
DO 14 K=1,NUM
READ(10,100)J,SIGO
READ(12,100)J,WNT
DATA(1,K)=SIGO
 EATA(1,K)=WNT
 DATA(2,K)=0.0
 EATA(2,K)=0.0
  SGO=SGO+SIGO*SIGO
14 CONTINUE
C
 CALL COROL(DATA,EATA,CROSS,ZATA,SATA,QATA,DUM,NUM,QUM)
C
  DO 15 K=1,QUM
15 CRSOSW(K)=CRSOSW(K)+CROSS(K)
C
REWIND 11
REWIND 12
C
DO 16 K=1,NUM
READ(11,100)J,SIGT
 READ(12,100)J,WNT
  DATA(1,K)=SIGT
 EATA(1,K)=WNT
 EATA(2,K)=0.0
  DATA(2,K)=0.0
16 CONTINUE
C
  CALL COROL(DATA,EATA,CROSS.ZATA,SATA,QATA,DUM.NUM,QUM)
C
DO 17 K=1,QUM
17 CRSTSW(K)=CRSTSW(K)+CROSS(K)
C
REWIND 11
REWIND 12
REWIND 10
REWIND 13
DO 18 K=1,NUM
READ(10,100)J,SIGO
READ(13,100)J,SLOP
 DATA(1,K)=SIGO
 EATA(1,K)=SLOP
 DATA(2,K)=0.0
 EATA(2.K)=0.0
18 CONTINUE
C
    CALL COROL(DATA,EATA,CROSS.ZATA,SATA,BATA,DUN,NUM,QUM)
C
```

```
L COL3T3

10  SUBROUTINE COROL(DATA,EATA,CROSS,ZATA,SATA,QATA,DUM,NUM,QUM)
30 INTEGER QUM,NUM
33 LUM=NUM
35 JUM=QUM
40  REAL NUN
45   REAL SATA(2,QUM)
50  REAL ZATA(2,NUM),DATA(2,NUM),EATA(2,NUM),CROSS(QUM)
60  REAL QATA(QUM),DUM(QUM)
70  NUN=1./FLOAT(NUM)
80  DO 12      K=1,QUM
82  SATA(1,K)=0.0
84  SATA(2,K)=0.0
90 12 CONTINUE
100C
102 DO 880 K=1,NUM
104C WRITE(19,1000)DATA(1,K),DATA(2,K),EATA(1,K),EATA(2,K)
106 880 CONTINUE
110    CALL FOURT(DATA,LUM,1,-1,0,0)
120    CALL FOURT(EATA,LUM,1,-1,0,0)
130C
140 DO 10 K=1,NUM
150  ZATA(1,K)=(DATA(1,K)*EATA(1,K)+DATA(2,K)*EATA(2,K))/LUM
160   ZATA(2,K)=(DATA(2,K)*EATA(1,K)-DATA(1,K)*EATA(2,K))/LUM
170 10 CONTINUE
180  DO 112 K=1,NUM
184  CROSS(K)=ZATA(1,K)
188  CROSS(NUM+K)=ZATA(2,K)
200 112 CONTINUE
210 RETURN
220 END
*
```

L CCA3G:

```
 SUBROUTINE CRSLTN(DATA,EATA,CROSS,ZATA,SATA,QATA,DUM,NUM,QUM)
INTEGER QUM,NUM
LUM=NUM
JUM=QUM
 REAL MUN
  REAL SATA(2,QUM)
 REAL ZATA(2,NUM),DATA(2,NUM),EATA(2,NUM),CROSS(QUM)
 REAL QATA(QUM),DUM(QUM)
C PRINT,"NUM=",NUM
 MUN=1./FLOAT(NUM)
 P=.33333333
 DO 12     K=1,QUM
 SATA(1,K)=0.0
 SATA(2,K)=0.0
12 CONTINUE
DO 10 K=1,NUM
 ZATA(1,K)=CROSS(K)
 ZATA(2,K)=CROSS(NUM+K)
10 CONTINUE
DO 23 K=3,(NUM/2)-2
  ZATA(1,K)=P*(P*(ZATA(1,K-2)+ZATA(1,K+2))+ZATA(1,K)+2.*P*(ZATA(1,K-1)
&+ZATA(1,K+1)))
  ZATA(2,K)=P*(P*(ZATA(2,K-2)+ZATA(2,K+2))+ZATA(2,K)+2.*P*(ZATA(2,K-1)
&+ZATA(2,K+1)))
23 CONTINUE
  ZATA(1,1)=.5*(ZATA(1,1)+P*ZATA(1,3)+2.*P*ZATA(1,2))
  ZATA(2,1)=.5*(ZATA(2,1)+P*ZATA(2,3)+2.*P*ZATA(2,2))
  ZATA(1,2)=(3./8.)*(P*ZATA(1,4)+ZATA(1,2)+2.*P*(ZATA(1,1)+ZATA(1,3)))
  ZATA(2,2)=(3./8.)*(P*ZATA(2,4)+ZATA(2,2)+2.*P*(ZATA(2,1)+ZATA(2,3)))
  ZATA(1,(NUM/2))=.5*(ZATA(1,(NUM/2))+P*ZATA(1,(NUM/2)-2)+2.*P*ZATA(
&1,(NUM/2)-1))
  ZATA(2,(NUM/2))=.5*(ZATA(2,(NUM/2))+P*ZATA(2,(NUM/2)-2)+2.*P*ZATA(
&2,(NUM/2)-1))
ZATA(1,(NUM/2)-1)=(3./8.)*(ZATA(1,(NUM/2)-1)+P*ZATA(1,(NUM/2)-3)+2.*P*(ZATA
&(1,(NUM/2)-2)+ZATA(1,(NUM/2))))
ZATA(2,(NUM/2)-1)=(3./8.)*(ZATA(2,(NUM/2)-1)+P*ZATA(2,(NUM/2)-3)+2.*P*(ZATA
&(2,(NUM/2)-2)+ZATA(2,(NUM/2))))
DO 156 K=1,NUM/2
ZATA(1,K+(NUM/2))=ZATA(1,K)
ZATA(2,K+(NUM/2))=-ZATA(2,K)
156 CONTINUE
DO 43 K=1,NUM/2
  SATA(1,K)=ZATA(1,K)
  SATA(1,QUM+1-K)=ZATA(1,NUM+1-K)
  SATA(2,QUM+1-K)=ZATA(2,NUM+1-K)
  SATA(2,K)=ZATA(2,K)
  43 CONTINUE
  CALL FOURT(SATA,JUM,1,-1,1,0)
DO 15 K=1,QUM
15 DUM(K)=SATA(1,K)
100 FORMAT(V)
DO 16 K=1,QUM/2
CROSS(K)=DUM(K+(QUM/2))
CROSS(QUM/2+K)=DUM(K)
16 CONTINUE
RETURN
 END
*
```

L SFCLOUT

```
PARAMETER NUM=128,QQ=.16666667
C  PARAMETER TRSHOLD=-10.0
REAL CATA(NUM),EATA(NUM),DATA(NUM),ZATA(NUM)
REAL QATA(NUM)
INTEGER SATA(NUM)
INTEGER AA
DO 78 J=1,5
 SUMS=0.0
 SUMP=0.0
 SUMST=0.0
 SUMPT=0.0
SUMPT=0.0
REWIND 30
 DO 56 L=1,NUM
 READ(40,100)AA,BB,CC,DD
 WRITE(30,100)AA,BB,CC,DD
56 CONTINUE
REWIND 30
 DO 10 K=1,NUM
 READ(30,100)SATA(K),CATA(K),EATA(K),DATA(K)
 ZATA(K)=DATA(K)
 QATA(K)=EATA(K)
 SUMS=SUMS+10.*ALOG10(DATA(K))
10 CONTINUE
 TRSHOLD=(SUMS/FLOAT(NUM))+6.
 SUMS=0.0
 DO 20 K=1,NUM
 IF(10.*ALOG10(DATA(K)).LT.TRSHOLD) GO TO 20
U1=0.0
 U2=0.0
U4=0.0
U5=0.0
IF(K.EQ.1) GO TO 344
IF(10.*ALOG10(DATA(K-1)).LT.TRSHOLD)   U2=2.*QQ
 IF(K.EQ.2)   GO TO 344
IF(10.*ALOG10(DATA(K-2)).LT.TRSHOLD)    U1=QQ
 IF(K.EQ.NUM) GO TO 554
344 CONTINUE
IF(10.*ALOG10(DATA(K+1)).LT.TRSHOLD)    U4=2.*QQ
 IF(K.EQ.NUM-1) GO TO 554
IF(10.*ALOG10(DATA(K+2)).LT.TRSHOLD)    U5=QQ
554 CONTINUE
  UU=U1+U2+U4+U5
 IF(UU.EQ.0.0)   PRINT,K
  DATA(K)=(U1*DATA(K-2)+U2*DATA(K-1)+U4*DATA(K+1)+U5*DATA(K+2))/UU
 EATA(K)=(U1*EATA(K-2)+U2*EATA(K-1)+U4*EATA(K+1)+U5*EATA(K+2))/UU
IF(DATA(K).NE.ZATA(K))WRITE(31,100)K,10.*ALOG10(ZATA(K)),10.*ALOG10(DATA(K))
&,10.*ALOG10(QATA(K)),10.*ALOG10(EATA(K)),TRSHOLD
20 CONTINUE
 DO 45 K=1,NUM
SUMS=SUMS+ZATA(K)
SUMP=SUMP+QATA(K)
SUMST=SUMST+DATA(K)
SUMPT=SUMPT+EATA(K)
45 CONTINUE
SUMS=10.*ALOG10(SUMS/FLOAT(NUM))
SUMP=10.*ALOG10(SUMP/FLOAT(NUM))
SUMST=10.*ALOG10(SUMST/FLOAT(NUM))
SUMPT=10.*ALOG10(SUMPT/FLOAT(NUM))
PRINT,"TRSHOLD",TRSHOLD,"SUMS",SUMS,"SUMP",SUMP,"SUMST",SUMST,"SUMPT",SUMPT
 DO 30 K=1,NUM
WRITE(35,100)SATA(K),CATA(K),EATA(K),DATA(K)
WRITE(34,100)K,DATA(K)
30 CONTINUE
WRITE(21,100)J,TRSHOLD
78 CONTINUE
100 FORMAT(V)
 STOP
 END
*
```

```
*L MDTRFNC

 08
INTEGER D,F,RAW
INTEGER NUM,AVE
PARAMETER V=128,U=128
PI=3.141593
Q=.33333
NUM=V
PARAMETER S=1280
REAL CRH(V),NORM(V)
DIMENSION ERH(V),AVRFUN(V)
DIMENSION DATA(2,V),EATA(2,V)
DIMENSION BULK(2,S)
DIMENSION AVCRS(2,V)
DIMENSION PURSPEC(V),PWS(V),GMAS(V),CROSPUR(V),FI(V)
DIMENSION PUSPEC(V),RFS(V),CHRENCE(V),FREQ(V)
DIMENSION GMASPEC(V),CROSPEC(2,V),RFUNC(2,V),RFSPEC(V)
DIMENSION AVRFUNC(U),AVFRQ(U),AVFI(U),AVPUR(U),AVGMA(U)
DIMENSION AVCSPUR(U),AVCOH(U)
C
PRINT, NUMBER OF PRCESSED TERMS TO BE AVERAGED/(AVE=?)'
READ,AVPTIN
AVE=AVPTIN
C
SUMPT=0.0
C
DO 111 K=1,S
READ(14,900)J,WHT,PUT,SIG
PRTN=PUT
SUMPT=SUMPT+PRTN
PRTN=PUT
BULK(1,K)=PRTN
BULK(2,K)=WHT
111 CONTINUE
C
DO 124 J=1,NUM
AVRFUN(J)=0.0
AVFI(J)=0.0
AVPUR(J)=0.0
AVGMA(J)=0.0
AVCSPUR(J)=0.0
AVCRS(1,J)=0.0
AVCRS(2,J)=0.0
AVCOH(J)=0.0
124 CONTINUE
C
AVEPT=SUMPT/S
PRINT,AVEPT
DO 115 F=1,AVE
RAW=(F-1)*NUM
C
DO 113 K=1,NUM
DATA(1,K)=BULK(1,(RAW+K))
DATA(2,K)=0.0
EATA(1,K)=BULK(2,(RAW+K))
EATA(2,K)=0.0
113 CONTINUE
C
CALL FOURT(DATA,NUM,1,-1,0,0)
CALL FOURT(EATA,NUM,1,-1,0,0)
C
DO 122 I=1,NUM
GMASPEC(I)=(EATA(1,I)*EATA(1,I)+EATA(2,I)*EATA(2,I))/NUM
PURSPEC(I)=(DATA(1,I)*DATA(1,I)+DATA(2,I)*DATA(2,I))/NUM
CROSPEC(1,I)=(DATA(1,I)*EATA(1,I)+DATA(2,I)*EATA(2,I))/NUM
CROSPEC(2,I)=(DATA(2,I)*EATA(1,I)-DATA(1,I)*EATA(2,I))/NUM
PUSPEC(I)=PURSPEC(I)
122 CONTINUE
C
```

MDTRFNC (cont'd.)

```
DO 211 J=1,NUM
K=J-1
FREQ(J)=FLOAT(K)/FLOAT(NUM)
211 CONTINUE
DO 117 D=1,NUM
AVCRS(1,D)=AVCRS(1,D)+CROSPEC(1,D)
AVCRS(2,D)=AVCRS(2,D)+CROSPEC(2,D)
AVPUR(D)=AVPUR(D)+PURSPEC(D)
AVGMA(D)=AVGMA(D)+GMASPEC(D)
117 CONTINUE
115 CONTINUE
 PRINT,"000790"
AVRG=0.0
DO 116 I=1,NUM
AVFRQ(I)=FREQ(I)
AVPUR(I)=AVPUR(I)/AVE
AVGMA(I)=AVGMA(I)/AVE
AVCRS(1,I)=AVCRS(1,I)/AVE
AVCRS(2,I)=AVCRS(2,I)/AVE
RFUNC(1,I)=AVCRS(1,I)/(AVEPT*AVGMA(I))
RFUNC(2,I)=AVCRS(2,I)/(AVEPT*AVGMA(I))
C AVFI(I)=ATAN(RFUNC(2,I)/RFUNC(1,I))
AVRFUN(I)=SQRT(RFUNC(1,I)*RFUNC(1,I)+RFUNC(2,I)*RFUNC(2,I))
NORM(I)=(AVEPT*AVGMA(I))
CRH(I)=SQRT(AVCRS(1,I)*AVCRS(1,I)+AVCRS(2,I)*AVCRS(2,I))
C ERH(I)=AVRFUN(I)*9.8/((2*PI*AVFRQ(I))**2)
116 CONTINUE
C
DO 203 J=1,NUM
K=J
WRITE(07,550)K,AVFRQ(J),CRH(J),NORM(J),AVGMA(J),AVEPT,AVRFUN(J)
203 CONTINUE
DO 210 I=4,(NUM-4)
AVPUR(I)=Q*(Q*AVPUR(I-2)+2*Q*AVPUR(I-1)+AVPUR(I)
&+2*Q*AVPUR(I+1)+Q*AVPUR(I+2))
NORM(I)=Q*(Q*NORM(I-2)+2*Q*NORM(I-1)+NORM(I)+2*Q*NORM(I+1)+Q*NORM(I+2))
CRH(I)=Q*(Q*CRH(I-2)+2*Q*CRH(I-1)+CRH(I)+Q*2*CRH(I+1)+Q*CRH(I+2))
210 CONTINUE
C
DO 214 I=4,(NUM-4)
AVRFUN(I)=CRH(I)/NORM(I)
ERH(I)=AVRFUN(I)*9.8/((2*PI*AVFRQ(I))**2)
214 CONTINUE
 DO 445 K=3,NUM-8
AVRFUN(K)=Q*(Q*(AVRFUN(K-2)+AVRFUN(K+2))+AVRFUN(K)+2.*Q*(AVRFUN
$(K+1)+AVRFUN(K-1)))
445  CONTINUE
DO 213 I=4,(NUM-4)
C WRITE(08,559)I,AVFRQ(I),AVRFUN(I),ERH(I),CRH(I),1000*NORM(I),100000000*AVPUR(I)
WRITE(05,100)AVFRQ(I),1000.*NORM(I)
WRITE(07,100)AVFRQ(I),100000000.*AVPUR(I)
213 CONTINUE
DO 667 K=5,(NUM-8)
WRITE(10,100)AVFRQ(K),AVRFUN(K)
667 CONTINUE
557 FORMAT(I3,4X,F5.3,4X,F9.2,4X,F9.2)
558  FORMAT(V)
C 558 FORMAT(I3,4X,F5.3,4X,F9.2,4X,F9.2,4X,F9.2,4X,F9.2)
C 900 FORMAT(I4,4X,F9.3,4X,F9.7)
900 FORMAT(V)
100 FORMAT(V)
559 FORMAT(I3,4X,F5.3,4X,F9.3,4X,F9.3,4X,F9.3,4X,F9.3,4X,F7.3)
STOP
END
```

Copy available to DTIC does not permit fully legible reproduction

L COHERENC

```
PARAMETER V=128,U=128,S=1280
INTEGER B,F,RAW
INTEGER NUM,AVE
PI=3.141593
Q=.33333
NUM=V
REAL NUN
REAL CRH(V),NORM(V)
DIMENSION ERH(V),AVRFUN(V)
DIMENSION DATA(2,V),EATA(2,V)
DIMENSION BULK(2,S)
DIMENSION AVCRS(2,V)
DIMENSION PURSPEC(V),PUS(V),GMAS(V),CROSPUR(V),FI(V)
DIMENSION PUSPEC(V),RFS(V),CHRENCE(V),FREQ(V)
DIMENSION GMASPEC(V),CROSPEC(2,V),RFUNC(2,V),RFSPEC(V)
DIMENSION AVRFUNC(U),AVFRQ(U),AVFI(U),AVPUR(U),AVGMA(U)
DIMENSION AVCSPUR(U),AVCON(U)
 NUN=1./FLOAT(NUM)
PRINT,'NUMBER OF PRCESSED TERMS TO BE AVERAGED/(AVE=?)'
READ,AVPTIN
AVE=AVPTIN
  EVA=1./FLOAT(AVE)
SUMPT=0.0
C
DO 111 K=1,S
READ(14,200)J,WHT,PWT,SIGO
PRTN=PWT
SUMPT=SUMPT+PRTN
PRTN=PWT
BULK(1,K)=PRTN
BULK(2,K)=WHT
111 CONTINUE
C
DO 124 J=1,NUM
AVRFUN(J)=0.0
AVFI(J)=0.0
AVPUR(J)=0.0
AVGMA(J)=0.0
AVCSPUR(J)=0.0
AVCRS(1,J)=0.0
AVCRS(2,J)=0.0
AVCON(J)=0.0
124 CONTINUE
C
AVEPT=SUMPT/S
C PRINT,AVEPT
DO 115 F=1,AVE
RAW=(F-1)*NUM
C
DO 113 K=1,NUM
DATA(1,K)=BULK(1,(RAW+K))
DATA(2,K)=0.0
EATA(1,K)=BULK(2,(RAW+K))
EATA(2,K)=0.0
113 CONTINUE
C
CALL FOURT(DATA,NUM,1,-1,0,0)
CALL FOURT(EATA,NUM,1,-1,0,0)
C
DO 122 I=1,NUM/2
GMASPEC(I)=(EATA(1,I)*EATA(1,I)+EATA(2,I)*EATA(2,I))/NUM
PURSPEC(I)=(DATA(1,I)*DATA(1,I)+DATA(2,I)*DATA(2,I))/NUM
CROSPEC(1,I)=(DATA(1,I)*EATA(1,I)+DATA(2,I)*EATA(2,I))/NUM
CROSPEC(2,I)=(DATA(2,I)*EATA(1,I)-DATA(1,I)*EATA(2,I))/NUM
PUSPEC(I)=PURSPEC(I)
122 CONTINUE
C
DO 211 J=1,NUM
K=J-1
FRCQ(K)=FLOAT(K)/FLOAT(NUM)
211 CONTINUE
```

COHERENC (cont'd.)

```
DO 117 D=1,NUM/2
   XI=SQRT((CROSPEC(1,D))*(CROSPEC(1,D))+(CROSPEC(2,D))*(CROSPEC(2,D)))
 AVCRS(1,D)=AVCRS(1,D)+EVA*XI
AVPUR(D)=AVPUR(D)+EVA*(PURSPEC(D))
AVGMA(D)=AVGMA(D)+EVA*(GMASPEC(D))
117 CONTINUE
115 CONTINUE
SUM=0.0
DO 346 K=1,NUM/2
AVCRS(2,K)=SQRT(AVGMA(K))*SQRT(AVPUR(K))
 CRH(K)=AVCRS(1,K)/AVCRS(2,K)
 CRH(K)=CRH(K)*CRH(K)
C PRINT,FREQ(K),CRH(K),AVCRS(1,K),AVCRS(2,K)
WRITE(08,100)FREQ(K),AVPUR(K),AVGMA(K),AVCRS(2,K),CRH(K)
 SUM=SUM+CRH(K)
346 CONTINUE
AVERAGE=SUM*2./NUM
SUM=0.0
DO 989 K=1,NUM/2
SUM=SUM+CRH(K)*CRH(K)-AVERAGE*AVERAGE
989 CONTINUE
STDEV=SUM*2./NUM
PRINT,'COHERENCE MEAN=',AVERAGE,'COHERENCE STAND. DEV.=',STDEV
100 FORMAT(5(1X,F12.9))
200 FORMAT(V)
STOP
END
*
```

*L FFT

```
      SUBROUTINE FOURT(DATA,NN,NDIM,ISIGN,IFORM,WORK)
c        bounded by 3*2**(-b)*sum(factor(j)**1.5), where b is the number
c        of bits in the floating point fraction and factor(j) are the
c        prime factors of ntot.
c
c        program by norman brenner from the basic program by charles
c        rader.  ralph alter suggested the idea for the digit reversal.
c        mit lincoln laboratory, august 1967.  this is the fastest and most
c        versatile version of the fft known to the author.  shorter pro-
c        grams four1 and four2 restrict dimension lengths to powers of two.
c        see-- ieee audio transactions (june 1967), special issue on fft.
c        see math explanation in pdp-15 documentation
c
c
c        the discrete fourier transform places three restrictions upon the
c        data.
c        1.  the number of input data and the number of transform values
c        must be the same.
c        2.  both the input data and the transform values must represent
c        equispaced points in their respective domains of time and
c        frequency.  calling these spacings deltat and deltaf, it must be
c        true that deltaf=2*pi/(nn(i)*deltat).  of course, deltat need not
c        be the same for every dimension.
c        3.  conceptually at least, the input data and the transform output
c        represent single cycles of periodic functions.
c
c        example 1.  three-dimensional forward fourier transform of a
c        complex array dimensioned 32 by 25 by 13 in fortran iv.
c        dimension data(32,25,13),work(50),nn(3)
c        complex data
c        data nn/32,25,13/
c        do 1 i=1,32
c        do 1 j=1,25
c        do 1 k=1,13
c     1  data(i,j,k)=complex value
c        call fourt(data,nn,3,-1,1,work)
c
c        example 2.  one-dimensional forward transform of a real array of
c        length 64 in fortran ii.
c        dimension data(2,64)
c        do 2 i=1,64
c        data(1,i)=real part
c     2  data(2,i)=0.
c        call fourt(data,64,1,-1,0,0)
c
      dimension data(1),nn(1),ifact(32),work(1)
      common /nam/ nnn
      twopi=6.283185307
      if(ndim-1)920,1,1
1      ntot=2
      do 2 idim=1,ndim
      if(nn(idim))920,920,2
2      ntot=ntot*nn(idim)
c
c        main loop for each dimension
c
      np1=2
      do 910 idim=1,ndim
      n=nn(idim)
      np2=np1*n
      if(n-1)930,900,5
c
c        factor n
c        decompose input into n discrete time
c        samples, n/2 odd and n/2 even.  keep decomposing until
c        n/2 contains two samples.
c
```

FFT (cont'd.)

```
5     n=n
      ntwo=np1
      if=1
      idiv=2
10      iquot=n/idiv
      irem=n-idiv*iquot
      if(iquot-idiv)50,11,11
11      if(irem)20,12,20
12      ntwo=ntwo+ntwo
      n=iquot
      go to 10
20      idiv=3
30      iquot=n/idiv
      irem=n-idiv*iquot
      if(iquot-idiv)60,31,31
31      if(irem)40,32,40
32      ifact(if)=idiv
      if=if+1
      n=iquot
      go to 30
40      idiv=idiv+2
      go to 30
50      if(irem)60,51,60
51      ntwo=ntwo+ntwo
      go to 70
60      ifact(if)=n
c
c      separate four cases--
c         1. complex transform or real transform for the 4th, 5th,etc.
c            dimensions.
c         2. real transform for the 2nd or 3rd dimension.  method--
c            transform half the data, supplying the other half by con-
c            jugate symmetry.
c         3. real transform for the 1st dimension, n odd.  method--
c            transform half the data at each stage, supplying the other
c            half by conjugate symmetry.
c         4. real transform for the 1st dimension, n even.  method--
c            transform a complex array of length n/2 whose real parts
c            are the even numbered real values and whose imaginary parts
c            are the odd numbered real values.  separate and supply
c            the second half by conjugate symmetry.
c
70      non2=np1*(np2/ntwo)
      icase=1
      if(idim-4)71,90,90
71      if(iform)72,72,90
72      icase=2
      if(idim-1)73,73,90
73      icase=3
      if(ntwo-np1)90,90,74
74      icase=4
      ntwo=ntwo/2
      n=n/2
      np2=np2/2
      ntot=ntot/2
      i=3
      do 80 j=2,ntot
      data(j)=data(i)
90      ifrng=np1
      if(icase-2)100,95,100
95      ifrng=np0*(1+nprev/2)
c
c      shuffle on the factors of two in n.  as the shuffling
c      can be done by simple interchange, no working array is needed
c      decomposed input must be shuffled to take
c      care of bit reversal in output.
c      example     f0,f4,f2,f6,f1,f5,f3,f7 will
```

FFT (cont'd.)

```
c     produce coefficients g0,g1,g2,g3,g4,g5 ....gn
c     fourier can then be done in place without
c     additional core.
c
  100   if(ntwo-np1)600,600,110
  110   np2hf=np2/2
      j=1
      do 150 i2=1,np2,non2
      if(j-i2)120,130,130
  120   i1max=i2+non2-2
      do 125 i1=i2,i1max,2
      do 125 i3=i1,ntot,np2
      j3=j+i3-i2
      tempr=data(i3)
      tempi=data(i3+1)
      data(i3)=data(j3)
      data(i3+1)=data(j3+1)
      data(j3)=tempr
  125   data(j3+1)=tempi
  130   m=np2hf
  140   if(j-m)150,150,145
  145   j=j-m
      m=m/2
      if(m-non2)150,140,140
  150   j=j+m
c
c     main loop for factors of two.  perform fourier transforms of
c     length four, with one of length two if needed.  the twiddle factor
c     w=exp(isign*2*pi*sqrt(-1)*m/(4*mmax)).  check for w=isign*sqrt(-1)
c     and repeat for w=isign*sqrt(-1)*conjugate(w). note j=sqrt(-1)
c
      non2t=non2+non2
      ipar=ntwo/np1
  310   if(ipar-2)350,330,320
  320   ipar=ipar/4
      go to 310
  330   do 340 i1=1,i1rng,2
      do 340 j3=i1,non2,np1
      do 340 k1=j3,ntot,non2t
      k2=k1+non2
      tempr=data(k2)
      tempi=data(k2+1)
      data(k2)=data(k1)-tempr
      data(k2+1)=data(k1+1)-tempi
      data(k1)=data(k1)+tempr
  340   data(k1+1)=data(k1+1)+tempi
  350   mmax=non2
  360   if(mmax-np2hf)370,600,600
  370   lmax=max0(non2t,mmax/2)
      if(mmax-non2)405,405,380
  380   theta=-twopi*float(non2)/float(4*mmax)
      if(isign)400,390,390
  390   theta=-theta
  400   wr=cos(theta)
      wi=sin(theta)
      wstpr=-2.*wi*wi
      wstpi=2.*wr*wi
  405   do 570 l=non2,lmax,non2t
      m=l
      if(mmax-non2)420,420,410
  410   w2r=wr*wr-wi*wi
      w2i=2.*wr*wi
      w3r=w2r*wr-w2i*wi
      w3i=w2r*wi+w2i*wr
  420   do 530 i1=1,i1rng,2
      do 530 j3=i1,non2,np1
      kmin=j3+ipar*m
      if(mmax-non2)430,430,440
  430   kmin=j3
  440   kdif=ipar*mmax
```

FFT (cont'd.)

```
450    kstep=4*kdif
       do 520 k1=kmin,ntot,kstep
       k2=k1+kdif
       k3=k2+kdif
       k4=k3+kdif
       if(mmax-nom2)460,460,480
460    u1r=data(k1)+data(k2)
       u1i=data(k1+1)+data(k2+1)
       u2r=data(k3)+data(k4)
       u2i=data(k3+1)+data(k4+1)
       u3r=data(k1)-data(k2)
       u3i=data(k1+1)-data(k2+1)
       if(isign)470,475,475
470    u4r=data(k3+1)-data(k4+1)
       u4i=data(k4)-data(k3)
       go to 510
475    u4r=data(k4+1)-data(k3+1)
       u4i=data(k3)-data(k4)
       go to 510
480    t2r=w2r*data(k2)-w2i*data(k2+1)
       t2i=w2r*data(k2+1)+w2i*data(k2)
       t3r=wr*data(k3)-wi*data(k3+1)
       t3i=wr*data(k3+1)+wi*data(k3)
       t4r=w3r*data(k4)-w3i*data(k4+1)
       t4i=w3r*data(k4+1)+w3i*data(k4)
       u1r=data(k1)+t2r
       u1i=data(k1+1)+t2i
       u2r=t3r+t4r
       u2i=t3i+t4i
       u3r=data(k1)-t2r
       u3i=data(k1+1)-t2i
       if(isign)490,500,500
490    u4r=t3i-t4i
       u4i=t4r-t3r
       go to 510
500    u4r=t4i-t3i
       u4i=t3r-t4r
510    data(k1)=u1r+u2r
       data(k1+1)=u1i+u2i
       data(k2)=u3r+u4r
       data(k2+1)=u3i+u4i
       data(k3)=u1r-u2r
       data(k3+1)=u1i-u2i
       data(k4)=u3r-u4r
520    data(k4+1)=u3i-u4i
       kmin=4*(kmin-j3)+j3
       kdif=kstep
       if(kdif-np2)450,530,530
530    continue
       m=mmax-m
       if(isign)540,550,550
540    tempr=wr
       wr=-wi
       wi=-tempr
       go to 560
550    tempr=wr
       wr=wi
       wi=tempr
560    if(m-lmax)565,565,410
565    tempr=wr
       wr=wr*wstpr-wi*wstpi+wr
570    wi=wi*wstpr+tempr*wstpi+wi
       ipar=3-ipar
       mmax=mmax+mmax
       go to 360
c
c       main loop for factors not equal to two.  apply the twiddle factor
c       w=exp(isign*2-pi*sqrt(-1)*(j2-1)*(j1-j2)/(np2*ifp1)), then
c       perform a fourier transform of length ifact(if), making use of
c       conjugate symmetries.
c       see differences in math main computer documentation
c
```

FFT (cont'd.)

```
600    if(ntwo-np2)605,700,700
605    ifp1=non2
      if=1
      np1hf=np1/2
610    ifp2=ifp1/ifact(if)
      j1rng=np2
      if(icase-3)612,611,612
611    j1rng=(np2+ifp1)/2
      j2stp=np2/ifact(if)
      j1rg2=(j2stp+ifp2)/2
612    j2min=1+ifp2
      if(ifp1-np2)615,640,640
615    do 635 j2=j2min,ifp1,ifp2
      theta=-twopi*float(j2-1)/float(np2)
      if(isign)625,620,620
620    theta=-theta
625    sinth=sin(theta/2.)
      wstpr=-2.*sinth*sinth
      wstpi=sin(theta)
      wr=wstpr+1.
      wi=wstpi
      j1min=j2+ifp1
      do 635 j1=j1min,j1rng,ifp1
      i1max=j1+i1rng-2
      do 630 i1=j1,i1max,2
      do 630 i3=i1,ntot,np2
      j3max=i3+ifp2-np1
      do 630 j3=i3,j3max,np1
      tempr=data(j3)
      data(j3)=data(j3)*wr-data(j3+1)*wi
630    data(j3+1)=tempr*wi+data(j3+1)*wr
      tempr=wr
      wr=wr*wstpr-wi*wstpi+wr
635    wi=tempr*wstpi+wi*wstpr+wi
640    theta=-twopi/float(ifact(if))
      if(isign)650,645,645
645    theta=-theta
650    sinth=sin(theta/2.)
      wstpr=-2.*sinth*sinth
      wstpi=sin(theta)
      kstep=2*n/ifact(if)
      krang=kstep*(ifact(if)/2)+1
      do 698 i1=1,i1rng,2
      do 698 i3=i1,ntot,np2
      do 690 kmin=1,krang,kstep
      j1max=i3+j1rng-ifp1
      do 680 j1=i3,j1max,ifp1
      j3max=j1+ifp2-np1
      do 680 j3=j1,j3max,np1
      j2max=j3+ifp1-ifp2
      k=kmin+(j3-j1+(j1-i3)/ifact(if))/np1hf
      if(kmin-1)655,655,665
655    sumr=0.
      sumi=0.
      do 660 j2=j3,j2max,ifp2
      sumr=sumr+data(j2)
660    sumi=sumi+data(j2+1)
      work(k)=sumr
      work(k+1)=sumi
      go to 680
665    kconj=k+2*(n-kmin+1)
      j2=j2max
      sumr=data(j2)
      sumi=data(j2+1)
      oldsr=0.
      oldsi=0.
      j2=j2-ifp2
670    tempr=sumr
```

FFT (cont'd.)

```
          tempi=sumi
          sumr=twowr*sumr-oldsr+data(j2)
          sumi=twowr*sumi-oldsi+data(j2+1)
          oldsr=tempr
          oldsi=tempi
          j2=j2-ifp2
          if(j2-j3)675,675,670
     675    tempr=wr*sumr-oldsr+data(j2)
          tempi=wi*sumi
          work(k)=tempr-tempi
          work(kconj)=tempr+tempi
          tempr=wr*sumi-oldsi+data(j2+1)
          tempi=wi*sumr
          work(k+1)=tempr+tempi
          work(kconj+1)=tempr-tempi
     680    continue
          if(kmin-1)685,685,686
     685    wr=wstpr+1.
          wi=wstpi
          go to 690
     686    tempr=wr
          wr=wr*wstpr-wi*wstpi+wr
          wi=tempr*wstpi+wi*wstpr+wi
     690    twowr=wr+wr
          if(icase-3)692,691,692
     691    if(ifp1-np2)695,692,692
     692    k=1
          i2max=i3+np2-np1
          do 693 i2=i3,i2max,np1
          data(i2)=work(k)
          data(i2+1)=work(k+1)
     693    k=k+2
          go to 698
c
c          complete a real transform in the 1st dimension, n odd, by con-
c          jugate symmetries at each stage.
c
     695    j3max=i3+ifp2-np1
          do 697 j3=i3,j3max,np1
          j2max=j3+np2-j2stp
          do 697 j2=j3,j2max,j2stp
          j1max=j2+j1rng2-ifp2
          j1cnj=j3+j2max+j2stp-j2
          do 697 j1=j2,j1max,ifp2
          k=1+j1-i3
          data(j1)=work(k)
          data(j1+1)=work(k+1)
          if(j1-j2)697,697,696
     696    data(j1cnj)=work(k)
          data(j1cnj+1)=-work(k+1)
     697    j1cnj=j1cnj-ifp2
     698    continue
          if=if+1
          ifp1=ifp2
          if(ifp1-np1)700,700,610
c
c          complete a real transform in the 1st dimension, n even, by con-
c          jugate symmetries.
c
     700    go to (900,800,900,701),icase
     701    nhalf=n
          n=n+n
          theta=-twopi/float(n)
          if(isign)703,702,702
     702    theta=-theta
     703    sinth=sin(theta/2.)
          wstpr=-2.*sinth*sinth
          wstpi=sin(theta)
          wr=wstpr+1.
          wi=wstpi
          imin=3
          jmin=2*nhalf-1
          go to 725
     710    j=jmin
```

```
---
      do 720 i=imin,ntot,np2
      sumr=(data(i)+data(j))/2.
      sumi=(data(i+1)+data(j+1))/2.
      difr=(data(i)-data(j))/2.
      difi=(data(i+1)-data(j+1))/2.
      tempr=wr*sumi+wi*difr
      tempi=wi*sumi-wr*difr
      data(i)=sumr+tempr
      data(i+1)=difi+tempi
      data(j)=sumr-tempr
      data(j+1)=-difi+tempi
 720     j=j+np2
      imin=imin+2
      jmin=jmin-2
      tempr=wr
      wr=wr*wstpr-wi*wstpi+wr
      wi=tempr*wstpi+wi*wstpr+wi
 725     if(imin-jmin)710,730,740
 730     if(isign)731,740,740
 731     do 735 i=imin,ntot,np2
 735     data(i+1)=-data(i+1)
 740     np2=np2+np2
      ntot=ntot+ntot
      j=ntot+1
      imax=ntot/2+1
 745     imin=imax-2*nhalf
      i=imin
      go to 755
 750     data(j)=data(i)
      data(j+1)=-data(i+1)
 755     i=i+2
      j=j-2
      if(i-imax)750,760,760
 760     data(j)=data(imin)-data(imin+1)
      data(j+1)=0.
      if(i-j)770,780,780
 765     data(j)=data(i)
      data(j+1)=data(i+1)
 770     i=i-2
      j=j-2
      if(i-imin)775,775,765
 775     data(j)=data(imin)+data(imin+1)
      data(j+1)=0.
      imax=imin
      go to 745
 780     data(1)=data(1)+data(2)
      data(2)=0.
      go to 900
c
c      complete a real transform for the 2nd or 3rd dimension by
c      conjugate symmetries.
c
 800     if(i1rng-np1)805,900,900
 805     do 860 i3=1,ntot,np2
      i2max=i3+np2-np1
      do 860 i2=i3,i2max,np1
      imin=i2+i1rng
      imax=i2+np1-2
      jmax=2*i3+np1-imin
      if(i2-i3)820,820,810
 810     jmax=jmax+np2
 820     if(idim-2)850,850,830
 830     j=jmax+np0
      do 840 i=imin,imax,2
      data(i)=data(j)
      data(i+1)=-data(j+1)
 840     j=j-2
 850     j=jmax
      do 860 i=imin,imax,np0
      data(i)=data(j)
      data(i+1)=-data(j+1)
 860     j=j-np0
c
```

FFT (cont'd.)

```
c     end of loop on each dimension
c
 900    np0=np1
      np1=np2
 910    nprev=n
      return
c
c     :we come here   only in error
c
 920    write (6, 9601) ndim
      return
c
 930    write (6, 9602) idim, nn (idim)
      return
c
c
 9601     format (3(/),10('<*>'),5x,'f o u r t   n o t',
&          '   e x e c u t e d',10x,'only',i2,' dimension: )
 9602     format (3(/),10('<*>'),5x,'f o u r t   n o t',3x,
&          'e x e c u t e d',10x,'length of dimension #',i2,
&          ' is only',i4)
      end
*
```

AD-A129 690 INTERACTION OF THE RADAR WAVES WITH THE CAPILLARY WAVES ON THE OCEAN..(U) KANSAS UNIV/CENTER FOR RESEARCH INC LAWRENCE REMOTE SENSING L.. S BARKESHLI ET AL. MAY 83 3/3

UNCLASSIFIED CRINC/RSL-TR-419-1 N00014-79-C-0533 F/G 17/9 NL

END
DATE
FILMED
7 83
DTIC

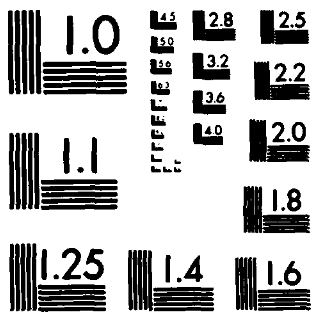

MICROCOPY RESOLUTION TEST CHART
NATIONAL BUREAU OF STANDARDS-1963-A

REFERENCES

Afarani, M., ''Directional Properties of Ocean Radar Backscatter—A Harmonic Regression Analysis of AAFE RADSCAT Circle Experiments,'' Remote Sensing Laboratory Technical Report 186-15, University of Kansas Center for Research, Inc., Lawrence, Kansas, October 1975.

Bass, F.G., I.M. Fuks et al., ''Very High Frequency Radiowave Scattering by a Disturbed Sea Surface,'' IEEE Transactions, vol. AP-16, 1968, pp. 554-567.

Chan, H.L. and A.K. Fung, ''Backscattering from a Two-Scale Rough Surface with Application to Radar Sea Return,'' NASA Contractor Report CR-2327, November 1973.

Chan, H.L. and A.K. Fung, ''A Theory of Sea Scatter at Large Incidence Angles,'' Journal of Geophysical Research, vol. 82, 1977, pp. 3429-3444.

Cox, C. and W. Munk, ''Statistics of the Sea Surface Derived from Sun Glitter,'' Journal of Marine Research, vol. 13, 1954, pp. 198-227.

Donelan, M. and Pierson, W.J., ''The Sampling Variability of Estimate of Wind-Generated Gravity Waves,''unpublished paper, 1981.

Fuks, I.M., ''Theory of Radiowave Scattering at a Rough Sea Surface,'' Soviet Radiophysics, vol. 9, 1969, pp. 513-519.

Hasselmann, K., ''On the Mass and Momentum Transfer Between Short Gravity Waves and Large-Scale Motions,'' Journal of Fluid Mechanics, vol. 50, 1971, pp. 189-205.

Jones, W.L., L.C. Schroeder and J.L. Mitchell, ''Aircraft Measurements of the Microwave Scattering Signature of the Ocean,'' IEEE Transactions, vol. AP-25, 1977, pp. 52-61.

Jones, W.L., L.C. Schroeder and J.L. Mitchell, ''Aircraft Measurements of the Isotropic Microwave Scattering Signature Over the Ocean for 1975 JONSWAP and 1976 East Coast Missions,'' NASA TMX-78646, NASA Langley Research Center, Hampton, Virginia, 1978.

Kalmykov, A.I. and V.V. Pustovogtenko, ''On Polarization Features of Radio Signal Scattered from the Sea Surface at Small Grazing Angles,'' Journal of Geophysical Research, vol. 81, no. 12, April 1976, pp. 1960-1964.

Keller, W.C. and J.W. Wright, ''Microwave Scattering and the Straining of Wind-Generated Waves,'' Radio Science, vol. 10, 1975, pp. 139-147.

Keller, W.C. and J.W. Wright, ''Modulation of Microwave Backscatter by Gravity Waves in a Wave Tank,'' NRL Report 7968, Naval Research Laboratory, Washington, D.C., 1976, pp. 1-21.

Kim, Y.S., ''Measurement of the Luneberg Lens Cross-Section,'' Remote Sensing Laboratory Technical Memorandum 419-4, University of Kansas Center for Research, Inc., Lawrence, Kansas, March 1982.

Kwoh, D.S.W. and B.M. Lake, ''Microwave Backscatter from Short Gravity Waves: Deterministic, Coherent, Dual-Polarized Study of the Relationship Between Backscatter and Water Wave Properties,'' presented at the IUCRM Symposium on Wave Dynamics and Radio Probing of the Ocean Surface, May 13-20, 1981, Miami Beach, Florida.

Larson, T.R. and J.W. Wright, ''Wind Generated Gravity-Capillary Waves: Laboratory Measurements of Temporal Growth Rates Using Microwave Backscatter,'' Journal of Fluid Mechanics, vol. 70, 1975, pp. 417-436.

Long, M.W., Radar Reflectivity of Land and Sea, Lexington Books, D.C. Heath and Company, Lexington, Massachusetts 1975.

Longuet-Higgins, M.S., ''The Effect of Non-Linearities on Statistical Distributions in the Theory of Sea Waves,'' Journal of Fluid Mechanics, vol. 17, part 3, 1963, pp. 459-480.

Longuet-Higgins, M.S. and R.W. Stewart, ''Radiation Stress in Water Waves: A Physical Discussion with Applications,'' Deep Sea Research, vol. 11, 1964, pp. 529-562.

Mitsuyasu, H. and T. Honda, ''The High Frequency Spectrum of Wind-Generated Waves,'' Journal of Oceanographical Society of Japan, vol. 30, 1974, pp. 185-198.

Moore, R.K., ''Effective Specular Events on Tower and Airborne Measurements of Ocean Backscatter,'' Remote Sensing Laboratory Technical Memorandum 419-3, University of Kansas Center for Research, Inc., Lawrence, Kansas, January 1982.

Neumann, G. and W.J. Pierson, Principles of Physical Oceanography, Prentice-Hall, Inc., Englewood Cliffs, New Jersey, 1966.

Phillips, O.M., The Dynamics of the Upper Ocean, Cambridge University Press, New York, New York, 1966.

Pierson, W.J. and Fife, P., ''Some Nonlinear Properties of Long-Crested Periodic Waves with Lengths Near 2.44 m,'' Journal of Geophysical Research, vol. 66, 1961, pp. 163-179.

Pierson, W.J. and R.A. Stacy, ''The Elevation, Slope and Curvature Spectra of a Wind-Roughed Sea,'' NASA Contract Report CR-2247, 1973.

Pierson, W.J., ''The Theory and Application of Ocean Wave Measuring Systems at and Below the Sea Surface, or the Land, from Aircraft and from Spacecraft,'' Contractor Report NAS 5-22041, NASA Goddard Space Flight Center, Greenbelt, Maryland, 1975.

Pierson, W.J., Private Communication, 1978.

Plant, W.J. and J.W. Wright, ''Growth and Equilibrium of Short Gravity- Capillary Waves in a Wind-Wave Tank,'' Journal of Fluid Mechanics, vol. 82, 1977, pp. 767-793.

Plant, W.J., W.C. Keller and J.W. Wright, ''Modulation of Coherent Microwave Backscatter by Shoaling Waves,'' Journal of Geophysical Research, vol. 83, 1978, pp. 1347-1352.

Plant, W.J., ''Measurement of Ocean Wave--Radar Modulation Transfer Functions,'' NRL Report (unpublished, 1980).

Valenzuela, G.R., ''Depolarization of EM Waves by Slightly Rough Surfaces,'' IEEE Transactions, vol. AP-15, 1967, pp. 552-557.

Valenzuela, G.R., ''Scattering of Electromagnetic Waves from a Tilted Slightly-Rough Surface,'' Radio Science, vol. 3, 1968, pp. 1057-1066.

Valenzuela, G.R. and M.B. Laing, ''Nonlinear Energy Transfer in Gravity- Capillary Wave Spectra, with Applications,'' Journal of Fluid Mechanics, vol. 54, 1972, pp. 507-520.

Wright, J.W., ''Backscattering from Capillary Waves with Application to Sea Clutter,'' IEEE Transactions, vol. AP-14, 1966, pp. 749-754.

Wright, J.W., ''A New Model for Sea Clutter,'' IEEE Transactions, vol. AP-16, 1968, pp. 217-223.

Wright, J.W., ''Detection of Ocean Waves by Microwave Radar: The Modulation of Short Gravity-Capillary Waves,'' Boundary-Layer Meteorology, vol. 13, 1978, pp.87-105.

Wright, J.W., W.J. Plant and W.C. Keller, ''Ocean Wave-Radar Modulation Transfer Functions from the West Coast Experiment,'' Journal of Geophysical Research, vol. 85, 1980, pp. 4957-4966.

Wu, S.T. and A.K. Fung, ''A Noncoherent Model of Microwave Emissons and Backscattering from the Sea Surface,'' Journal of Geophysical Research, vol. 77, no. 30, 1973, pp. 5917-5929.

CRINC LABORATORIES

Chemical Engineering Low Temperature Laboratory

Remote Sensing Laboratory

Flight Research Laboratory

Chemical Engineering Heat Transfer Laboratory

Nuclear Engineering Laboratory

Environmental Health Engineering Laboratory

Information Processing Laboratory

Water Resources Institute

Technical Transfer Laboratory

Air Pollution Laboratory

Satellite Applications Laboratory